



Universidad de Concepción  
Dirección de Postgrado  
Facultad de Farmacia -Programa de Ciencias y Tecnología Analítica.

**A NOVEL METABOLOMICS APPROACH AS INTEGRATIVE  
STRATEGY FOR UNDERSTANDING CHANGES IN PINUS  
RADIATA D.DON METABOLOME IN RESPONSE TO  
INFESTATION BY SIREX NOCTILIO F.**



Tesis para optar al grado de Doctor en Ciencias y Tecnología Analítica

por

**SEBASTIÁN ANDRES RIQUELME RIFO**

Profesor Guía: Dr. Andy Jorge Pérez de Armas  
Profesor Co-Guía: Dr. Oliver Fiehn

Diciembre, 2022.  
Concepción, Chile.

© The total or partial reproduction, for academic purposes, by any means or procedure, including the bibliographic citation of the document, is authorized.



## Acknowledgement

I want to thank conicyt (ANID) for funding my education and the work reported in this thesis. Specially to the project ANID/CONICYT Fondecyt Regular 1181915 and Conicyt doctoral scholarship N°: 21161407”

I thank Professor Oliver Fiehn (UC Davis) and his staff for providing me access to novel techniques and metabolomics equipment; I appreciate the invaluable opportunity he gave me.



# Table of Contents

ACKNOWLEDGEMENT .....	III
TABLE OF CONTENTS .....	IV
LIST OF TABLES.....	VIII
LIST OF FIGURES .....	IX
ABSTRACT .....	XIX
<b>1. CHAPTER N°1 .....</b>	<b>21</b>
1. INTRODUCTION .....	22
1.1 Conifers Forest in the world.....	22
1.2 The forest industry in Chile .....	23
1.3 <i>Sirex noctilio</i> in Chile.....	25
1.4 <i>Sirex noctilio</i> worldwide spreading.....	28
1.5 <i>Sirex noctilio</i> biology and life cycle .....	29
1.6 <i>S. nocitilio</i> and <i>A. areolatum</i> pathosystem.....	33
1.7 <i>Sirex</i> venom and initial symptoms of infection in <i>P. radiata</i> trees.....	35
2. STATE OF THE ART.....	38
2.1 Strategies for control of <i>S. noctilio</i> .....	38
2.2 Biological control of <i>S. noctilio</i> in Chile.....	39
2.3 Plant Metabolomics.....	42
2.4 Plant Lipidomics.....	45
2.5 Metabolomics in pine-stress interaction .....	50
3. HYPOTHESIS AND OBJECTIVES .....	53
3.1 Hypothesis .....	53
3.2 Objectives .....	53
4. RESEARCH STRATEGY .....	55
5. METHODOLOGIES .....	57

5.1	<i>Plant material</i> .....	57
5.2	<i>Extraction of metabolome and lipidome</i> .....	58
5.3	<i>LC-MS analysis for metabolomics</i> .....	59
5.4	<i>LC-MS analysis for lipidomics</i> .....	61
5.5	<i>Data analysis, statistical treatment and annotation</i> .....	63
6.	REFERENCES.....	66
<b>2.</b>	<b>CHAPTER N°2</b> .....	<b>75</b>
1.	GRAPHICAL ABSTRACT .....	76
2.	ABSTRACT .....	78
3.	INTRODUCTION .....	80
4.	RESULTS .....	84
4.1	<i>Initial metabolome changes in <i>P. radiata</i> as a response to <i>S. noctilio</i> infestation</i> .....	84
4.2	<i>Biomarker model evaluation for early diagnosis of infestation</i> .....	89
4.3	<i>Long-term metabolome changes</i> .....	92
5.	DISCUSSION .....	97
6.	CONCLUSIONS.....	112
7.	EXPERIMENTAL .....	114
7.1	<i>General experimental procedures</i> .....	114
7.2	<i>Origin of plant material and sampling.</i> .....	115
7.3	<i>Sample preparation and metabolome extraction.</i> .....	117
7.4	<i>LC-MS metabolomics analysis.</i> .....	118
7.5	<i>Data processing and statistics.</i> .....	120
7.6	<i>Biomarker model evaluation.</i> .....	121
7.7	<i>Metabolite annotation.</i> .....	122
8.	ACKNOWLEDGMENTS.....	125
9.	DATA AVAILABILITY STATEMENT .....	125

8	REFERENCES.....	131
9	SUPPORTING INFORMATION .....	138
<b>3.</b>	<b>CHAPTER N°3 .....</b>	<b>157</b>
1.	SUMMARY .....	159
2.	INTRODUCTION .....	161
3.	EXPERIMENTAL PROCEDURES.....	165
3.1	<i>Origin of plant material and collection.....</i>	<i>165</i>
3.2	<i>Sample preparation and lipidome extraction .....</i>	<i>166</i>
3.3	<i>LC-MS lipidomics analysis .....</i>	<i>167</i>
3.4	<i>Data processing and statistics .....</i>	<i>168</i>
4.	RESULTS .....	171
4.1	<i>Lipids profile in P. radiata needles under S. noctilio infestation .....</i>	<i>171</i>
4.2	<i>Statistical models of P. radiata trees upon infestation by S. noctilio.....</i>	<i>171</i>
4.3	<i>The Early effect of S. noctilio infestation in lipids of P. radiata trees .....</i>	<i>175</i>
4.4	<i>The prolonged effect of S. noctilio infestation in lipids of P. radiata trees .....</i>	<i>177</i>
5.	DISCUSSION .....	179
6.	CONCLUSION .....	186
7.	ACKNOWLEDGMENTS.....	188
8.	SUPPORTING INFORMATION .....	189
9.	REFERENCES.....	202
<b>4.</b>	<b>CHAPTER 4.....</b>	<b>210</b>
1.	CONCLUSION .....	210
1.1	<i>General conclusions.....</i>	<i>210</i>
1.2	<i>Specific conclusions: .....</i>	<i>212</i>
2.	ANEXOS.....	214
1.	RESEARCH PROJECT PARTICIPATION .....	214

2. SCHOLARSHIP.....	215
3. COLLABORATION IN OTHER PUBLICATIONS .....	215
4. PATENTS.....	217



## List of Tables

Table 1-2: Annotation of significant metabolites that changed their levels in <i>P. radiata</i> needles and/or wood during <i>S. noctilio</i> infestation. ....	126
---	-----





## List of Figures

Figure 1-1: The global distribution of all conifer species is represented with black dots. The numbers of genera and taxa (species and infraspecific taxa) were calculated per 10-degree latitude band (From Farjon and Filer 2013). ...23	
Figure 2-1: National <i>S. noctilio</i> distribution map delimited with risk zone in colors (From Sandoval et al., 2018) .....27	
Figure 3-1: <i>S. noctilio</i> female (Extracted from sawflies.org.uk/sirex-noctilio/) .....30	
Figure 4-1: Life cycle of <i>S. noctilio</i> (Image extract from Ryan and Hurley 2011).....32	
Figure 5-1: Analytical strategy for metabolomics and lipidomics analysis .....56	
Figure 6-1: Plant material sampling and pretreatment.....58	
Figure 7-1: Milled samples extraction. ....59	
Figure 8-1: Proposed metabolomics protocol by HPLC-MSMS platform .....61	
Figure 9-1: Proposed lipidomics protocol by HPLC-MSMS platform .63	
Figure 1-2: Metabolomics uncovered the <i>P. radiata</i> response to <i>S. noctilio</i> infestation, highlighting photoprotection and auxin expression as tolerance traits and the oxidative stress causing death.....76	

Figure 2-2: PCA score plots based on the LC-MS dataset showing cluster patterns between the first two principal components (PC1 and PC2). Blue triangles and red diamonds represent samples from HT and IT, respectively, with their 95% confidence interval (shadowed regions). Needles at T1 in –ESI (a) and +ESI (b). Wood at T1 in –ESI (c) and +ESI (d). Needles at T2 in –ESI (e) and +ESI (f). Wood at T2 in –ESI (g) and +ESI (h).....85

Figure 3-2: OPLS-DA model based on LC-MS datasets obtained from *P. radiata* needle leaves collected at T1. Scores plots showing separation of samples labeled as healthy (HT, blue triangles) and infested (IT, red diamonds) trees with their 95% confidence intervals (shadowed regions) for –ESI (a) and +ESI (b) acquisition modes. This is a regression method to find a relationship between data tables represented by X, the LC-MS data, and Y, a binary vector with the value 0 for HT class and 1 for IT class. The Y-predictive component (T score [1]) for variation in the dataset correlated to class separation is shown on the x-axis, while the orthogonal component that refers to uncorrelated variation for class separation is shown on the y-axis. S-plots showing significant features with their numbers assigned according to Table 1-2 for –ESI (c) and +ESI (d), indicating features fragmented in the ion source as “in source”. The S-plots visualize the features’ influence in the predictive component of the model, combining the covariance (p[1]) and correlation (p(corr)[1]) loading

profiles. Covariance plotted on the x-axis visualizes the contribution to the predictive component, while correlation plotted on the y-axis spans between  $\pm 1$  as the reliability has a theoretical minimum of -1 and a maximum of +1 to predict the class 1 (IT). In this way, variables/features visualized toward the right-hand side contribute to class separation by high correlation with label IT [ $Y = 1$ ] and the opposite. Thus, significant metabolites were selected based on the combined high covariance ( $> 2000$ ) and high correlation ( $> 0.5$ ). Quantitative data for significant metabolites are presented in Fig. S4 and S5.

.....87

Figure 4-2: ROC curve-based model to assess biomarker quality for a set of 21 metabolites up-regulated in *P. radiata* needles after initial infestation by *S. noctilio* at T1. ROC curve plot for the created biomarker model showing on the x-axis the highest possible specificity (false-positive rate) and the y-axis the highest sensitivity (true-positive rate) with the 95% of confidence interval, contributing to the maximum area under the curve,  $AUC = 1$  **(a)**. Plot of predicted class probabilities for each sample using the created biomarker model showing classification boundary at the center ( $x = 0.5$ ) and a perfect separation between HT (white circles) and IT (black circles) samples **(b)**. Permutation test for model validation presented as a histogram using the predictive accuracy of the model as a measure of performance, showing the AUC distribution for all

permutations (in blue) and the distribution for the original model (red arrow), along with the empirical p-value (c). ..... 90

Figure 5-2 : OPLS-DA models based on LC-MS datasets obtained from wood of *P. radiata* at T2. Scores plots showing separation of samples labeled as healthy (HT, blue triangles) and infested (IT, red diamonds) trees with their 95% confidence intervals (shadowed regions) for -ESI (a) and +ESI (b) acquisition modes. The Y-predictive component (T score [1]) for variation in the dataset correlated to class separation is shown on the x-axis, while the orthogonal component that refers to uncorrelated variation for class separation is shown on the y-axis. S-plots showing significant features with their numbers assigned according to Table 1-2 for -ESI (c) and +ESI (d), indicating atypical adduct ions and features fragmented in the ion source as “in source”. The S-plots visualize the features’ influence in the predictive component of the model, combining the covariance (p[1]) and correlation (p(corr)[1]) loading profiles. Covariance plotted on the x-axis visualizes the contribution to the predictive component, while correlation plotted on the y-axis spans between  $\pm 1$  as the reliability has a theoretical minimum of -1 and a maximum of +1 to predict the class 1 (IT). In this way, variables/features visualized toward the right-hand side contribute to class separation by high correlation with label IT [Y = 1] and the opposite. Thus, significant metabolites were selected based on the combined

high covariance set at 1500 and 200 for -ESI and +ESI, respectively, and high correlation ( $> 0.5$ ). Quantitative data for significant metabolites are presented from Fig. S8-2. ....94

Figure 6-2: OPLS-DA models based on LC-MS datasets obtained from needles of *P. radiata* at T2. Scores plots showing separation of samples labeled as healthy (HT, blue triangles) and infested (IT, red diamonds) trees with their 95% confidence intervals (shadowed regions) for -ESI (a) and +ESI (b) acquisition modes. The Y-predictive component (T score [1]) for variation in the dataset correlated to class separation is shown on the x-axis, while the orthogonal component that refers to uncorrelated variation for class separation is shown on the y-axis. S-plots showing significant features with their numbers assigned according to Table 1-2 for -ESI (c) and +ESI (d), indicating atypical adduct ions and features fragmented in the ion source as “in source”. The S-plots visualize the features’ influence in the predictive component of the model, combining the covariance ( $p[1]$ ) and correlation ( $p(\text{corr})[1]$ ) loading profiles. Covariance plotted on the x-axis visualizes the contribution to the predictive component, while correlation plotted on the y-axis spans between  $\pm 1$  as the reliability has a theoretical minimum of -1 and a maximum of +1 to predict the class 1 (IT). In this way, variables/features visualized toward the right-hand side contribute to class separation by high correlation with label IT [ $Y = 1$ ] and the

opposite. Thus, significant metabolites were selected based on the combined high covariance (> 2000) and high correlation (> 0.5). Quantitative data for significant metabolites are presented from Fig. S6-2 and S7-2.....96

Figure 7-2: Scheme for the pathway analysis of changes systemically induced in the metabolome of *P. radiata* needles immediately after infestation by *S. noctilio*. Metabolite nodes are shown as rectangles with annotated names and assigned numbers where available. Colour set-1 refers to expression data according to  $\log_2FC$ , where  $FC = ITHT$ , and  $ITHT$  is the average intensity ratio for the metabolite, and with the scale adjusted between -3 and 3 for ease of interpretation. Colour set-2 shows statistical significance in a t-test, where white indicates significant ( $p < 0.001$ ) and yellow not significant ( $p > 0.001$ ). Metabolites filled in grey were not detected. Enzymes involved in specific transformations are shown as rounded rectangles, labeled, if possible, with their KEEG Ortholog number (KO). Downstream transformation pathways are shown as rounded grey rectangles. Dashed lines indicate known metabolic pathways containing several conversion steps or proposed ones. .... 100

Figure S1-2: Original photos of *P. radiata* trees from the sampling place, showing the visual symptoms of infestation by *S. noctilio*. The black arrow shows a hole drilled by a female woodwasp in the act of oviposition (a). Oleoresin exudation as droplets in drilling sites of a tree being under attack (b).

Wilting and chlorotic needles in the whole foliage **(c)** and in the crown **(d)** of two infested trees. Holes left in the trunk of an already dead tree by the emergence of woodwasp adults approximately after a year from the oviposition **(e)**. ..... 140

Figure S2-2 Validation of OPLS-DA models based on LC-MS dataset by random permutation test of class membership with 1000 permutations, showing the observed and cross-validated  $R^2Y$  and  $Q^2$  coefficients for needles at T1 in –ESI **(a)** and +ESI **(b)**, for wood at T2 in –ESI **(c)** and +ESI **(d)**, and for needles at T2 in –ESI **(e)** and +ESI **(f)**. ..... 141

Figure S3-2: ROC curves obtained for each individual metabolite up-regulated **(a)** and down-regulated **(b)** in needles at T1, sorted in descending order of their AUC value..... 142

Figure S4-2: Quantitative data for metabolites significantly overexpressed in the needles of *P. radiata* infested trees at T1. Per each compound, box-and-whisker plots on the left show the original values of peak intensities in healthy (HT, blue) and infested trees (IT, red). The plots on the right summarize the normalized values. In each box plot, black dots represent the actual concentration (intensity) of the given metabolite in each analysed sample, the notch indicates the 95% confidence interval around the median of

each group, and the yellow diamond indicates the mean concentration of each group.....144

Figure S5-2: Quantitative data for metabolites significantly suppressed in the needles of *P. radiata* infested trees at T1. Per each compound, box-and-whisker plots on the left show the original values of peak intensities in healthy (HT, blue) and infested trees (IT, red). The plots on the right summarize the normalized values. In each box plot, black dots represent the actual concentration (intensity) of the given metabolite in each analysed sample, the notch indicates the 95% confidence interval around the median of each group, and the yellow diamond indicates the mean concentration of each group. ...146

Figure S6-2: Quantitative data for metabolites significantly overexpressed in the needles of *P. radiata* infested trees at T2. Per each compound, box-and-whisker plots on the left show the original values of peak intensities in healthy (HT, blue) and infested trees (IT, red). The plots on the right summarize the normalized values. ....148

Figure S7-2: Quantitative data for metabolites significantly suppressed in the needles of *P. radiata* infested trees at T2. Per each compound, box-and-whisker plots on the left show the original values of peak intensities in healthy (HT, blue) and infested trees (IT, red). The plots on the right summarize the normalized values.....149



Figure S8-2: Quantitative data for metabolites significantly up and down-regulated in wood of *P. radiata* infested trees at T2. Per each compound, box-and-whisker plots on the left show the original values of peak intensities in healthy (HT, blue) and infested trees (IT, red). The plots on the right summarize the normalized values..... 150

Figure S9-2: Quantitative data for the metabolite Pinosylvin found not significantly changed in the wood of *P. radiata* trees at T2. Box-and-whisker plots on the left show the original values of peak intensities in healthy (HT, blue) and infested trees (IT, red). The plots on the right summarize the normalized values..... 151

Figure 1-3: Score plot of OPLS-DA models based on combined datasets (+) ESI and (-) ESI among healthy trees (HT, green circles) and infested (IT, red circles), with their 95% confidence regions for (a) T1 (sampling 1) and (b) T2 (sampling 2). Graphics of OPLS-DA predictive model performance by (c) cross-validation, and (d) permutation with 1000 random permutation tests of class membership for T1 and (e) and (f) T2 respectively. .... 174

Figure 2-3: Volcano plot of IT vs HT in T1 from using Fold Change (FC) analysis and T-tests to select significant features based on biological significance and statistical significance of features present in *P. radiata* needles under *S. noctilio* infestation (a) and whisker and box plot of the first 9

significant feature related with IT plotted by decreasing magnitude order **(b)**.  
(Suggested 2-column fitting image)..... 176

Figure 3-3: Volcano plot of IT vs HT in T2 from using Fold Change (FC) analysis and T-tests to select significant features based on biological significance and statistical significance of features present in *P. radiata* needles under *S. noctilio* infestation **(a)** and whisker and box plot of the first 9 significant feature related with IT plotted by decreasing magnitude order **(b)**.  
..... 178



## ABSTRACT

The production of renewable resources in forest plantations is one of Chile's most important industrial activities since it serves as the basis for essential primary industries such as wood, boards, pulp and chips.

Consistent with the global trend, our country's most extensive commercial plantations are monoculture forests, with *Pinus radiata* as the predominant planted species. Plantations of the species account for more than fifty per cent of the commercial plantations registered by 2021.

Productivity and long-term viability of the forest economic sector in Chile, based on *P. radiata* plantations, are constantly threatened by droughts, fires, and disease outbreaks caused by exotic pests. Among these harmful pests, the insect *Sirex noctilio* (*S. noctilio*) may cause significant economic losses because it can kill trees quickly after just one infestation.

The primary focus of scientific research regarding *S. noctilio* has been its symbiotic relationship with the fungus *Amylostereum areolatum* and the composition and physiological effects of the venom injected during oviposition. However, no studies have been published describing the biochemical processes triggered in the plant during infection.

It is so far unknown the resistance and tolerance traits induced in *Pinus radiata* metabolome after *S. noctilio* infestation. Therefore, in the present thesis,

we report the usefulness of LC-MS-based untargeted metabolomics for uncovering the systemic metabolome changes in needles (leaves) and wood of 14-year-old *P. radiata* trees in response to initial and long-term *S. noctilio* infestation. Needles suffered severe consequences from the chlorosis degrading photosystems after infestation. Photoprotection was immediately induced via up-regulation of catechin and procyanidin B1. Also, proline serves as an alternative substrate for respiration. In addition, extraordinary oxidative stress was also registered by an acute decrease in ascorbate levels (90-fold). Detoxification of venom toxin (noctilisin) via conjugation with glutathione (dropped by 17-fold) was hypothesized preceding the inevitable premature senescence observed within infested trees. Nonetheless, significant overexpression of auxins was detected, suggesting the activation of a tolerance mechanism. Finally, we evidenced that metabolomics accurately revealed the biochemical response of trees to the woodwasp infestation, indicating, in addition, the upstream molecular functions involved in the biochemical processes, as well as potentially new research and breeding targets.

## 1. CHAPTER N°1

**“A Novel Metabolomics Approach as Integrative Strategy for Understanding Changes in *Pinus Radiata* D.Don Metabolome in Response to Infestation by *Sirex Noctilio*”**



## 1. INTRODUCTION

### 1.1 Conifers Forest in the world

Conifers are considered living fossils. Their forests have proliferated for more than 200 million years, with a natural lifespan of several hundred years in some species (Hao et al., 2015a). The lineage and longevity of conifers have been usually attributed to their ability to resist biotic stresses caused by pathogens, insects, and herbivorous, depending on plant systemic or localized physiological and biochemical responses (Ralph et al., 2006a; Warren et al., 2015a; Celedon & Bohlmann, 2019a; Whitehill et al., 2019a) as well as their ability to resist abiotic stress such as drought, high temperatures, and ultraviolet radiation exposure (de Miguel et al., 2016; de Simón et al., 2017; Escandón et al., 2018). Conifers also established a long-aged symbiotic relationship with fungi forming ectomycorrhizal systems, which extend the surface area for water and nutrient uptake. In disturbance cycles, they are the first to spread seed on the new soil, taking advance of the most angiosperm (Farjon, 2018).

The global distribution of conifers occurs in several habitats covering five continents (see Figure 1-1). They can resist several altitude ranges, covering from the sea level up to 5000 m in the Himalayas, and are predominant in climates under suboptimal conditions for plant growth (Farjon Aljos & Filer Denis, 2013).



Figure 1-1: The global distribution of all conifer species is represented with black dots. The numbers of genera and taxa (species and infraspecific taxa) were calculated per 10-degree latitude band (From Farjon and Filer 2013).

From an economic point of view, conifers are one of the most important forest species, providing about 50% of the annual wood production worldwide (Eckenwalder, 2018a). *Pinus radiata* D. Don is the conifer species most extensively planted worldwide, covering around 4.2 million hectares of plantations (Mead, 2013a). The largest planted areas of this species are currently held by Chile, New Zealand, and Australia, with 1.5, 1.3, and 0.7 million ha, respectively (Forestry Corporation, 2016a; Clough et al., 2019a; Gysling Caselli et al., 2019).

## 1.2 The forest industry in Chile

According to the most recent report of the Chilean Statistical Yearbook of Forestry 2021, despite the global health emergency of Covid-19 and its

socioeconomic effects, the forest industry contributed 2.3% to the national gross domestic products, and the forestry exportations accounted for USD 4.948 million FOB. Commercial forest plantations in Chile were 2.321.257 ha, 56% corresponding to *P. radiata* D. Don (Pinaceae) (Soto Aguirre *et al.*, 2021).

This species was introduced in Chile in 1893, with the first plantation of about 10 ha near Concepcion (Mead, 2013). Current *P. radiata* plantations are mainly distributed within three regions, including Biobío (339.254 ha), Araucanía (245.783 ha), and Maule (356.544 ha), with 72% of the total planted area of the country (Soto Aguirre *et al.*, 2021). The forest industry has provided raw materials for several other national initiatives, such as sawing, chipping, pulp, boards, and sheets, as well as posts and poles, consuming more than 43 million m<sup>3</sup> of wood in logs per year (Gysling & Bañados, 2017; Soto Aguirre *et al.*, 2021). An essential part of that volume, 30 million m<sup>3</sup> approx., exclusively belongs to *P. radiata* species (Gysling *et al.*, 2017). Despite the severe contraction of the global economy in 2020 and, consequently, national economy contraction by 5.8%, the forest sector only decreased by 2.7%. The Chilean Forest Industry employed more than 112 thousand people in 2020, with a positive social impact performance regardless of pandemic restrictions (Soto Aguirre *et al.*, 2021).



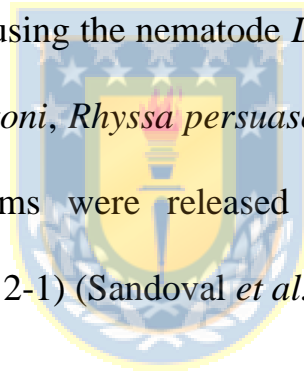
Despite its permanent growth and importance to the country, forestry activity is not exempt from difficulties that negatively affect its development, such as fires, droughts, and plagues. Despite a century of research and management programs, *Sirex noctilio* Fabricius (Hymenoptera: Siricidae) remains one of the most destructive pests for *P. radiata* plantations, spreading continuously to new geographical areas (Slippers et al., 2015a).

### **1.3 *Sirex noctilio* in Chile**

During the 1980s, *S. noctilio* was first detected in Argentina, Uruguay, and Brazil, driven to programs for its earlier detection in South America. The early detection program for *S. noctilio* was implemented in our country in 1990. The surveillance program was done by a joint effort between the Agricultural and Livestock Service (SAG) and the leading forestry companies present in the country. The strategy focused on funnel lure traps with pine volatiles for *S. noctilio* adult detection, based on the International Standards for Phytosanitary Measurements (ISPM) No. 6 (IPPC/FAO, 2016).

The first record in Chile of *S. noctilio* detection was reported in February 2001 in Guardia Vieja, Valparaíso. Such detection was associated with large quantities of equipment packed in wood, possibly infested, imported from Europe by a hydroelectric power plant near the town. At the same time, the possible migrations of immature individuals from Argentina could contribute to

the proliferation of the plague in our country (Beèche, 2012). In the same year, specimens were found in the provinces of Llanquihue and Osorno (Los Lagos region). A year later, woodwasp was also reported in Temuco (Araucanía), which led to declaring a mandatory control in Chile of this pest. In 2006, SAG implemented a program for the biological control and quarantine zones, registering the protocols in Resolution No. 5366/06. These measures aimed to decrease the country's pest population and mitigate the negative impact on *P. radiata* plantations and wood exports and products. The strategy was mainly based on biological control using the nematode *Deladenus siricidicola* and the parasitoids *Megarbyssa nortoni*, *Rhyssa persuasoria*, and *Ibalia leucospoides*. Biological control organisms were released within the high-risk areas demarcated by SAG (Figure 2-1) (Sandoval *et al.*, 2018).



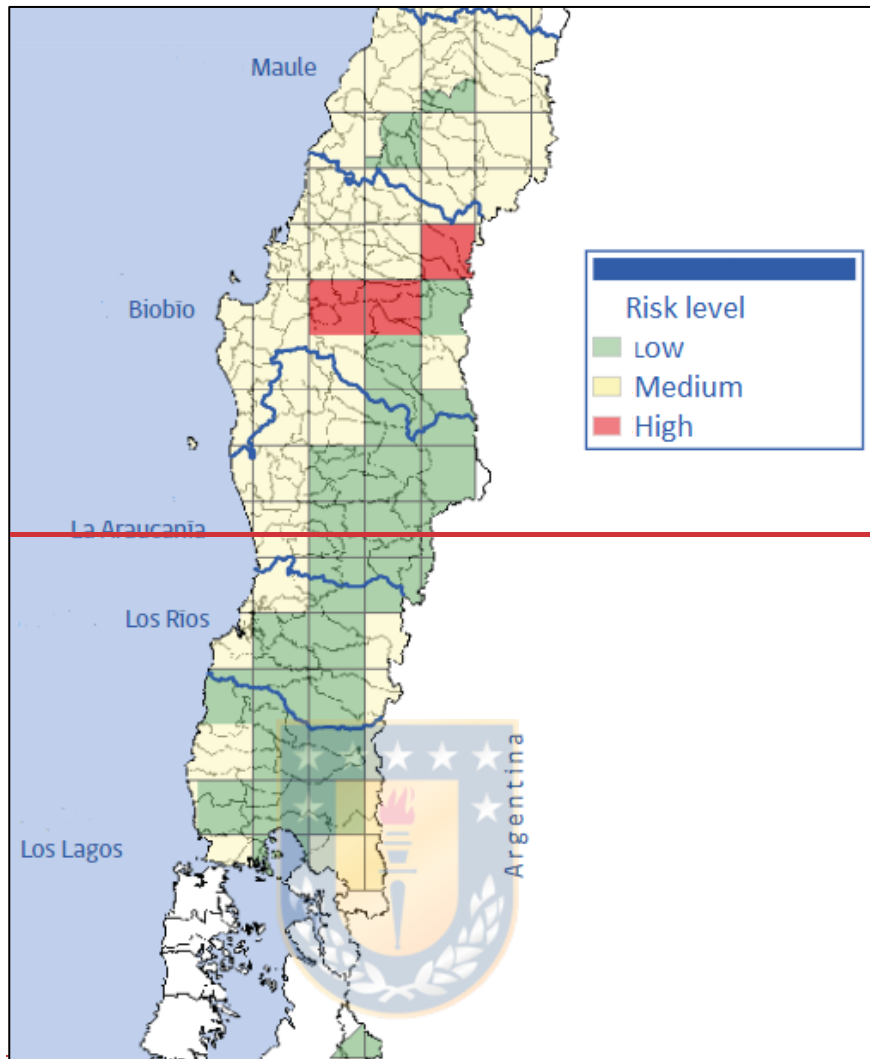


*Figure 2-1: National S. noctilio distribution map delimited with risk zone in colours (From Sandoval et al., 2018)*

The SAG program also included a binational plan in collaboration with Argentina to reduce insect population levels in the adjacent high-risk Andean-Patagonian locations (Beèche, 2012).

#### 1.4 *Sirex noctilio* worldwide spreading

The spread of *Sirex noctilio* Fabricius (Hymenoptera: Siricidae, *Sirex*) has occurred repeatedly and from multiple sources. The insect is endemic to Eurasia and North Africa. In various regions of the world, such as Australia and the United States of America, it is considered an invasive species within the top 10 most serious forest pests (Wang et al., 2016). It represents a significant threat to unaffected *Pinus* spp. plantation in Africa, Australia, South America, and Asia (Slippers et al., 2015a). Adults *S. noctilio* are powerful fliers, spreading around 25-50 km per year in Australia (Haugen *et al.*, 1990), being the only woodwasp species known to kill trees, especially in those regions where it has been accidentally introduced (Ryan & Hurley, 2012a). Consequently, it has colonized all continents where it has been accidentally introduced, except for Antarctica (Sun *et al.*, 2020). In contrast, the woodwasp attacks only weakened or recently dead trees in endemic geographic areas (Spradbery & Kirk, 1978b).

Several outbreaks of *S. noctilio* have also been reported worldwide, but the most devastating occurred in New Zealand between 1946 and 1951, causing the loss of 120.000 ha of forest (Mead, 2013b). Short-term periods of physiological stress in pine trees appear sufficient for attracting *S. noctilio*. Stressors may involve damages caused by wind or felling operations, defoliation, herbicides application, fires, cone harvesting, thinning, or droughts,

mainly when they take place during the *S. noctilio* flight season (Madden, 1988). Even though such significant *S. noctilio* outbreaks have not occurred for decades, the USDA Forest Service estimated a cost between \$2.8 and \$17 billion in losses if it became a nationwide established pest in the USA (New York Invasive Species Information, 2019a).

### **1.5 *Sirex noctilio* biology and life cycle**

*S. noctilio* has a cryptic lifestyle and spent most of its life cycle as a larva within its host's sapwood. The life cycle starts with a larval stage, usually between 1 and 3 years, but in most regions, the emergence occurs after the first year (Ryan & Hurley, 2012a). Adults (see Figure 3-1) emerge from early or mid-summer until autumn (December to March in Chile). Such a period is commonly named “flight season”.

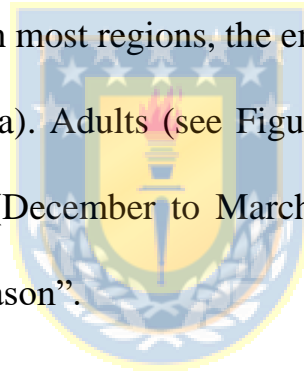




*Figure 3-1: S. noctilio female (Extracted from sawflies.org.uk/sirex-noctilio/)*

In this period, mature females locate a tree host for oviposition after mating or in the absence of mating. The female *Sirex* roves the surface of the pine bark, testing the sapwood with its antennae and inspecting for the possible host for oviposition, which is finally done in the phloem (Madden, 1988). When the female finds a proper host, she begins depositing eggs from the bottom to the top of the tree, drilling single, double, triple, or quadruple sets of oviposition chambers every 7.5-50 cm along the stem. However, the eggs are only placed in conditions that maximize the larvae's survival rate. Thereby, numerous holes are drilled during the initial phases of the Sirex strike (Approximately 19 mm deep), but only a few have eggs. Instead, *Amylostereum areolatum* (*A. areolatum*) arthrospores and *S. noctilio* mucus (phytotoxic substance) are inoculated into each drilled hole, contributing to stress the host tree (Ryan &

Hurley, 2012a). Sometimes, a single hole is drilled in each tree when conditions are not optimal, which stresses the tree and makes it susceptible to future attacks(Madden, 1988; Ryan & Hurley, 2012a). Finally, the eggs hatch within 15-28 days, originating the larvae that begin to feed through the wood infected by fungi, creating galleries into the wood. The life cycle of *S. noctilio* is graphically summarized in Figure 4-1.



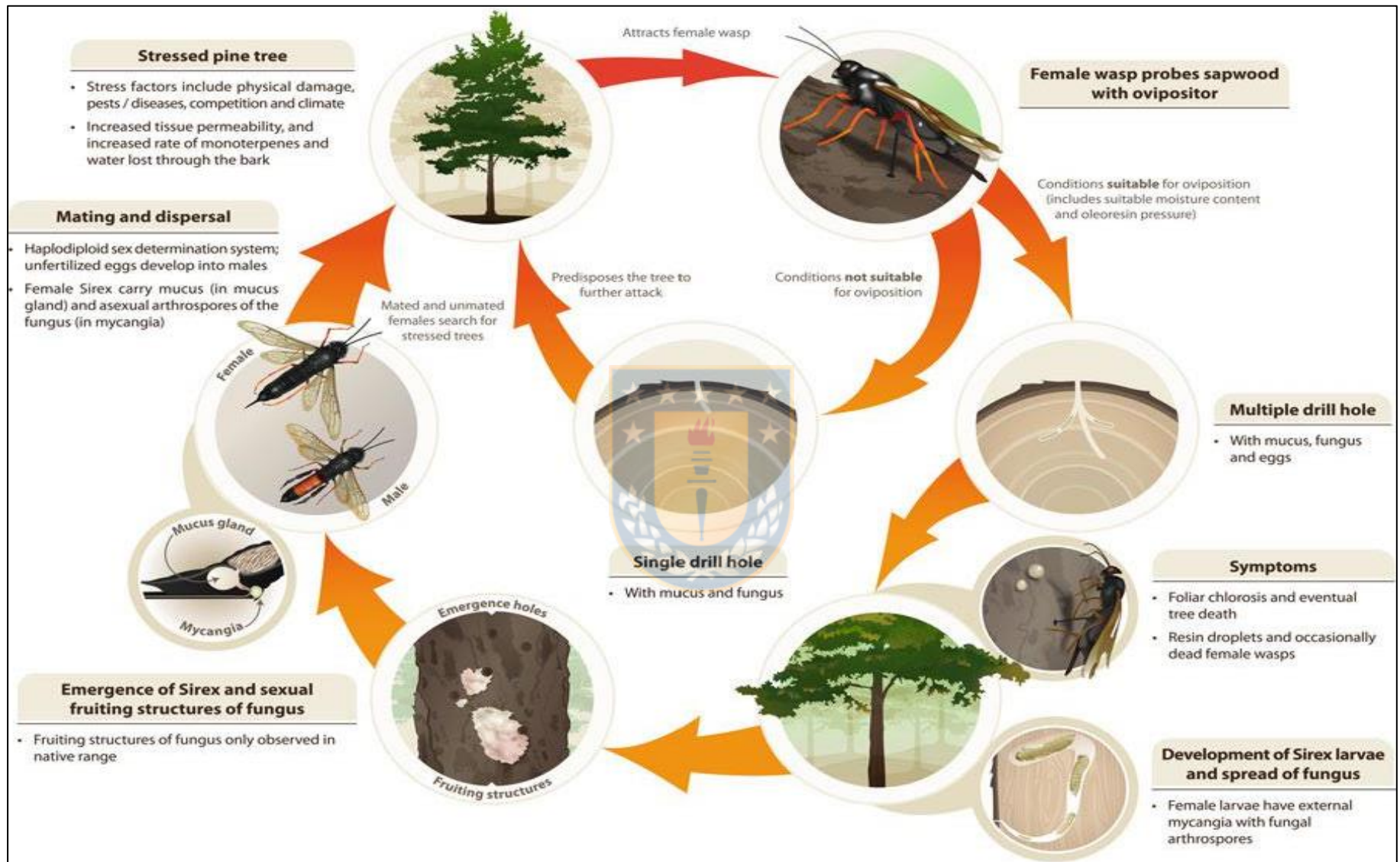


Figure 4-1: Life cycle of *S. noctilio* (Image extract from Ryan and Hurley 2011)



It is well recognized that the most robust trees, without mechanical or other damage, are typically more resistant to *S. noctilio* infestation. Some authors have categorized such resistance as non-preference, antibiosis, and tolerance. The first occurs when an initially appealing tree becomes unsightly upon closer scrutiny. Antibiosis requires filling oviposition holes with resin, which kills *S. noctilio* eggs and *A. areolatum*, together with a polyphenolic barrier for isolating *A. areolatum* growth. Tolerance inhibits mucus, lowering transpiration and precipitating the premature senescence of afflicted needles (Madden, 1988).

### **1.6 *S. noctilio* and *A. areolatum* pathosystem**

In general, insects can use a flexible symbiosis with fungus to achievement nutrients from a hostile food source. Exposure to new symbionts may increase the likelihood of symbiont shifts. Genus *Sirex* obligates nutritional ectosymbioses with white fungi in the genus *Amylostereum*. The flexibility of the association could provide *Siricidae*s using resources with the ability to thrive under a variety of conditions (Hajek *et al.*, 2013). *A. areolatum* is the primary symbiont of *S. noctilio* worldwide. The first report of its relationships was in New Zealand around 1900, Tasmania in the 1950s, Australia in 1960, South America in the 1980s and Africa in the 1990s (Hurley *et al.*, 2007). The insect predominantly spreads the fungus in the asexually produced oidia

(=asthrospores). The female *S. noctilio* emerges from trees carrying *A. areolatum* in mycangia, a specialized organ in animals designed for transporting fungus symbionts, located at the anterior end part end of the female body (Slippers *et al.*, 2003). In addition to the ovipositing egg, the fungus is inoculated into the sapwood of the host tree through a secondary bore. When the adult insect incorporates the fungus into the mycangia when she sheds her pupal skin, a continuing link with the fungus is created (Slippers *et al.*, 2012). Sirex larvae may obtain nutrients by eating the rotten wood or directly from the fungus (Wermelinger & Thomsen, 2012). The fungus supplies enzymes that aid in the digestion of the xylem. Sirex larvae acquire enzymes (cellulases and xylanases) after swallowing *A. areolatum* tissue produced in the wood where the larvae feed. These enzymes allow the larvae to exploit significant fungal and plant polysaccharides in their meal (Kukor & Martin, 1983). *Amylostereum spp.* is a weak parasite, and numerous trees resist its attack. The fungus was not responsible for any systemic toxicity, and a small number of fungal infestations did not affect the tree (Coutts, 1969a).

The plan or mere coincidence of the organized symbiote attack is the insect's injection of toxic mucus, which weakens the tree's defences and facilitates the subsequent fungus colonization.

### **1.7 *Sirex* venom and initial symptoms of infection in *P. radiata* trees**

Multiple recovery findings in trees inoculated exclusively with *A. areolatum* indicate that the fungus would fail as a pathogen (Coutts, 1969b; Bordeaux *et al.*, 2012).

Female *Sirex* has paired glands in the abdomen that secrete colourless mucus (*S. noctilio* venom). Mucus reservoirs contain between 10 and 25 mg of mucus, depending on the insect size (Coutts, 1969c). The simultaneously inoculated venom by *S. noctilio* alters tree physiology and defence responses, allowing the fungus infection, eventually overwhelming the tree (Bordeaux & Dean, 2012a). The published proteome analysis of *S. noctilio* mucus reveals that it is composed of a complex mixture of proteins and peptides. Several of these proteins were discovered as potential poisons, including noctilisin (venom glycopeptide of *S. noctilio*). Also, proteins such as acph-1 (venom acid phosphatase), ADAMTS (disintegrin and metalloproteinase with thrombospondin), VSPs (venom serine proteases), and MANF (mesencephalic astrocyte-derived neurotrophic factor) were described. In addition, the presence of chemosensory binding proteins belonging to the three families identified in hexapods insects, such as OBPs (odorant-binding proteins), CSPs (chemosensory proteins), and NPC2 (Niemann-Pick type C2 proteins), were

also detected, suggesting a possible sensorial requirement for host tree selection (Wang et al., 2016c).

Forty days after oviposition, needles in the top of the tree begin to bend at the fascicle sheath and subsequently turn yellow and wilt (chlorosis), signifying the onset of the first apparent signs of infection (Fong & Crowdent, 1973a). Other early responses of trees include increased stem respiration, decreased photosynthate transport from photosynthetic tissues, and streaming of resin at the oviposition site (Bordeaux et al., 2014a). These early symptoms have been attributed to the *S. noctilio* mucus since they occur before egg hatching or significant fungus growth (Coutts, 1969b). Artificial injection of the mucus into the tree induces premature senescence only in the older needles, and the venom alone can kill the trees (Fong & Crowdent, 1973a). Also, mucus triggers a starch accumulation in the tree needles and affects the translocation in the sink organs for the photosynthate in the stem (Coutts, 1969b).

Other physiological responses include the appearance of darkly stained necrotic lesions in the cambium upon removal of the bark above the oviposition holes. Commonly, there are vertically elongated, lens-shaped, reddish-brown discolourations on the wood surrounding the oviposition site (Bordeaux *et al.*, 2012). Typically, this event has been linked to the accumulation of polyphenolic compounds due to the activation of the phenylpropanoid pathway in response

to a fungal pathogen infestation (Madden, 1988). However, it may also be associated with a polyphenol oxidase activity of woodwasp mucus (Bordeaux *et al.*, 2012). However, mucus has a physiological effect on trees, weakening them and fostering the growth of fungi. By reversing the sap flow, fungus colonization in the sapwood's prolonged infestation stage leads to the tree's death (Coutts, 1969c).



## 2. STATE OF THE ART

### 2.1 Strategies for control of *S. noctilio*

Research about Sirex woodwasp in *P. radiata* plantations has focused on the insect's biology and biochemistry and the parasitic organisms used for its biological control. However, apart from volatile profiles in the stem, very little is known about the phytochemistry of the tree during an infestation by *S. noctilio*. Slippers and colleagues (2015a) addressed this concern in assessing the most critical features of this invasive forest pest control (Slippers et al., 2015a). Another relevant aspect for the future of resistance breeding programs is the recognition that the defence mechanisms presented by specific individuals are linked to their genetic basis (Bordeaux *et al.*, 2012).

Control measures for *S. noctilio* are being developed, such as new traps based on a genetic analysis undermining the symbiotic relationship between *A. areolatum* and *S. noctilio*. The research indicates that clusters of sesquiterpene synthase genes are present in fungi. *A. areolatum* volatile components attracted female woodwasps more than those of the plant hosts. Authors suggest that sesquiterpene molecules could play a role in the host selection process (Fu *et al.*, 2020).

On the other hand, new study evidence the potential of the incidental fungi in pinus trees as a biological control for *S. noctilio*, sample logs inoculated

with *Ophiostoma minus* (Hedgc.) Sydow *Phlebiopsis gigantea* (Fr.) Jülich, *Trichoderma atroviride* Bissett, *Trichoderma viride* Pers, and *Trichoderma harzianum* Rifai larval mortality was significantly increased. Inoculation of logs with *Ophiostoma minus* resulted in the most significant mortality and wood moisture content reductions. These fungi grew faster than *A. areospermum* mycelium on artificial media and inhibited its growth. The detrimental effects of incidental fungi on the survival of *S. noctilio* larvae are at least partially caused by an indirect mechanism involving the inhibition of the fungal symbiont. Mongolian pine is colonized by native bark beetles *I. sexdentatus* and *I. acuminatus*. They can spread their associated blue-stain fungus *Ophiostoma minus* creating competition for resources with Sirex. *Ophiostoma minus* can block water flow in the xylem, reducing wood moisture and making the habitat inhospitable for *S. noctilio* larvae (Wang *et al.*, 2020).

## **2.2 Biological control of *S. noctilio* in Chile**

The biological control programs focus on suppressing the pest with the parasitic nematode *Deladenus* (= *Beddingia*) *siricidicola*, insect parasitoids *Ibalia leucospoides*, *Megarhyssa nortoni* and *Rhyssa persuasoria* (Beèche, 2012). The nematode *D. siricidicola* is considered the cornerstone of *S. noctilio* biological control programs across the Southern Hemisphere (Bedding & Iede, 2005). The nematode sterilizes the female of *S. noctilio*, although it does not

affect oviposition and is consequently spread by the female woodwasp through infected eggs (Slippers *et al.*, 2012). However, *S. noctilio* is adaptable to all climatic regions it has encountered, including mediterranean climates like its origin in Europe and Africa. It covers cool to warm temperate semi-tropical areas. Unfortunately, *D. siricidicola* has not adapted to every environment equally well (Hurley *et al.*, 2007; Slippers & Wingfield, 2012). The adaptability lacks causes significant variation in its efficacy across regions, with parasitism rates ranging from 5% to >99% (Slipper *et al.* 2012a). This appears to have a similar effect on the biological control in Chile, as the distribution of parasitism levels observed in *S. noctilio* in 2009 was irregular, absent in some areas and reaching nearly 80 per cent in others. In the Biobío Region, the parasitism rate in female *S. noctilio* was almost 11.5 per cent and in males, 12.0 per cent, while in the Los Ríos and Los Lagos regions, it was over 85 per cent (Beèche, 2012). Another factor that can impact the response could be attributable to the significantly higher woodwasp population in Biobío compared to other regions or perhaps because pest biological control was first implemented in Araucanía, Los Ríos and Los Lagos Regions.

However, the latest field research carried out between 2015 and 2018 on long-term inoculation with *D. siricidicola* in our country established similar levels in three with different geographic conditions, pre Andean sites, the



Central Valley and the Nahuelbuta mountain range in the Biobío region (a region with a high incidence of *S. noctilio*). The reduction of *S. noctilio* populations and the associated decrease in *P. radiata* infestation after parasitism by the nematode *D. siricidicola* for three years reached 90% in all localities, demonstrating that control is feasible to implement if long periods of inoculation are considered (Castillo, et al. 2018).

From another point of view, the investigations developed in Chile, researcher at the Instituto de Investigaciones Agropecuarias (INIA) (Ceballos, 2015) focus on the “on-site” volatiles components in stems of attacked, artificially weakened (by herbicide injection), and healthy *P. radiata* trees. The objective was to establish an early warning system for detecting *S. noctilio* woodwasps, attracting the insects into lure-baited traps with a mixture of volatiles compounds. Their results show that the detected volatiles profile matches those previously reported in the literature (Simpson, 1976). However, in areas with a low woodwasp population, the utility of this type of trap appears to be limited, as it is sometimes ineffective (Hurley *et al.*, 2015).

The focus on insect attraction to specific individuals is not restricted to the composition of the volatiles. Instead, factors such as the recently discovered chemosensory interaction between the insect and its host tree through proteomics were described. As well as the attractiveness of the volatile

compounds synthesized by *A. areolatum*, these findings shed new light on the plant-insect relationship and suggest novel research methods for its control.

### 2.3 Plant Metabolomics

Metabolomics is a trend in analytical chemistry positioning a novel strategy in the scientific community to understand external or pathological stressors in a biological system. The analysis of hundreds to thousands of metabolites in biological samples provides a holistic view of the metabolic status and biochemical events taking place within an organism (Ren *et al.*, 2015). It has been stated that metabolome variability, as measured by metabolite level changes, is more sensitive to systematic perturbations than either the transcriptome or the proteome. Consequently, metabolome variability can be viewed as the ultimate response to genetic or environmental (biotic/abiotic) factor changes (Kell *et al.*, 2005).

In metabolomics, the most common analytical platforms have been Nuclear Magnetic Resonance (NMR) spectroscopy and Mass Spectrum (MS) spectroscopy coupled to liquid chromatography (LC) or gas chromatography (GC) (Ren *et al.*, 2015). NMR has lower sensitivity than MS, detecting only medium to high abundance metabolites (Smolinska *et al.*, 2012). Then, multivariate statistical analysis is used to extract the most significant features (data consisting of pairs of retention time and mass-to-charge ratio ( $m/z$ )) of

molecules, fragments, and peak area/intensity concerning the studied biological condition.

Metabolomics has aided in the comprehension of followed presented critical plant concerns. Thus, the application of metabolomics has advanced our understanding of phenomena such as how the global spread of invasive alien species may damage ecosystems. The study of *Chromolaena odorata* (Asteraceae), *Datura stramonium* (Solanaceae), and *Xanthium strumarium* (Asteraceae) studied for their metabolomic profiles in their natural environments (USA) and Kruger National Park (South Africa, ZA) show the invasive species have more phytochemical diversity than their native counterparts and statistically different metabolomic profiles (Skubel *et al.*, 2020). The increasing plant diversity has widely divergent effects on the performance of individual plant species. Systematic, untargeted metabolite profiling on a variety of plants from a grassland biodiversity experiment revealed the physiological responses of certain plant species to increasing plant diversity. The research demonstrates that metabolite profiling is a valuable diagnostic tool for evaluating metabolic phenotypes in response to plant diversification and ecophysiological adaptation (Scherling *et al.*, 2010). Uncertainties remain about how evolution impacts plant metabolism. The application of metabolomics to plant evolution revealed that metabolites play

crucial roles in plant development, adaptation to climate, and evolution. However, the analysis of metabolomics data from leaf and seed tissues in maize and rice reveals that maize flavonoids are more variable than rice flavonoids, highlighting their importance to interspecific metabolic divergence. Defining that metabolomics is beneficial for monitoring evolutionary history and augmenting maize and rice interspecific genetic information with metabolomic data (Deng *et al.*, 2020). Also, it has been successfully applied to determine metabolites that contribute most to the distinction between the metabolome of genetically closed plants, for example, the qualitative and quantitative variations between the metabolomes of toxic *B. decumbens* and harmless *B. brizantha*. In this line, applying the metabolomics approach in plant-based health medicine could improve the nutritional quality of crops, accelerate the discovery of plant-derived bioactive leads through disease diagnostics, or increase the therapeutic efficacy of medications. The advances in this topic have been summarized in the review by Marchev and collaborators, where applications in this field are exemplified and discussed. The potential value of metabolite profiling in agricultural development, medicinal plant use, prognosis, diagnosis, and management of complicated diseases (Marchev *et al.*, 2021).

## 2.4 Plant Lipidomics

In the beginning, metabolomics relied on normal and reversed phase columns, which covered predominantly polar and mildly polar compounds. However, with the progress of metabolomics, there was an increasing concern about lipids and other non-polar substances. In this context, approaches were developed to characterize the lipidome (the set of lipids within a biological system) (Kishimoto *et al.*, 2001). Lipidomics uses a variety of approaches to quantify tens of thousands of chemically distinct lipids in cells and identify how they contribute to cellular function. Electrospray ionization mass spectrometry (ESI/MS) has enabled the identification and quantification of lipidome alterations following cellular perturbations. The review of Han & Gross in 2003 provided the first overview of the essential role of ESI/MS in lipidomics, presenting a broad strategy for generating lipidomes directly from cellular extracts of biological samples. They summarized examples of strategies used to conquer the lipidome. The ESI/MS technique could provide a crucial link for collecting extremely accurate data that fingerprint cellular lipidomes, hence facilitating the comprehension of the functional importance of subcellular membrane compartments and microdomains in mammalian cells (Han & Gross, 2003). However, lipidomics analysis requires the ability to distinguish enantiomers and structural isomers. However, using reversed-phase

chromatography can make this difficult. In 2003, new analytical innovations were developed to respond to the challenge based on the use of non-normal-phase chromatography with chiral columns to improve enantiomer and isomer resolution, coupled with electron capture in APCI-MS/MS to improve sensitivity. The method helped to define a lipidomics profile from cultivated rat epithelial cells and evaluate a non-selective lipoxygenase inhibitor (Lee *et al.*, 2003).

Furthermore, The United States National Institute of General Medical Sciences funded a project with \$ 35 million dollars entitled “Lipid metabolites and path-ways strategy”. The research team headed by Edward Dennis formulated “Lipids are in many ways the most important biomolecules because they are the ultimate controllers and regulators of our bodily processes; they are key to signalling events in cells’ ([www.lipidmaps.org](http://www.lipidmaps.org)) (Lagarde *et al.*, 2003). These landmarks set the basis for contemporary lipidomics.

Scientists have studied lipids and their roles in biological systems for many years. It has been demonstrated that even small modifications to lipids' structure and composition can deeply affect vital biological functions. For example, membrane cell fluidity and permeability are directly affected by lipid membrane changes (Harayama & Riezman, 2018). The first step in lipid analysis is the successful extraction of lipids from the target tissue, which

requires a rapid, simple, and efficient method. Lipidomics most widespread sample preparation technique is liquid–liquid extraction. Most liquid–liquid plant lipid extraction methods are derived from animal tissue extraction protocols, such as the Folch, and Bligh and Dyer methods (FOLCH *et al.*, 1957; Bligh & Dyer, 1959). However, the most used modern methods in plants involve reducing the volume of solvents, modifying extraction temperatures, and substituting solvents to ensure broad coverage of lipid extraction and avoid artefacts. Several studies have demonstrated, for instance, that chloroform/methanol mixtures are unsuitable for the extraction of plant sphingolipids like glycosylinositol phosphorylceramides (Markham *et al.*, 2006; Lange *et al.*, 2018; Kehelpannala *et al.*, 2020). For instance, the method developed by Roche and collaborators deactivates lipolytic enzymes by boiling 2-propanol (de la Roche *et al.*, 1973).

Additionally, the improve oh the methodologies with the addition of antioxidants such as butyl hydroxy toluene to the extraction solvent to prevent lipid oxidation (Shiva *et al.*, 2018), the substitution of chloroform for methyl tert-butyl ether (Matyash *et al.*, 2008), or the application of the supercritical fluid such CO<sub>2</sub> or another green solvent to avoid carcinogenic toxicity where proposed by several authors (Kumar *et al.*, 2017b; Cvjetko Bubalo *et al.*, 2018; de Jesus & Filho, 2020). The plant lipidome is extremely complex, and the

composition of lipids in different tissues and their specific roles in plant development, growth, and stress responses are not yet fully understood. Numerous techniques are currently employed to extract lipids from plant tissues. However, there is always a trade-off between extraction method efficiency, selectivity, and reproducibility (Kehelpannala *et al.*, 2020).

In contemporary lipidomics, several forms of liquid chromatography are used. According to the meta-study conducted by Cajka and Fiehn on 185 original publications reporting LC–MS lipidomics applications, 71% of the experiments were conducted using reversed-phase chromatography (RP-LC), followed by normal phase (NP-LC) with 19%, hydrophilic interaction liquid chromatography (HILIC) with 8%, and supercritical fluid chromatography (SFC) with 2% (Cajka & Fiehn, 2014).

The structural variety of lipids exceeds 40 thousand substances. In order to address this complicated system, comprehensive lipidome atlas systems with information on retention time, collision cross-section, and tandem mass spectrometry have been developed, and an automated workflow independent of mass spectrometry data has been implemented into the analysis program (MS-DIAL). MS-Dial has fragmentations of lipid mass spectral into 117 lipid subclasses, allowing the annotation and semiquantification of 8051 lipids with an estimated 1-2% false discovery rate. Using simultaneous liquid



chromatography and mass spectrometry to validate the platform with 1056 samples from over 80 distinct lipidomics research (Tsugawa *et al.*, 2020).



## 2.5 Metabolomics in pine-stress interaction

Integrative omics is needed to identify the molecular pathways of plants driving the adaptation to climate change. For example, the metabolomics and proteomic study of *Pinus radiata* under heat stress. The 30-day old plant exposed to 40°C for five days has changes in cytokinins, fatty acid metabolism, flavonoid and terpenoid levels, with zeatin riboside and isopentenyl adenosine as the main hormones. The integrative approach allowed elucidation of key metabolic mechanisms involved in heat response in *P. radiata* and identification of thermotolerance metabolic biomarkers (L-phenylalanine, hexadecanoic acid, and dihydromyricetin), aiding to the metabolic strategy to adapt plant to high temperature (Escandón *et al.*, 2018b). Knowing tree-species tolerance to UV irradiation is important for designing new forest productivity strategies. They increased UV irradiation-induced system-level changes in *Pinus radiata* needles. Early responses reduced photosystem activity, the electron transfer chain, and photorespiration. The core metabolism was modified to deal with oxidative stress while decreasing ROS generation.

Additionally, to UV-induced photosynthesis reduction, the main metabolism was altered to reduce reactive oxygen species (ROS) production. This adaptation was possible by preferring photorespiration over carboxylation and changing sugar metabolism to create NADPH for UV-enhanced secondary

metabolism. After UV exposure, accumulation of flavonoids with enhanced photoprotective activities (flavan-3-ols, precursors of UV screens and antioxidants) corroborated this observation (Pascual et al., 2017a).

On another hand, a metabolomics approach of the needles from three closely related *Pinus* species with distant coevolutionary histories with the caterpillar of the processionary moth, demonstrates that the investigated pines species had different metabolomes and metabolic responses to herbivorous attack. The results suggest that both macroevolutionary history (phylogeny) and the coevolutionary history between plants and insects may play important roles in determining the metabolomic responses of pines to herbivory attack, giving new approaches to study and understanding plant-insect relationships (Rivas-Ubach et al., 2016).

The metabolome of *Pinus pinaster* (*P. pinaster*) was examined to understand the adaptation to drought and phenotypic diversity. Ten provenances of *P. pinaster* from France, Spain, and Morocco were cultivated for five years in a communal garden. The metabolomes of needles and buds were examined, revealing that provenance differences were maintained and that most metabolites in each organ are connected to amino acid metabolism. When organs were individually studied, provenances were distinguished mostly by secondary metabolism. Integration of metabolome, environmental, and growth

data highlighted the adaptability of conifers. The study concluded that studying the metabolome of *P. pinaster* is feasible and identified two major plant families: Atlantic and Mediterranean (Meijõn *et al.*, 2016).



### 3. HYPOTHESIS AND OBJECTIVES

#### 3.1 Hypothesis

Application of metabolomics analysis for metabolome comparison of *Pinus radiata* trees infected by *Sirex noctilio* with those of nearly growing healthy trees of the same age and management could reveal significant differences leading to identifying meaningful biomarkers related to the pine defensive response and resistance to this pest.

#### 3.2 Objectives

##### 3.2.1 Main objective

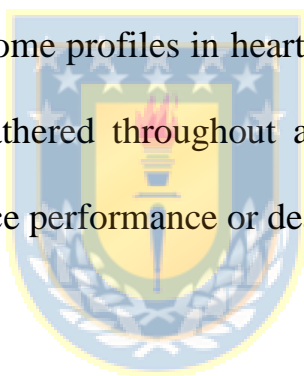
To identify biomarkers in *Pinus radiata* directly correlated to its defensive response and resistance to *Sirex noctilio* attack, by using a combined LC-MS based metabolomics and LC-MS based lipidomic strategy for an integrative metabolome comparison of infected and healthy trees

##### 3.2.2 Specific objectives

- To compare the metabolome profiles of polar extracts obtained from bark, heartwood and needles between infected (IT) and healthy (HT) *P. radiata* trees, using a metabolomics processing of their LC-MS data.
- To identify the nature of biomarkers detected from metabolomics processing of LC-MS data of polar extracts, using molecular formula

calculated from their exact masses, MS/MS fragmentation pattern, and matching in on-line free access data bases.

- To compare the metabolome profiles of non-polar extracts obtained from bark, heartwood and needles between infected (IT) and healthy (IT) *P. radiata* trees using a lipidomics LC-MS approach.
- To identify the nature of biomarkers detected from metabolomics processing of LC-MS data of non-polar extracts, using matching in lipdblast data base.
- To compare the metabolome profiles in heartwood and needles of infected *P. radiata* trees (IT) gathered throughout a year to identify significant changes related to defence performance or death tree process.



#### 4. RESEARCH STRATEGY

To comprehend the defensive response and resistance to *S. noctilio* attack in *P. radiata*, we proposed to compare the metabolomes of infected (IT) and healthy trees (HT). For this study, the bark, heartwood, and needles of each chosen tree were employed, and both polar to medium polar and lipophilic components were evaluated. Infested (IT) and healthy (HT) individual trees were sampled. The strategy is described in Figure 5-1.

Ten IT with the same age, management, and condition were selected for the study. Additionally, ten HT closer to each IT were acquired. The sampling was made in April 2018 (the conclusion of the Sirex flight season), and the same individuals were sampled every three months until their deaths.

Each sampling consists of 20 samples per plant organ (bark, heartwood, and needles). The IT and HT samples were undergone simultaneous polar/non-polar solvent extraction, and subsequent analysis by Liquid Chromatography coupled to Mass Spectrometry (LC-MS) for metabolomics and lipidomics, respectively. Then, the generated experimental data (LC/MS-chromatograms) were used as the basis for a metabolomics study using various chemometric approaches to identify significant variations (biomarkers) between the groups under consideration. Thus, the metabolome comparison (each plant organ handled separately) between IT and HT could identify biomarkers in the

metabolome of IT expressed in response to *Sirex* infection. In contrast, biomarkers highly connected to HT may be responsible for defence/resistance mechanisms. Lastly, HT and IT were collected and tested simultaneously to prevent seasonal metabolic fluctuation.

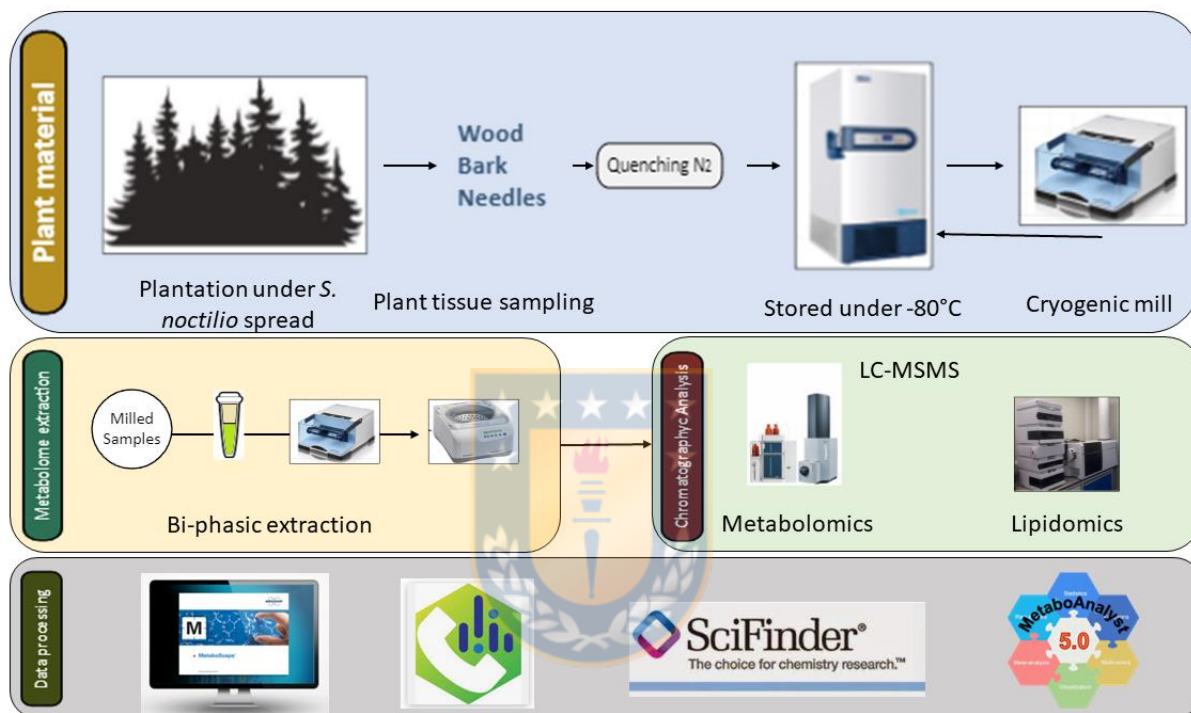


Figure 5-1: Analytical strategy for metabolomics and lipidomics analysis



## 5. METHODOLOGIES

### 5.1 Plant material

The plant material used for this study was collected at San Nicolás, in the Ñuble region of Chile (MININCO Forestry Company plantations). The initial collection was conducted during the *S. noctilio* flying season in April 2018. Bark flakes without physical damage were collected using a razor-sharp steel blade. Approximately a square of 5 x 5 cm and 1 cm of thickness were cut from each selected tree at a height of 1.5 meters and facing north. Needles were collected from the living crown using a pruning pole. The wood of trees was sampled using a Pressler incremental borer (HAGLOF), and the samples were taken at breast height. After sampling, all plant materials were frozen in liquid nitrogen and transported to the laboratory, where they were subjected to cryogenic homogenization in a bead mill (Retsch MM400). Then, powdered, frozen fresh samples were stored at -80°C until extraction. The methodology is detailed in Figure 6-1.

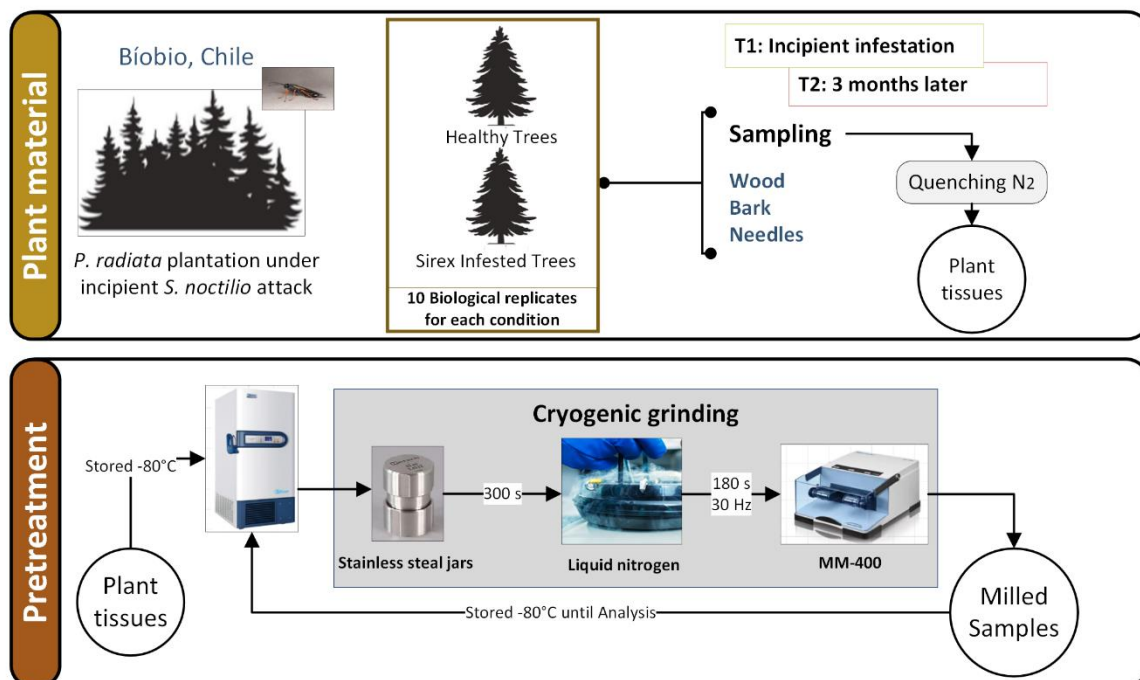


Figure 6-1: Plant material sampling and pretreatment

## 5.2 Extraction of metabolome and lipidome

According to the method described by Valledor et al., metabolome extraction was performed in triplicate and random order (Valledor et al., 2014a). Briefly, 100 mg (dry weight basis) of each type of tissue (bark, heartwood and needles) were mixed with 800 ml of cold (4°C) extraction solution (methanol/chloroform/water, 2.5:1:0.5). The mixture was vigorously shaken in a mixer mill (Retsch MM400) for 30 sec. Then, each sample tube was centrifuged for 10 minutes at 14,000 g at 4°C, and the metabolite-containing supernatant was transferred to a fresh tube for liquid-liquid extraction. After adding chloroform and water, 400 µl each, the mixture was vortexed and

centrifuged at 10,000 g for 5 minutes at 4°C. The upper layer (methanol/water) contained polar metabolites, while the bottom organic layer (chloroform) contained non-polar substances. These fractions were transferred to new microcentrifuge tubes and dried by centrifugation under a vacuum. This protocol is described in Figure 7-1.

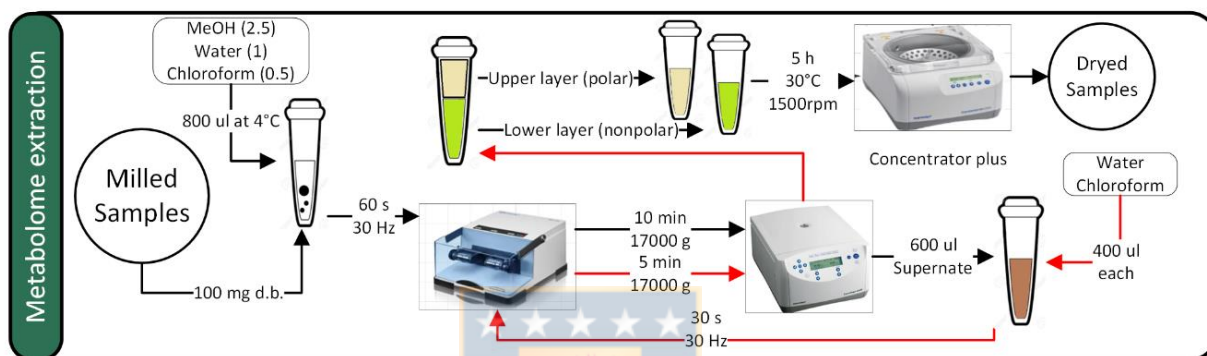
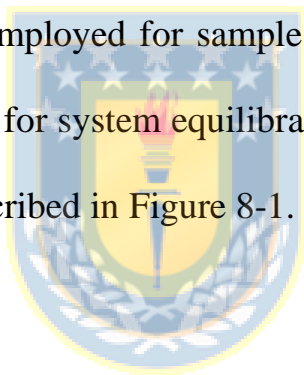


Figure 7-1: Milled samples extraction.

### 5.3 LC-MS analysis for metabolomics

Dried polar extracts were reconstituted with 600 µl of mobile phase [water/methanol (20:80 v/v)], homogenized in the MM-400 for 30 seconds, and centrifuged for 10 minutes at 4°C. Then, samples were analyzed in a UHPLC-HR-QTOF-MS (Elute UHPLC, Bruker Daltonik GmbH, Bremen, Germany). Quality control samples (QCs) were used to evaluate instrumental reproducibility (Dunn *et al.*, 2012). Equal amounts of each extract (100 µl) were combined to create quality control samples. Chromatographic separations were performed on a Kinetex C18 column (100 mm length x 2.1 mm id, 1.7 µm

particle size, Phenomenex) maintained at 30°C, with a mobile phase formed by solvent A (0.1% formic acid in Milli-Q water, v/v) and solvent B (0.1% formic acid in acetonitrile hypergrade) in gradient elution mode, at a flow rate of 0.4 ml/min. The mass spectrometer was operated in both negative and positive modes using electrospray ionization method (ESI). The range of the mass scan was set between 50 and 1500 m/z. The MS/MS were obtained in a data-dependent mode, using two precursors (max) for each scan. Internal calibrations were done by infusing 10 mM sodium formate solution into the ions source. A randomized sequence was employed for sample injection, with blanks at the beginning, followed by QCs for system equilibration and reconstituted sample extracts. The protocol is described in Figure 8-1.



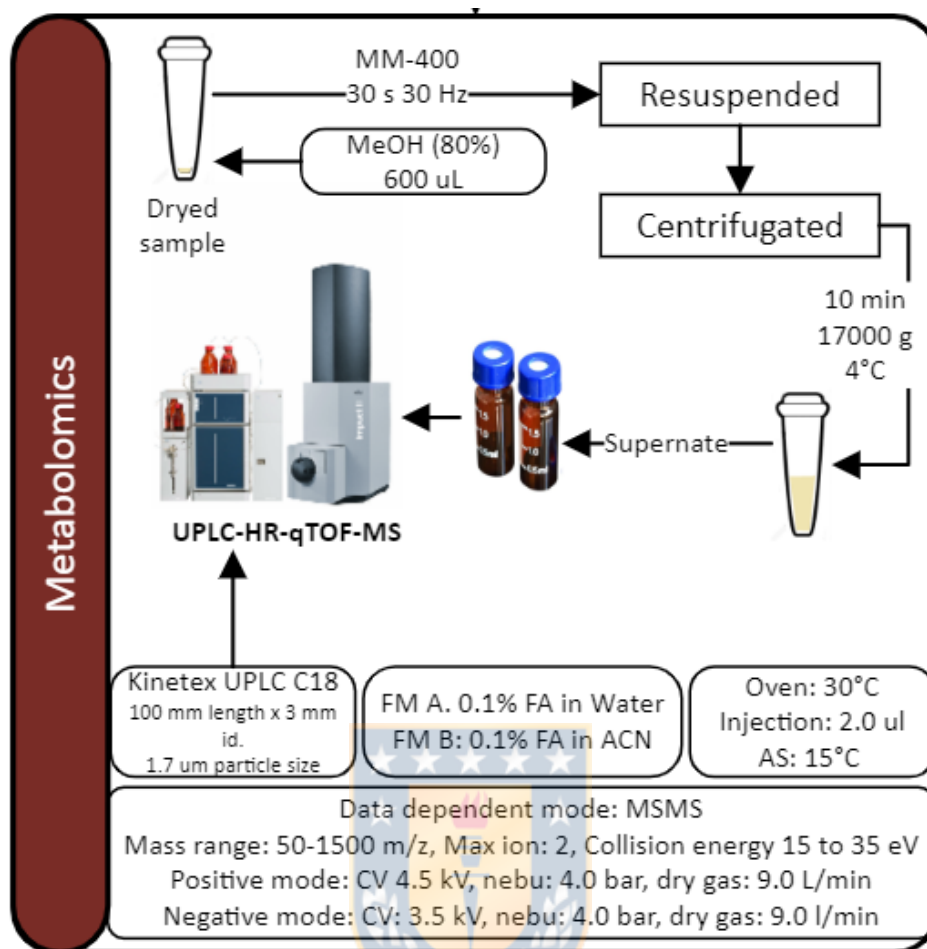


Figure 8-1: Proposed metabolomics protocol by HPLC-MSMS platform

#### 5.4 LC-MS analysis for lipidomics

Dried lipophilic extracts were resuspended in 488  $\mu$ l of ice-cold (3:10 v/v) methanol: methyl tertbutyl ether containing a quality control mix of 22:1 cholesterol ester standard, vortex for 10 sec, and dried for 4 hrs at 248 g in a vacuum centrifuge. Then, 1000  $\mu$ l of methanol:toluene (9:1 v/v) with 12-[[[(cyclohexylamino)carbonyl]amino]-dodecanoic acid (50 ng/ml) were added to each sample. The samples were vortexed for 10 sec, sonicated for 5 min, and

centrifuged for 2 min at 16000 g. Aliquots of 50  $\mu$ l per sample were collected for a pooled quality control (QC) sample, and two aliquots of 450  $\mu$ l each were separated for analyzing in positive and negative ESI modes. Analysis was performed by LC-MS/MS on an ultra-high performance liquid chromatography system Agilent 1290 Infinity LC system (Agilent Technologies, Santa Clara, CA, USA). Lipids were separated on an Acquity UPLC CSH C18 column (100 mm length, 2.1 mm id; 1.7  $\mu$ m) coupled to an Acquity CSH C18 VanGuard pre-column (5 mm length, 2.1 mm id and 1.7  $\mu$ m particle size). Separations were carried out at 65 °C at a flow rate of 0.6 ml/min. The mobile phases consisted of (A) 60:40 (v/v) acetonitrile:water and (B) 90:10 (v/v) isopropanol:acetonitrile for negative mode, each mobile phase (A, B) containing 10 mM ammonium acetate, and for positive mode each mobile phase (A, B) contain ammonium formate 10 mM plus 0.1% formic acid. Gradient elution was set as follows: 0 min 15 % (B); 0–2 min 30 % (B); 2–2.5 min 48 % (B); 2.5–11 min 82 % (B); 11–11.5 min 99 % (B); 11.5–12 min 99 % (B); 12–12.1 min 15 % (B); 12.1–15 min 15 % (B) (Cajka et al., 2017; Cajka & Fiehn, 2016). The chromatography protocol for lipidomics is described in Figure 9-1.

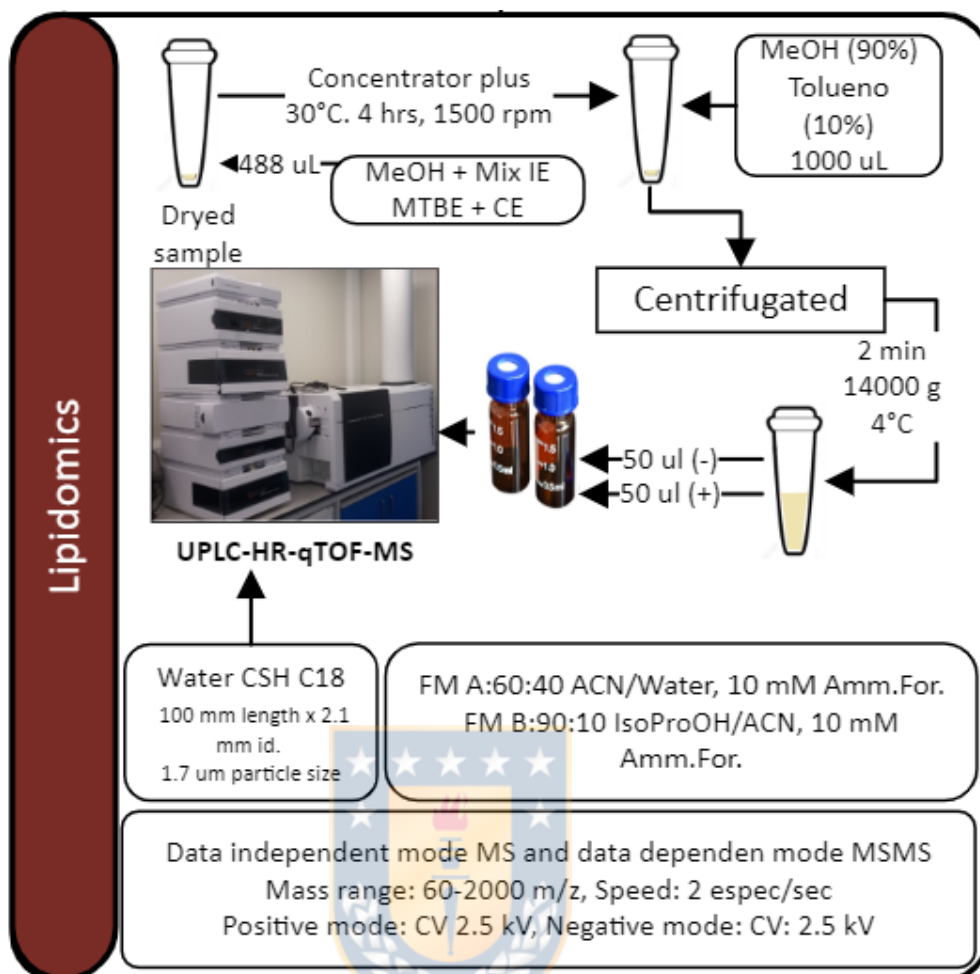


Figure 9-1: Proposed lipidomics protocol by HPLC-MSMS platform

## 5.5 Data analysis, statistical treatment and annotation

Significant metabolites were manually annotated using an integrated MetaboScape workflow. SmartFormula determines molecular formulas based on extracted feature mass and isotopic patterns. SmartFormula 3D calculations are applied to all features with MS/MS spectra in this step, improving the molecular formula. SmartFormula 3D ranked ion formulas according to MS/MS fragment explanation and intensity coverage for each possible explanation of

the precursor's  $m/z$  and isotopic pattern of a feature. The Compound Crawler tool sends queries for a given molecular formula to databases such as ChEBI, ChemSpider, and PubChem and returns results that can be used to annotate compounds. MetFrag was used to select the correct structure after Compound Crawler found multiple candidates for a given elemental composition. MetFrag searches for ions matching in-silico fragmentation of Compound Crawler candidates and ranks them by fragment peaks and intensity coverage (Ruttkies et al., 2016). The MS/MS Library Search tool compares the MS/MS spectrum of a given feature with Spectral Libraries previously imported in MetaboScape, such as Bruker MetaboBASE Plant Library and Vaniya/Fiehn Natural Products Library of the MassBank of North America (MoNA). SIRIUS 4.0, a free web service that integrates isotopic pattern analysis and fragmentation trees, was used to improve annotation.

The lipidomics data files acquired in MassHunter (extension .d) were transformed to “Analysis Base File” (ABF) using Reifycs File Converted (Reifycs, 2021), allowing the analysis in MS-dial. Time correction for the annotation of the Lipidblast library was performed using a Microsoft Excel sheet with the retention time of the standards quality control mixture. The general workflow for data processing was done as follows: MS-DIAL was utilized for data collection, peak detection, deconvolution, identification,



adducts, and alignment (Tsugawa et al., 2015a). Initially, bucket tables were manually cured using Microsoft Excel for blank subtraction, feature filtering with intragroup covariance upper limits of 50 per cent, presence of the feature in nearly 50 per cent of biological replicates per group, and signal-to-noise ratios greater than 10. Using MS-FLO, potential duplicates, adducts, and isotopes were filtered out. For statistical analysis, curated data containing only annotated lipids species from (+) and (-) ESI modes were combined into a single dataset (DeFelice et al., 2017b). The Metaboanalyst platform was used for statistical analysis.

The metabolome and lipidome comparison (each plant organ handled separately) between IT and HT led to identifying biomarkers in the IT metabolome that were expressed in response to the *Sirex noctilio* infestation. Metabolomics analysis of IT samples collected before the flight season in Chile (sampling 1) and three months later (sampling two) from the same individuals allowed the observation of metabolic changes under prolonged infestation.

## 6. REFERENCES

- Bedding RA, Iede ET. 2005. Application of *Beddingia siricidicola* for *Sirex* woodwasp control. In: Grewal PS, Ehlers RU, Shapiro-Ilan DI, eds. *Nematodes as biocontrol agents*. Wallingford: CABI Publishing, 385–399.
- Beèche M. 2012. *Sirex noctilio* (Hym.: Siricidae) *Situación y marco regulatorio en Chile*.
- Bligh EG, Dyer WJ. 1959. A rapid method of total lipid extraction and purification. *Canadian Journal of Biochemistry and Physiology* 37: 911–917.
- Bordeaux JM, Dean JFD. 2012. Susceptibility and Response of Pines to *Sirex noctilio*. In: Slippers B, de Groot P, Wingfield MJ, eds. *The Sirex Woodwasp and its Fungal Symbiont*: Dordrecht: Springer Netherlands, 31–50.
- Bordeaux JM, Lorenz WW, Dean JFD. 2012. Biomarker genes highlight intraspecific and interspecific variations in the responses of *Pinus taeda* L. and *Pinus radiata* D. Don to *Sirex noctilio* F. acid gland secretions. *Tree Physiology* 32: 1302–1312.
- Bordeaux JM, Lorenz WW, Johnson D, Badgett MJ, Glushka J, Orlando R, Dean JFD. 2014. Noctilisin, a venom glycopeptide of *Sirex noctilio* (Hymenoptera: Siricidae), Causes needle wilt and defense gene responses in pines. *Journal of Economic Entomology* 107: 1931–1945.
- Cajka T, Fiehn O. 2014. Comprehensive analysis of lipids in biological systems by liquid chromatography-mass spectrometry. *TrAC - Trends in Analytical Chemistry* 61: 192–206.
- Cajka, T., & Fiehn, O. (2016). Increasing lipidomic coverage by selecting optimal mobile-phase modifiers in LC–MS of blood plasma. *Metabolomics*, 12(2), 1–11. <https://doi.org/10.1007/s11306-015-0929-x>
- Cajka, T., Smilowitz, J. T., & Fiehn, O. (2017). Validating Quantitative Untargeted Lipidomics Across Nine Liquid Chromatography-High-Resolution Mass Spectrometry Platforms. *Analytical Chemistry*, 89(22), 12360–12368. <https://doi.org/10.1021/acs.analchem.7b03404>
- Castillo, M., Sanfuentes, E., Angulo, A., Becerra, J., Romero-Romero, J. L., & Arce-Johnson, P. (2018). Biocontrol of *Sirex noctilio* by the parasitic nematode *Deladenus siricidicola*: A five season field study in southern Chile. *PLOS ONE*, 13(11), e0207529. <https://doi.org/10.1371/JOURNAL.PONE.0207529>

- Ceballos R. 2015. Informe final Proyecto CORFO 12BPC2-13355. "Fortalecimiento del sector forestal mediante el diseño e implementación de un sistema de vigilancia temprana para el manejo integrado de la plaga *Sirex noctilio*, basado en el uso de semioquímicos." Los Ángeles, Chile.
- Celedon JM, Bohlmann J. 2019. Oleoresin defenses in conifers: chemical diversity, terpene synthases and limitations of oleoresin defense under climate change. *New Phytologist* 224: 1444–1463.
- Clough S, McLaughlin S, Murray S. 2019. *National Exotic Forest Description* (C Riley, Ed.). Wellington: Ministry for Primary Industries New Zealand.
- Coutts M. 1969a. The Mechanism of Pathogenicity of *Sirex Noctilio* on *Pinus Radiata* I. Effects of the Symbiotic Fungus *Amylostereum* Sp. (Thelophoraceae). *Australian Journal of Biological Sciences* 22: 915.
- Coutts M. 1969b. The Mechanism of Pathogenicity of *Sirex Noctilio* on *Pinus Radiata* II. Effects of *S. Noctilio* Mucus. *Australian Journal of Biological Sciences* 22: 1153.
- Coutts M. 1969c. The Mechanism of Pathogenicity of *Sirex Noctilio* on *Pinus Radiata* II. Effects of *S. Noctilio* Mucus. *Australian Journal of Biological Sciences* 22: 1153.
- Cvjetko Bubalo M, Vidović S, Radojčić Redovniković I, Jokić S. 2018. New perspective in extraction of plant biologically active compounds by green solvents. *Food and Bioproducts Processing* 109: 52–73.
- DeFelice BC, Mehta SS, Samra S, Čajka T, Wancewicz B, Fahrman JFJF, Fiehn O. 2017. Mass Spectral Feature List Optimizer (MS-FLO): A Tool To Minimize False Positive Peak Reports in Untargeted Liquid Chromatography-Mass Spectroscopy (LC-MS) Data Processing. *Analytical Chemistry* 89: 3250–3255.
- Deng M, Zhang X, Luo J, Liu H, Wen W, Luo H, Yan J, Xiao Y. 2020. Metabolomics analysis reveals differences in evolution between maize and rice. *The Plant Journal* 103: 1710–1722.
- Dunn WB, Wilson ID, Nicholls AW, Broadhurst D. 2012. The importance of experimental design and QC samples in large-scale and MS-driven untargeted metabolomic studies of humans. *Bioanalysis* 4: 2249–2264.
- Eckenwalder JE. 2018. Conifer. *Encyclopedia Britannica*.

- Escandón M, Meijón M, Valledor L, Pascual J, Pinto G, Cañal MJ. 2018a. Metabolome Integrated Analysis of High-Temperature Response in *Pinus radiata*. *Frontiers in Plant Science* 9: 1–15.
- Escandón M, Meijón M, Valledor L, Pascual J, Pinto G, Cañal MJ. 2018b. Metabolome integrated analysis of high-temperature response in *Pinus radiata*. *Frontiers in Plant Science* 9.
- Farjon A. 2018. The Kew Review Conifers of the World. *Kew Bulletin* 73: 1–16.
- Farjon Aljos, Filer Denis. 2013. *An Atlas of the World's Conifer*.
- Folch J, Lees M, Sloane Stanley Gh. 1957. A simple method for the isolation and purification of total lipides from animal tissues. *Journal of Biological Chemistry* 226: 497–509.
- Fong LK, Crowdent RK. 1973. Physiological effects of mucus from the wood wasp, *Sirex noctilio* F., on the foliage of *Pinus radiata* D. Don. *Australian Journal of Biological Science* 26: 365–378.
- Forestry Corporation. 2016. Forest Fact No 04. : 3.
- Fu N, Wang M, Wang L, Luo Y, Ren L. 2020. Genome Sequencing and Analysis of the Fungal Symbiont of *Sirex noctilio*, *Amylostereum areolatum*: Revealing the Biology of Fungus-Insect Mutualism (G Suen, Ed.). *mSphere* 5: 1–15.
- Gysling AJ, Bañados G. 2017. *Anuario forestal 2017*. Santiago.
- Gysling Caselli AJ, Álvarez González VDC, Soto Aguirre DA, Pardo Velasquez EJ, Poblete Hernandez PA, Kahler González C. 2019. *Chilean statistical yearbook of forestry*. Santiago: Forestry Institute (INFOR).
- Hajek AE, Nielsen C, Kepler RM, Long SJ, Castrillo L. 2013. Fidelity among *Sirex* woodwasps and their fungal symbionts. *Microbial Ecology* 65: 753–762.
- Han X, Gross RW. 2003. Global analyses of cellular lipidomes directly from crude extracts of biological samples by ESI mass spectrometry: A bridge to lipidomics. *Journal of Lipid Research* 44: 1071–1079.
- Hao DC, Gu X-J, Xiao PG. 2015. *Taxus medicinal resources*. In: *Medicinal Plants*. Elsevier, 97–136.
- Harayama T, Riezman H. 2018. Understanding the diversity of membrane lipid composition. *Nature Reviews Molecular Cell Biology* 2018 19:5 19: 281–296.

- Haugen D, Bedding R, Underdown M, Neumann F. 1990. *National-sirex-control-strategy-1990*.
- Hurley BP, Garnas J, Cooperband MF. 2015. Assessing trap and lure effectiveness for the monitoring of *Sirex noctilio*. *Agricultural and Forest Entomology* 17: 64–70.
- Hurley BP, Slippers B, Wingfield MJ. 2007. A comparison of control results for the alien invasive woodwasp, *Sirex noctilio*, in the southern hemisphere. *Agricultural and Forest Entomology* 9: 159–171.
- de Jesus SS, Filho RM. 2020. Recent advances in lipid extraction using green solvents. *Renewable and Sustainable Energy Reviews* 133: 110289.
- Kehelpannala C, Rupasinghe TWT, Hennessy T, Bradley D, Ebert B, Roessner U. 2020. A comprehensive comparison of four methods for extracting lipids from *Arabidopsis* tissues. *Plant Methods* 16: 1–16.
- Kell DB, Brown M, Davey HM, Dunn WB, Spasic I, Oliver SG. 2005. Metabolic footprinting and systems biology: the medium is the message. *Nature Reviews. Microbiology* 3: 557–565.
- Kishimoto K, Urade R, Ogawa T, Moriyama T. 2001. Nondestructive quantification of neutral lipids by thin-layer chromatography and laser-fluorescent scanning: Suitable methods for “lipidome” analysis. *Biochemical and Biophysical Research Communications* 281: 657–662.
- Kukor JJ, Martin MM. 1983. Acquisition of digestive enzymes by Siricid woodwasps from their fungal symbiont. *Science* 220: 1161–1163.
- Kumar SPJ, Prasad SR, Banerjee R, Agarwal DK, Kulkarni KS, Ramesh K v. 2017. Green solvents and technologies for oil extraction from oilseeds. *Chemistry Central Journal* 11: 1–7.
- de la Roche IA, Andrews CJ, Kates M. 1973. Changes in Phospholipid Composition of a Winter Wheat Cultivar during Germination at 2 C and 24 C. *Plant Physiology* 51: 468–473.
- Lagarde M, Géloën A, Record M, Vance D, Spener F. 2003. Lipidomics is emerging. *Biochimica et Biophysica Acta - Molecular and Cell Biology of Lipids* 1634: 61.
- Lange M, Ni Z, Criscuolo A, Fedorova M. 2018. Liquid Chromatography Techniques in Lipidomics Research. *Chromatographia* 2018 82:1 82: 77–100.

- Lee SH, Williams M v., DuBois RN, Blair IA. 2003. Targeted lipidomics using electron capture atmospheric pressure chemical ionization mass spectrometry. *Rapid Communications in Mass Spectrometry* 17: 2168–2176.
- Madden JL. 1988. Sirex in Australasia. In: Berryman AA, ed. Dynamics of forest insect populations. Patterns, causes, implications. New York: Springer Science+Business Media, 407–429.
- Marchev AS, Vasileva L v., Amirova KM, Savova MS, Balcheva-Sivenova ZP, Georgiev MI. 2021. Metabolomics and health: from nutritional crops and plant-based pharmaceuticals to profiling of human biofluids. *Cellular and Molecular Life Sciences* 2021 78:19 78: 6487–6503.
- Markham JE, Li J, Cahoon EB, Jaworski JG. 2006. Separation and identification of major plant sphingolipid classes from leaves. *The Journal of biological chemistry* 281: 22684–22694.
- Matyash V, Liebisch G, Kurzchalia T v., Shevchenko A, Schwudke D. 2008. Lipid extraction by methyl-tert-butyl ether for high-throughput lipidomics. *Journal of Lipid Research* 49: 1137–1146.
- Mead DJ. 2013a. *Sustainable management of Pinus radiata plantations*. Rome: FAO Forestry Paper No. 170.
- Meijõn M, Feito I, Oravec M, Delatorre C, Weckwerth W, Majada J, Valledor L. 2016. Exploring natural variation of *Pinus pinaster* Aiton using metabolomics: Is it possible to identify the region of origin of a pine from its metabolites? *Molecular Ecology* 25: 959–976.
- de Miguel M, Guevara MÁ, Sánchez-Gómez D, de María N, Díaz LM, Mancha JA, Fernández de Simón B, Cadahía E, Desai N, Aranda I, *et al.* 2016. Organ-specific metabolic responses to drought in *Pinus pinaster* Ait. *Plant Physiology and Biochemistry* 102: 17–26.
- New York Invasive Species Information. 2019. Sirex Woowasp. : 1.
- Pascual J, Canal MJ, Escandon M, Meijon M, Weckwerth W, Valledor L. 2017. Integrated physiological, proteomic, and metabolomic analysis of ultraviolet (UV) stress responses and adaptation mechanisms in *pinus radiata*. *Molecular and Cellular Proteomics* 16: 485–501.

- Ralph SG, Yueh H, Friedmann M, Aeschliman D, Zeznik JA, Nelson CC, Butterfield Y s. N, Kirkpatrick R, Liu J, Jones S j. M, *et al.* 2006. Conifer defence against insects: microarray gene expression profiling of Sitka spruce (*Picea sitchensis*) induced by mechanical wounding or feeding by spruce budworms (*Choristoneura occidentalis*) or white pine weevils (*Pissodes strobi*) reveals large-scale. *Plant, Cell and Environment* 29: 1545–1570.
- Reifycs. 2021. Reifycs Abf Converter. <https://www.reifycs.com/AbfConverter/>.
- Ren S, Hinzman AA, Kang EL, Szczesniak RD, Lu LJ. 2015. Computational and statistical analysis of metabolomics data. *Metabolomics* 11: 1492–1513.
- Riquelme, S., Campos, J. v., Pecio, Ł., Alzamora, R., Mardones, C., Simonet, A. M., Arteaga-Pérez, L. E., Rubilar, R., Fiehn, O., & Pérez, A. J. (2022). *Sirex noctilio* infestation led to inevitable pine death despite activating pathways involved in tolerance. *Phytochemistry*, 203, 113350. <https://doi.org/10.1016/J.PHYTOCHEM.2022.113350>
- Ryan K, Hurley BP. 2012. Life History and Biology of *Sirex noctilio*. In: Slippers B, de Groot P, Wingfield MJ, eds. *The Sirex Woodwasp and its Fungal Symbiont*: Dordrecht: Springer Netherlands, 15–30.
- Sandoval A, Opazo A, Velazquez P, Schafer M, Aravena JC, Barrientos C, Sievert H, Gonzalez M, Valenzuela J, Peragallo M, *et al.* 2018. Programa Control Biológico de *Sirex noctilio* F. (Hymenoptera: Siricidae): 2006-2017. : 37.
- Scherling C, Roscher C, Giavalisco P, Schulze ED, Weckwerth W. 2010. Metabolomics Unravel Contrasting Effects of Biodiversity on the Performance of Individual Plant Species. *PLoS ONE* 5: 1–13.
- Shiva S, Enniful R, Roth MR, Tamura P, Jagadish K, Welti R. 2018. An efficient modified method for plant leaf lipid extraction results in improved recovery of phosphatidic acid. *Plant Methods* 14: 1–8.
- de Simón BF, Sanz M, Cervera MT, Pinto E, Aranda I, Cadahía E. 2017. Leaf metabolic response to water deficit in *Pinus pinaster* Ait. relies upon ontogeny and genotype. *Environmental and Experimental Botany* 140: 41–55.

- Simpson RF. 1976. Bioassay of pine oil components as attractants for *Sirex noctilio* (Hymenoptera: Siricidae) using electroantennogram techniques. *Entomologia Experimentalis et Applicata* 19: 11–18.
- Skubel SA, Su X, Poulev A, Foxcroft LC, Dushenkov V, Raskin I. 2020. Metabolomic differences between invasive alien plants from native and invaded habitats. *Scientific Reports* 2020 10:1 10: 1–9.
- Slippers B, Coutinho TA, Wingfield BD, Wingfield MJ. 2003. A review of the genus *Amylostereum* and its association with woodwasps. *South African Journal of Science* 99: 70–74.
- Slippers B, de Groot P, Wingfield MJ. 2012. The sirex woodwasp and its fungal symbiont: Research and management of a worldwide invasive pest. *The Sirex Woodwasp and its Fungal Symbiont: Research and Management of a Worldwide Invasive Pest*: 1–301.
- Slippers B, Hurley BP, Wingfield MJ. 2015. *Sirex* Woodwasp: A model for evolving management paradigms of invasive forest pests. *Annual Review of Entomology* 60: 601–619.
- Slippers B, Wingfield MJ. 2012. *Sirex* research and management: Future prospects. In: Slippers B, de Groot P, Wingfield MJ, eds. *The Sirex woodwasp and its fungal symbiont: Research and management of a worldwide invasive pest*. Dordrecht Heidelberg London New York: Springer, 287–295.
- Smolinska A, Blanchet L, Buydens LMC, Wijmenga SS. 2012. NMR and pattern recognition methods in metabolomics: From data acquisition to biomarker discovery: A review. *Analytica Chimica Acta* 750: 82–97.
- Soto Aguirre D, Caselli JG, Kahler González C, Poblete Hernández P, Álvarez González V, Pardo Velásquez E, Carlos Bañados J, Rocha DB. 2021. *ANUARIO FORESTAL*.
- Spradbery JP, Kirk AA. 1978. Aspects of the ecology of siricid woodwasps (Hymenoptera: Siricidae) in Europe, North Africa and Turkey with special reference to the biological control of *Sirex noctilio* F. in Australia. *Bulletin of Entomological Research* 68: 341–359.
- Sun X, Xu Q, Luo Y. 2020. A maximum entropy model predicts the potential geographic distribution of *Sirex noctilio*. *Forests* 11.



- Tsugawa H, Cajka T, Kind T, Ma Y, Higgins B, Ikeda K, Kanazawa M, Vandergheynst J, Fiehn O, Arita M. 2015. MS-DIAL: Data-independent MS/MS deconvolution for comprehensive metabolome analysis. *Nature Methods* 12: 523–526.
- Tsugawa H, Ikeda K, Takahashi M, Satoh A, Mori Y, Uchino H, Okahashi N, Yamada Y, Tada I, Bonini P, *et al.* 2020. A lipidome atlas in MS-DIAL 4. *Nature Biotechnology* 2020 38:10 38: 1159–1163.
- Valledor L, Escandón M, Meijón M, Nukarinen E, Cañal MJ, Weckwerth W. 2014. A universal protocol for the combined isolation of metabolites, DNA, long RNAs, small RNAs, and proteins from plants and microorganisms. *Plant Journal* 79: 173–180.
- Wang L, Li C, Shi J, Li C, Li J, Ren L, Luo Y, Sullivan B. 2020. Incidental Fungi in Host Trees Disrupt the Development of *Sirex noctilio* (Hymenoptera: Siricidae) Symbiotic Fungus and Larvae. *Journal of Economic Entomology* 113: 832–838.
- Wang T, Zhao M, Rotgans BA, Ni G, Dean JFD, Nahrung HF, Cummins SF. 2016a. Proteomic analysis of the venom and venom sac of the woodwasp, *Sirex noctilio* - Towards understanding its biological impact. *Journal of Proteomics* 146: 195–206.
- Wang T, Zhao M, Rotgans BA, Ni G, Dean JFD, Nahrung HF, Cummins SF. 2016b. Proteomic analysis of the venom and venom sac of the woodwasp, *Sirex noctilio* - Towards understanding its biological impact. *Journal of Proteomics* 146: 195–206.
- Warren RL, Keeling CI, Yuen MM saint, Raymond A, Taylor GA, Vandervalk BP, Mohamadi H, Paulino D, Chiu R, Jackman SD, *et al.* 2015. Improved white spruce (*Picea glauca*) genome assemblies and annotation of large gene families of conifer terpenoid and phenolic defense metabolism. *Plant Journal* 83: 189–212.
- Wermelinger B, Thomsen IM. 2012. The woodwasp *Sirex noctilio* and its associated fungus *Amylostereum areolatum* in Europe. In: Slippers B, de Groot P, Wingfield MJ, eds. *The Sirex woodwasp and its fungal symbiont: Research and management of a worldwide invasive pest*. Dordrecht Heidelberg London New York: Springer, 65–80.
- Whitehill JGA, Yuen MMS, Henderson H, Madilao L, Kshatriya K, Bryan J, Jaquish B, Bohlmann J. 2019. Functions of stone cells and oleoresin terpenes in the conifer defense syndrome. *New Phytologist* 221: 1503–1517.



## 2. CHAPTER N°2

***Sirex noctilio* infestation led to inevitable pine death despite activating pathways involved in tolerance**



# 1. GRAPHICAL ABSTRACT

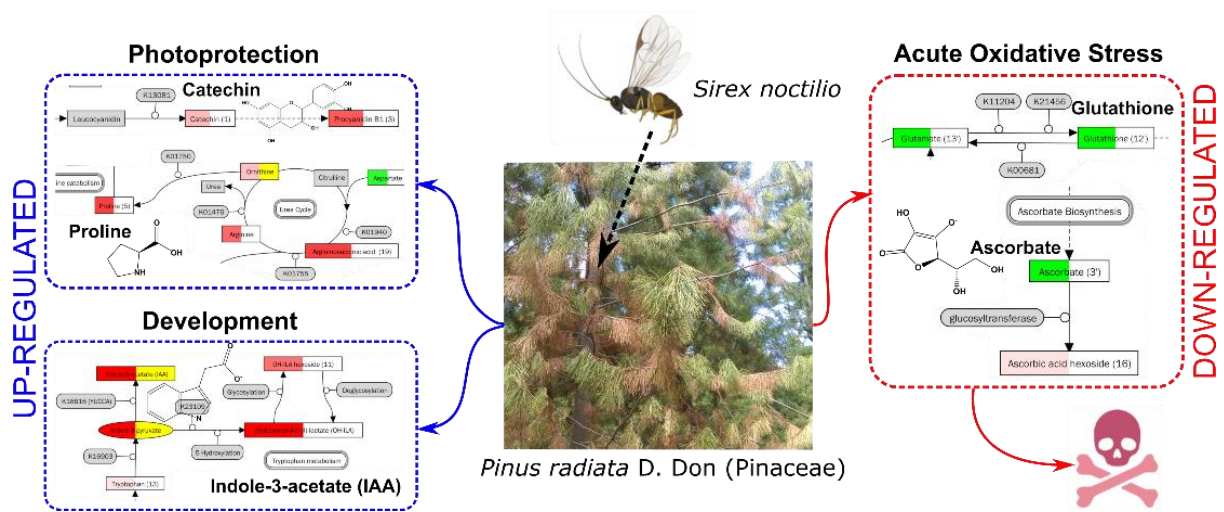


Figure 1-2: Metabolomics uncovered the *P. radiata* response to *S. noctilio* infestation, highlighting photoprotection and auxin expression as tolerance traits and the oxidative stress causing death.



***Sirex noctilio* infestation led to inevitable pine death despite activating pathways involved in tolerance.**

Sebastián Riquelme<sup>a</sup>, Jasna V. Campos<sup>a</sup>, Łukasz Pecio<sup>c</sup>, Rosa Alzamora<sup>d,e</sup>, Claudia Mardones<sup>a,b</sup>, Ana M. Simonet<sup>f</sup>, Luis E. Arteaga-Pérez<sup>g</sup>, Rafael Rubilar<sup>e,h</sup>, Oliver Fiehn<sup>i</sup>, Andy J. Pérez<sup>a,b,\*</sup>

<sup>a</sup> Departamento de Análisis Instrumental, Facultad de Farmacia, Universidad de Concepción, Concepción, Chile.

<sup>b</sup> Unidad de Desarrollo Tecnológico, UDT, Universidad de Concepción, Coronel, Chile.

<sup>c</sup> Department of Biochemistry and Crop Quality, Institute of Soil Science and Plant Cultivation, State Research Institute, ul. Czartoryskich 8, 24-100 Puławy, Poland.

<sup>d</sup> Departamento Manejo de Bosques y Medio Ambiente, Facultad de Ciencias Forestales, Universidad de Concepción, Concepción, Chile.

<sup>e</sup> Centro UC de Innovación en Madera, Pontificia Universidad Católica de Chile, Santiago, Chile.

<sup>f</sup> Allelopathy Group, Department of Organic Chemistry, Institute of Biomolecules (INBIO), Campus de Excelencia Internacional (ceiA3), School of Science, University of Cadiz, Puerto Real, Cadiz, Spain.

<sup>g</sup> Laboratory of Thermal and Catalytic Processes (LPTC), Department of Wood Engineering, University of Bío-Bío, Chile.

<sup>h</sup> Cooperativa de Productividad Forestal, Departamento de Silvicultura, Facultad de Ciencias Forestales, Universidad de Concepción, Concepción, Chile.

<sup>i</sup> NIH West Coast Metabolomics Center, UC Davis Genome Center, University of California, Davis, CA 95616, USA.

\* Corresponding author E-mail: aperezd@udec.cl. Phone: + 56 41 220 3027

Phytochemistry . 2022 Nov; 203:113350.

doi:10.1016/j.phytochem.2022.113350. Epub 2022 Aug 13.

## 2. ABSTRACT

Defense-related metabolome traits in pine species after infestation by *Sirex noctilio* are largely unknown, despite, in most cases, trees being overwhelmed. Using LC-MS-based untargeted metabolomics, we revealed the systemic metabolic changes induced by this insect in 14-year-old *Pinus radiata* trees, the most affected species worldwide. An immediate metabolome alteration was expressed in needles after infestation, including the up-regulation of flavonols, flavan-3-ols, oxycneolignans, auxins, proline, and tryptophan, among others. The flavan-3-ols (catechin and procyanidin B1) suggested a rapidly induced photoprotection mechanism aided by diverting proline as an alternative substrate for respiration to compensate for the progressive chlorosis that degrades photosystems. Meanwhile, glutathione, glutamate, and ascorbate levels significantly dropped in needles, which may indicate the critical oxidative stress that trees had to face since the onset of the infestation. They were not fully replenished after long-term infestation, and redox homeostasis was probably not achieved, compromising tree survival. Nevertheless, a huge auxins overexpression detected in needles throughout the infestation may reflect tolerance against the premature senescence caused by the woodwasp venom. In contrast, the metabolome of wood tissues remained initially unchanged, although it seems to collapse after three months. Overall, the metabolomics

strategy adopted in this work evidenced its usefulness in uncovering the fundamental roles of plants' chemical defense that govern interactions with specific stressors.

**Keywords:** *Pinus radiata* D. Don; Pinaceae; Radiata pine; LC-MS metabolomics; Plant-insect interaction; Plant defense; *Sirex noctilio*; Woodwasp.



### 3. INTRODUCTION

Coniferous forests have proliferated over 200 million years, with some species reaching natural lifespans of several hundred years (Hao et al., 2015b). Their speciation and longevity have usually been attributed to their ability to withstand biotic stresses caused by microbes, insects, and herbivores, depending on systemic or localized physiological and biochemical responses (Ralph et al., 2006b; Warren et al., 2015b; Celedon & Bohlmann, 2019b; Whitehill et al., 2019b). Conifers currently provide about 50% of the world's annual timber production (Eckenwalder, 2018b), with the North American conifer, *Pinus radiata* D. Don (Pinaceae), being the most extensively planted worldwide. It covers approximately 4.2 million ha (Mead, 2013a), with the largest plantations currently located in Chile, New Zealand, and Australia, with 1.5, 1.3, and 0.7 million ha, respectively (Forestry Corporation, 2016b; Clough et al., 2019b; Gysling Caselli et al., 2019).

However, growing *P. radiata* has been constantly threatened by pests that cause significant losses (Klapwijk et al., 2016a). The woodwasp, *Sirex noctilio* Fabricius (Hymenoptera: Siricidae), is one of the most important pests of pine plantations, which may cause severe physiological damage leading to death (Lantschner et al., 2014a; Xu et al., 2019a). It is a wood borer insect native to Eurasia and North Africa that lays eggs into conifers, especially *Pinus* spp. In



contrast to its behavior in foreign regions where it can kill established trees, decaying or already dead trees are its preferred hosts in its native area (Spradbery & Kirk, 1978a).

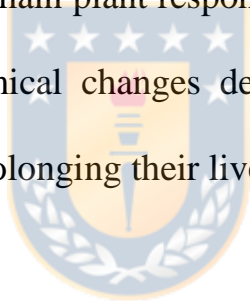
With the worldwide adoption of *Pinus* spp. for commercial purposes, the woodwasp has accidentally spread beyond its native domain, causing serious problems for foresters. For example, the first *S. noctilio* outbreak in Chile was detected in January 2001 and was associated with a hydroelectric power plant installed nearby the discovery site that imported large quantities of wood-packed equipment from Europe (Beèche et al., 2012). Several outbreaks have also been reported worldwide, but by far the most devastating one occurred in New Zealand between 1946 and 1951, causing the loss of 120.000 ha of forest (Mead, 2013a). Although such a large *S. noctilio* outbreak has not occurred in decades, the USDA Forest Service estimates that *S. noctilio* could cause between \$2.8 and \$17 billion in losses if it becomes a nationwide established species in the USA (New York Invasive Species Information, 2019b).

The damage caused by *S. noctilio* is due to a combination of two factors. When females select a host tree for oviposition, they drill tunnels through the bark into the xylem, depositing eggs along with venom (a complex mixture of proteins and peptides) and arthrospores of the symbiotic fungus, *Amylostereum areolatum* (Coutts 1969a, 1969b; Ryan and Hurley, 2012). As soon as two

weeks following oviposition, needles in the tree crown begin to bend at the fascicle sheath, wilting and becoming yellowish before their premature senescence. At the same time, respiration increases in the stem tissues, photosynthates transport from the photosynthetic tissues decreases, and droplets of resin flow from oviposition holes (Fong & Crowdent, 1973b; Bordeaux & Dean, 2012b). All these early symptoms have been attributed to the *S. noctilio* venom since they appear before egg hatching or before significant fungus colonization (Coutts 1969b). Finally, most infested trees are overwhelmed by the combined action of *A. areolatum* and the physiological changes caused by the woodwasp venom, dying several weeks later (Coutts, 1969d; Bordeaux & Dean, 2012b; Wang et al., 2016b). However, resistance and tolerance strategies deployed by the tree that relies on changes at primary or specialized metabolism in response to such a lethal infestation are still unknown, despite a century of research and well-established management programs. The importance of such knowledge for understanding the chemical traits that govern this interaction and for resistant breeding programs leading to effective and sustained integral management was recognized by Slippers and co-workers a few years ago (Slippers et al., 2015b).

As metabolites are downstream products of cellular biochemical processes, their identification and quantification in *P. radiata* organs during

woodwasp infestation can provide a sensitive measure of associated upstream molecular function, including genes, transcripts, or enzymes. Analytical platforms commonly used in metabolomics studies, facilitate simultaneous quantitative comparison of hundreds to thousands of metabolites in a living system, enabling good coverage of the chemical responses to abiotic or biotic stresses (Kumar et al., 2017a; Sharma et al., 2018; Evans et al., 2020; Fraga-Corral et al., 2020). In this context, by using an untargeted LC-MS-based metabolomics approach we compared the metabolomes of healthy and infested *P. radiata* trees, to reveal the main plant response to such lethal challenge and describe the specific biochemical changes deployed by pines that provide tolerance and resistance for prolonging their lives.



## 4. RESULTS

### 4.1 Initial metabolome changes in *P. radiata* as a response to *S. noctilio* infestation

After LC-MS analysis of sample extracts obtained from *P. radiata* trees showing initial symptoms of infestation at T1, raw data were processed in MetaboScape software to generate bucket tables as the main matrix for statistical treatments. A total of 6722 (–ESI) and 8914 (+ESI) features ( $m/z - R_t$  pairs) were detected in the needle dataset, while 2175 (–ESI) and 6125 (+ESI) features were detected in the wood dataset.

We first examined clustering patterns in the datasets obtained from both plant organs and acquisition modes using unsupervised multivariate Principal Component Analyses (PCA) (Figure 2-2). Scores plots for the distribution of needle samples between the first two Principal Components (PCs) showed a clear separation between infested (IT) and healthy (HT) trees along PC1, with 49.8% of the total explained variance of data in –ESI, and 40.9% in +ESI

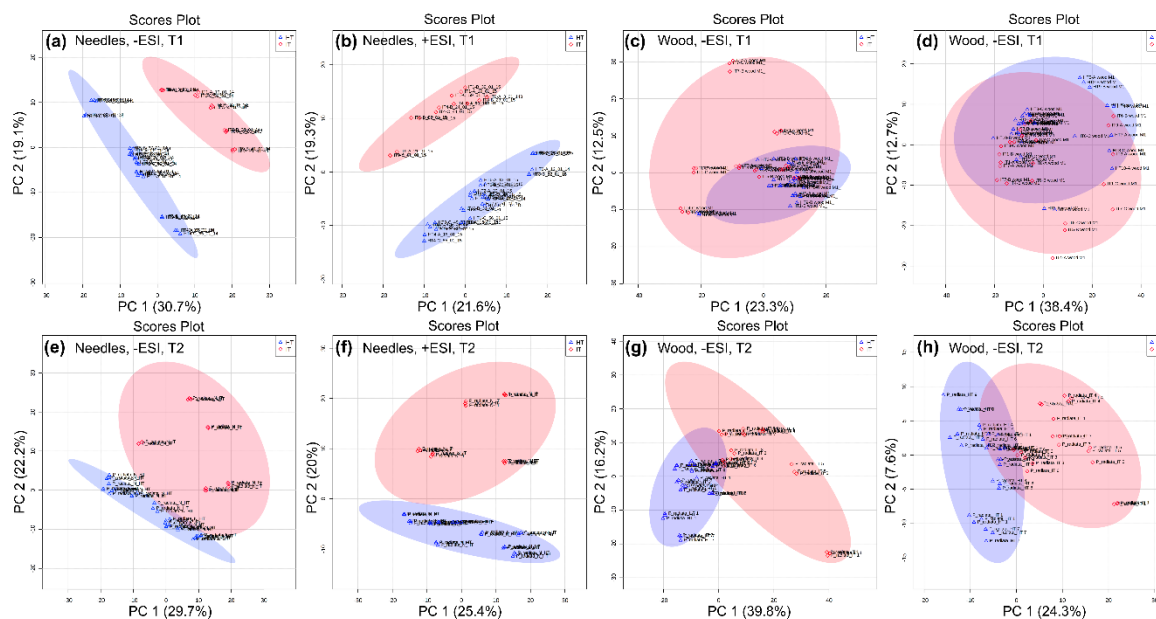


Figure 2-2: PCA score plots based on the LC-MS dataset showing cluster patterns between the first two principal components (PC1 and PC2). Blue triangles and red diamonds represent samples from HT and IT, respectively, with their 95% confidence interval (shadowed regions). Needles at T1 in  $-ESI$  (a) and  $+ESI$  (b). Wood at T1 in  $-ESI$  (c) and  $+ESI$  (d). Needles at T2 in  $-ESI$  (e) and  $+ESI$  (f). Wood at T2 in  $-ESI$  (g) and  $+ESI$  (h).

On the other hand, the distribution of wood samples showed a complete overlap of IT samples with that of HT between PC1 and PC2 in both ionization modes, with 35.8% of the explained data variance for  $-ESI$  and 51.1% for  $+ESI$  (Figure 2-2c,d). This indicates that metabolic activity in wood tissues remains unchanged.

The chemical nature of features significantly up-regulated or down-regulated in the needles at the onset of the infestation, relevant to discriminate between

group labels (IT and HT), were identified using the OPLS-DA model (Figure 3-2).

As expected, the scores plot showed perfect separation between the two classes in both acquisition modes (Figure 3-2 **a,b**). The results of the random permutation test of class labels with internal leave-*n*-out cross-validation showed  $Q^2=0.98$  and  $R^2Y=0.987$  for -ESI, and  $Q^2=0.984$  and  $R^2Y=0.992$  for +ESI, and with complete separation between original model statistics and distribution statistics for all permutations (Fig. S2-2a,b). This demonstrates a good assessment of the statistical quality of the model, indicating consistency between predicted and original data ( $Q^2$ ), with a good degree of model fit to data ( $R^2Y$ ).



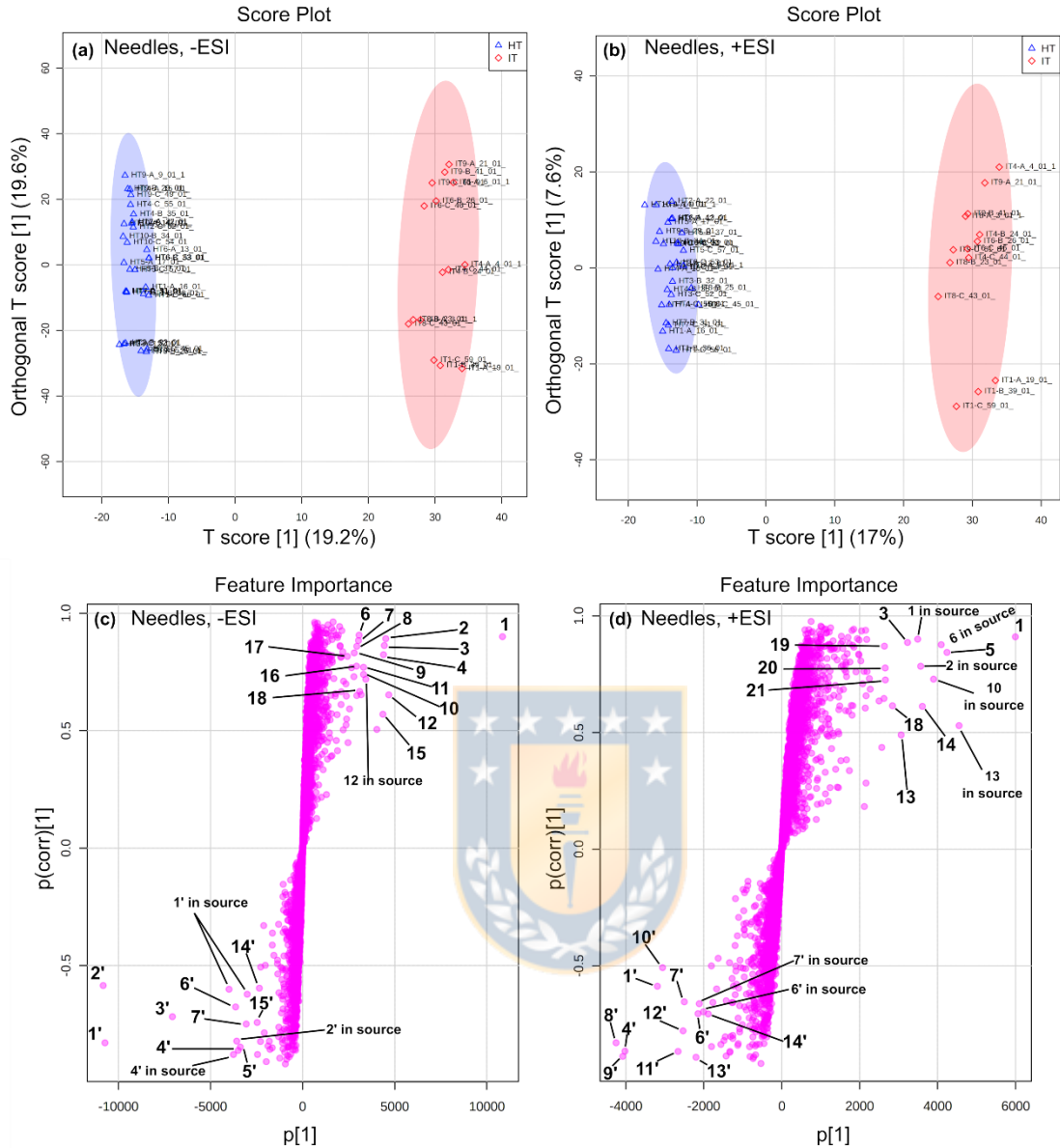


Figure 3-2: OPLS-DA model based on LC-MS datasets obtained from *P. radiata* needle leaves collected at T1. Scores plots showing separation of samples labeled as healthy (HT, blue triangles) and infested (IT, red diamonds) trees with their 95% confidence intervals (shadowed regions) for -ESI (a) and +ESI (b) acquisition modes. This is a regression method to find a relationship between data tables represented by X, the LC-MS data, and Y, a binary vector with the value 0 for HT class and 1 for IT class. The Y-predictive component (T score [1]) for variation in the dataset correlated to class separation is shown on the x-axis, while the orthogonal component that refers to uncorrelated variation for class separation is shown on the y-axis. S-plots showing significant features with their numbers assigned according to

Table 1-2 for  $-ESI$  (c) and  $+ESI$  (d), indicating features fragmented in the ion source as “in source”. The S-plots visualize the features’ influence in the predictive component of the model, combining the covariance ( $p[1]$ ) and correlation ( $p(\text{corr})[1]$ ) loading profiles. Covariance plotted on the x-axis visualizes the contribution to the predictive component, while correlation plotted on the y-axis spans between  $\pm 1$  as the reliability has a theoretical minimum of  $-1$  and a maximum of  $+1$  to predict the class 1 (IT). In this way, variables/features visualized toward the right-hand side contribute to class separation by high correlation with label IT [ $Y = 1$ ] and the opposite. Thus, significant metabolites were selected based on the combined high covariance ( $> |2000|$ ) and high correlation ( $> |0.5|$ ). Quantitative data for significant metabolites are presented in Fig. S4 and S5.

The S-plots of the OPLS-DA models provide the most relevant features (metabolites) to distinguish between infested and healthy trees. Figure 3-2c,d show S-plots of OPLS-DA models derived from needle datasets acquired in both ionization modes. Each data point in the S-plot represents a specific feature ( $m/z$ ;  $R_t$  pair), being those located at the end of both sides of the “S” that contributes most to class distinction. Thus, features located at the right end are correlated with infested trees (IT), and the metabolites they represent are up-regulated or occurring *de-novo*. In contrast, features at the left end are correlated with healthy trees (HT), representing their down-regulation in needles after infestation. Full chemical data for each significant metabolite are given in Table 1.

We found that 21 metabolites were significantly up-regulated in *P. radiata* needles following the initiation of infestation by *S. noctilio* (Figure 3-2 c,d).



The major classes of metabolites were flavonoids and lignans, each of which includes five. Flavonoids were identified as three glycosylated flavonols (**2**, **10**, and **18**), a flavan-3-ol (**1**), and a proanthocyanidin (**3**) (Table 1-2). Lignans were identified as a classical lignan (**6**) and four oxyneolignans (**9**, **15**, **17**, and **21**). These were followed by three amino acids (**5**, **13**, and **19**), two carboxylic acids of the citrate cycle (**4** and **12**), two sugar alcohols (**14** and **20**), an acetophenone glycoside (**7**), an iridoid-type monoterpenoid (**8**), a potential auxin (hydroxy indole-3-yl)-lactate glycoside (**11**), and an ascorbic acid glycoside (**16**).

Meanwhile, additional 15 metabolites were down-regulated in needles (Figure 3 **c,d**). These were identified as two cyclitol carboxylic acids of the shikimate pathway (**1'** and **2'**), two acetylated flavonol glycosides (**6'** and **7'**), two hydroxybenzoate (**5'** and **8'**), two dicarboxylic acids (**4'** and **11'**), two amino acids, one of which is an oligopeptide (**12'** and **13'**), ascorbic acid (**3'**), a vitamer of vitamin B6 (**10'**), a phenylpropanoid glycoside (**14'**), a lignan glycoside (**15'**), and an unknown substance (**9'**).

#### **4.2 Biomarker model evaluation for early diagnosis of infestation**

All the above metabolites were tested for their biomarker quality by using the receiver operating characteristic (ROC) curve-based approach, which provided a measure of their ability to diagnose trees as being infested by *S. noctilio* (Chong et al., 2019). Individual ROC curves are shown in Fig. S2-3. However,

given the diversity of metabolic pathways involved in the tree response judged by the different chemical families of the above-mentioned metabolites, a more integrative ROC-based tester was used. In this case, a combination of the up-regulated metabolites immediately after the woodwasp attack (**1 – 21**) was set up to create a biomarker model, testing their joint ability to predict classes for new samples without a class label (Figure 4-2).

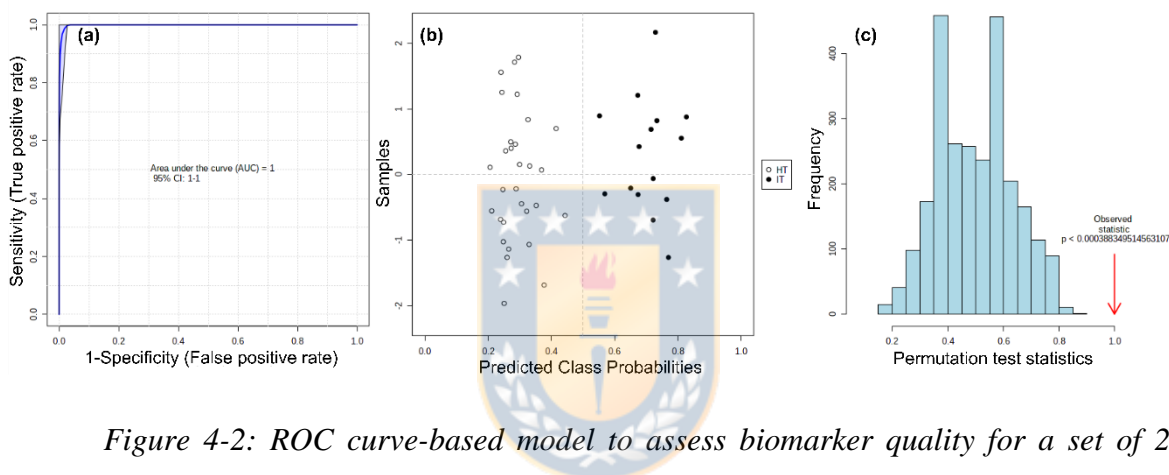


*Figure 4-2: ROC curve-based model to assess biomarker quality for a set of 21 metabolites up-regulated in *P. radiata* needles after initial infestation by *S. noctilio* at T1. ROC curve plot for the created biomarker model showing on the x-axis the highest possible specificity (false-positive rate) and the y-axis the highest sensitivity (true-positive rate) with the 95% of confidence interval, contributing to the maximum area under the curve, AUC = 1 (a). Plot of predicted class probabilities for each sample using the created biomarker model showing classification boundary at the center ( $x = 0.5$ ) and a perfect separation between HT (white circles) and IT (black circles) samples (b). Permutation test for model validation presented as a histogram using the predictive accuracy of the model as a measure of performance, showing the AUC distribution for all permutations (in blue) and the distribution for the original model (red arrow), along with the empirical p-value (c).*

The ROC curve of the created biomarker model showed very good performance, with the maximum possible value of the area under the curve, AUC=1.0 (Figure 4-2a). This means that the best sensitivity and specificity were achieved with such a combination of metabolites, which is even more evident in the plot of the predicted class probabilities for all samples using this created model (Figure 4-2 b). In this case, the model worked blind with no class label for all samples, grouping them into two clusters separated by the classification boundary at  $x=0.5$  (center), corresponding to their actual origin, healthy or infested.

Results of the random permutation test, presented as a histogram using the predictive accuracy of the created model as a measure of performance (Figure 4-2c), showed 0% overlap between the AUC of the original model (observed statistic, in red) and the AUC distribution of the model based on all permutations (in blue), indicating a significantly higher  $R^2$  (model efficiency) for the original model, with an empirical  $p$ -value  $<0.0003$  for 100 permutations. These confirmed the ability of a biomarker model based on the combination of the 21 up-regulated metabolites to diagnose early infestation by *S. noctilio* in *P. radiata* trees.

### 4.3 Long-term metabolome changes

To monitor the metabolic performance of pine a while after the onset of infestation by *S. noctilio*, the same trees were sampled three months later during the winter season (T2) despite scarce greenish needles being found at this time in the foliage of IT individuals. After processing the raw LC-MS data and generating bucket tables, 4926 and 5378 features were detected in needles for –ESI and +ESI modes, respectively. For wood samples, 2750 (–ESI) and 1616 (+ESI) features were detected.

In contrast to the completely overlapping pattern between the wood samples of HT and IT at T1, the exploratory analysis with PCA models at T2 suggested differentiation of their metabolomes (Figure 3-2g,h). Two defined clusters were observed in the scores plots between PC1 and PC2, which accounted for a total explained variance of 56.1% and 36.2%, for –ESI and +ESI, respectively.

As with needles at T1, features relevant for the variation in wood metabolome between HT and IT individuals were collected from the OPLS-DA models. The S-plot for the –ESI-derived data suggested that metabolism in wood tissues is being significantly down-regulated by long-term infestation (Figure 5-2c). Although some features appear to be up-regulated (in the upward and right end direction, Figure 5-2c), they are much less important for class distinction. This is consistent with the S-plot obtained from the +ESI dataset, although a much

smaller number of features with lower significance were detected (Figure 5-2d). Cross-validation of the permutation tests for the latter model indicates a not very good statistics quality assessment, with a lower agreement between the predicted and original data ( $Q^2=0.894$ ) and with an overlap between the statistics of the original model and the permutation distribution (Fig. S2-2d). In contrast, the discriminant model built from the –ESI data was successfully validated (Fig. S2-2c). Therefore, presenting results regarding wood metabolome changes is focused on statistical models obtained from the –ESI acquisition mode.

Ten metabolites were significantly down-regulated in the *P. radiata* wood after three months of infestation (Figure 5-2c,d). They were annotated as three oligosaccharides (**16'**, **18'**, and **21'**), three flavonoids (**1**, **3**, and **22'**), two lignans (**17'** and **19'**), cyclitol carboxylic acid (**1'**), and hydroxycinnamic acid glycoside (**20'**). Three up-regulated metabolites, although of lesser significance for class distinction, were also annotated as flavanone (**22**), dicarboxylic acid (**23**), and sugar alcohol (**24**).

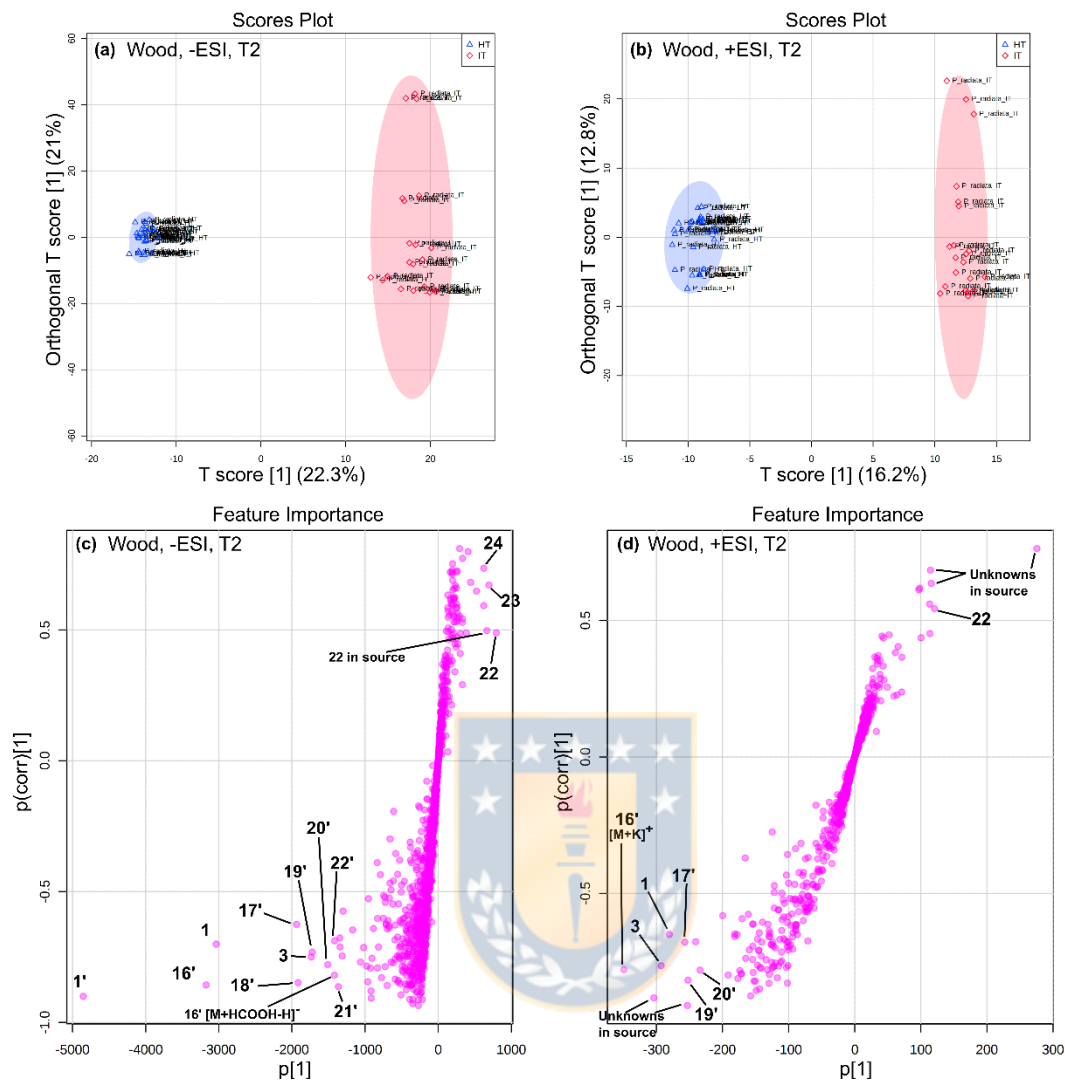


Figure 5-2: OPLS-DA models based on LC-MS datasets obtained from wood of *P. radiata* at T2. Scores plots showing separation of samples labeled as healthy (HT, blue triangles) and infested (IT, red diamonds) trees with their 95% confidence intervals (shadowed regions) for  $-ESI$  (a) and  $+ESI$  (b) acquisition modes. The Y-predictive component (T score [1]) for variation in the dataset correlated to class separation is shown on the x-axis, while the orthogonal component that refers to uncorrelated variation for class separation is shown on the y-axis. S-plots showing significant features with their numbers assigned according to Table 1-2 for  $-ESI$  (c) and  $+ESI$  (d), indicating atypical adduct ions and features fragmented in the ion source as “in source”. The S-plots visualize the features’ influence in the predictive component of the model, combining the covariance ( $p[1]$ ) and

*correlation (p(corr)[1]) loading profiles. Covariance plotted on the x-axis visualizes the contribution to the predictive component, while correlation plotted on the y-axis spans between  $\pm 1$  as the reliability has a theoretical minimum of -1 and a maximum of +1 to predict the class 1 (IT). In this way, variables/features visualized toward the right-hand side contribute to class separation by high correlation with label IT [ $Y = 1$ ] and the opposite. Thus, significant metabolites were selected based on the combined high covariance set at |1500| and |200| for -ESI and +ESI, respectively, and high correlation ( $> |0.5|$ ). Quantitative data for significant metabolites are presented from Fig. S8-2.*

The needle metabolome remains altered for IT individuals at T2, as shown by the PCA scores plots where class-specific clusters are clearly defined (Figure 3-2e,f). According to the validated OPLS-DA models (Figure 6-2 and Figure S2-2e,f), eight metabolites were significantly up-regulated in needles. Six of them (**1**, **3**, **4**, **11**, **13**, and **21**) were up-regulated from the beginning of the infestation, while the other two (**25** and **26**) appeared as significant for the first time (Table 1-2). Of the latter two, metabolite **25** was identified as an isomer of **11** (potential auxin glycoside), probably differing in the position of glycosylation. While compound **26** remains unknown.

Of the fifteen metabolites found to be down-regulated in needles at the beginning of infestation (T1), nine (**1'-4'**, **6'**, **8'**, **9'**, **11'**, and **13'**) are still significant at T2 (Figure 6-2c,d). In addition, another three carbohydrate metabolites (**16'**, **18'**, and **21'**) were significantly down-regulated for the first

time. Interestingly, these three compounds, along with **1'**, were also down-regulated in wood at T2.

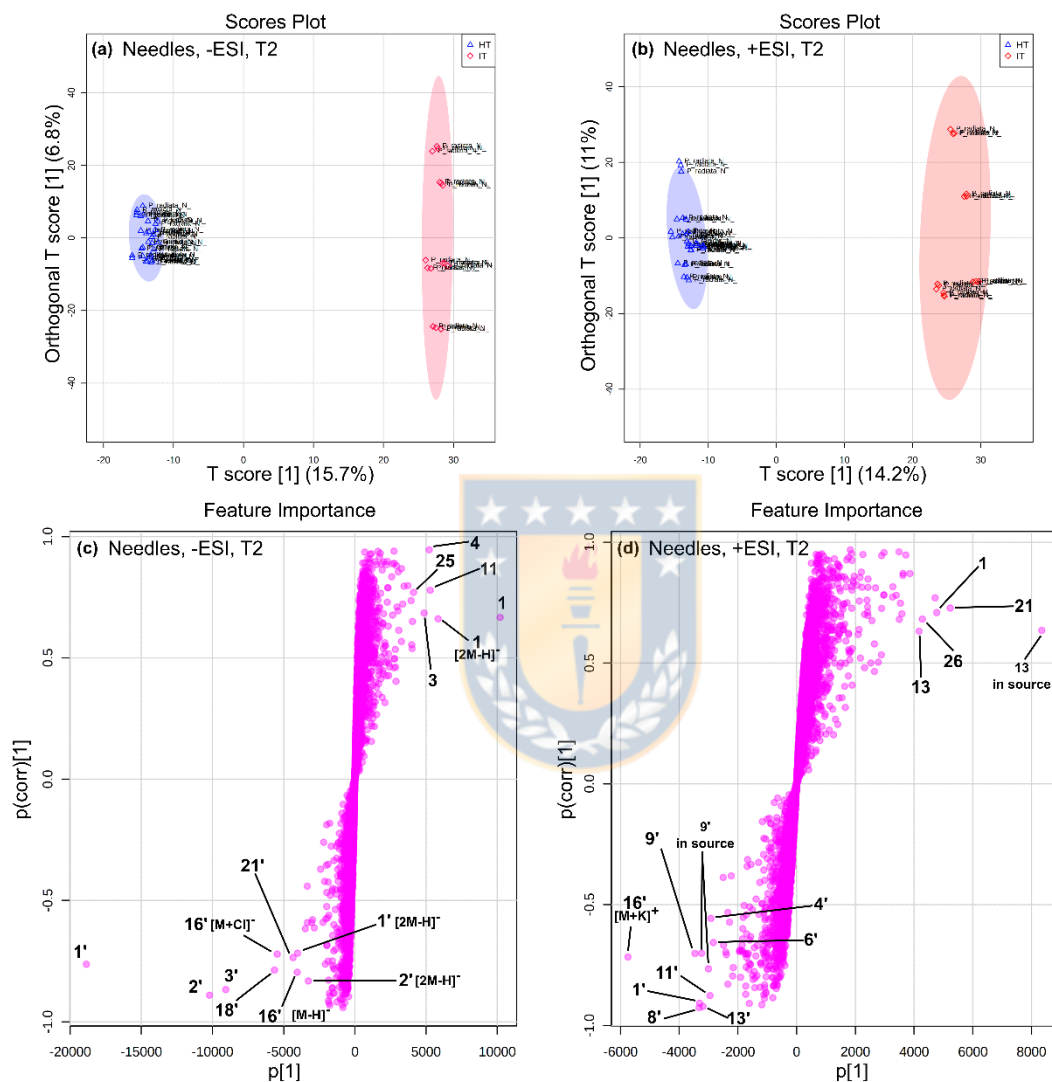



Figure 6-2: OPLS-DA models based on LC-MS datasets obtained from needles of *P. radiata* at T2. Scores plots showing separation of samples labeled as healthy (HT, blue triangles) and infested (IT, red diamonds) trees with their 95% confidence intervals (shaded regions) for  $-ESI$  (a) and  $+ESI$  (b) acquisition modes. The Y-predictive component (T score [1]) for variation in the dataset correlated to class separation is shown on the x-axis, while the orthogonal component that refers to uncorrelated variation for class separation is shown on the y-axis. S-plots showing significant



features with their numbers assigned according to Table 1-2 for  $-ESI$  (c) and  $+ESI$  (d), indicating atypical adduct ions and features fragmented in the ion source as “in source”. The S-plots visualize the features’ influence in the predictive component of the model, combining the covariance ( $p[1]$ ) and correlation ( $p(corr)[1]$ ) loading profiles. Covariance plotted on the x-axis visualizes the contribution to the predictive component, while correlation plotted on the y-axis spans between  $\pm 1$  as the reliability has a theoretical minimum of  $-1$  and a maximum of  $+1$  to predict the class 1 (IT). In this way, variables/features visualized toward the right-hand side contribute to class separation by high correlation with label IT [ $Y = 1$ ] and the opposite. Thus, significant metabolites were selected based on the combined high covariance ( $> |2000|$ ) and high correlation ( $> |0.5|$ ). Quantitative data for significant metabolites are presented from Fig. S6-2 and S7-2.

Additional chemical defense triggered in foliage after the *S. noctilio* infestation is reported in Note S2-2.

## 5. DISCUSSION



Metabolomics results presented here reveal the biochemical response of the downstream definitive cellular function expressed in needle and wood tissues of *P. radiata* following infestation by the woodwasp *S. noctilio*. As the needle’s metabolome rapidly responds to the woodwasp attack, an overall integral view of the primary and specialized metabolism pathways that most significantly changed in this organ is presented in Figure 7-2. However, only those metabolic changes that were considered highly relevant to this study are discussed below.

As described above, from the 21 metabolites most significantly up-regulated in needles immediately after infestation, the flavonoid family is one of the two

most numerous groups, with five total metabolites (**1-3**, **10**, and **18**). Phenylpropanoid pathway is therefore systemically activated, providing key precursors for boosting flavonoid biosynthesis after converting Phenylalanine into *p*-coumaroyl-CoA (Figure 7-2) (Ferrer et al., 2008b).



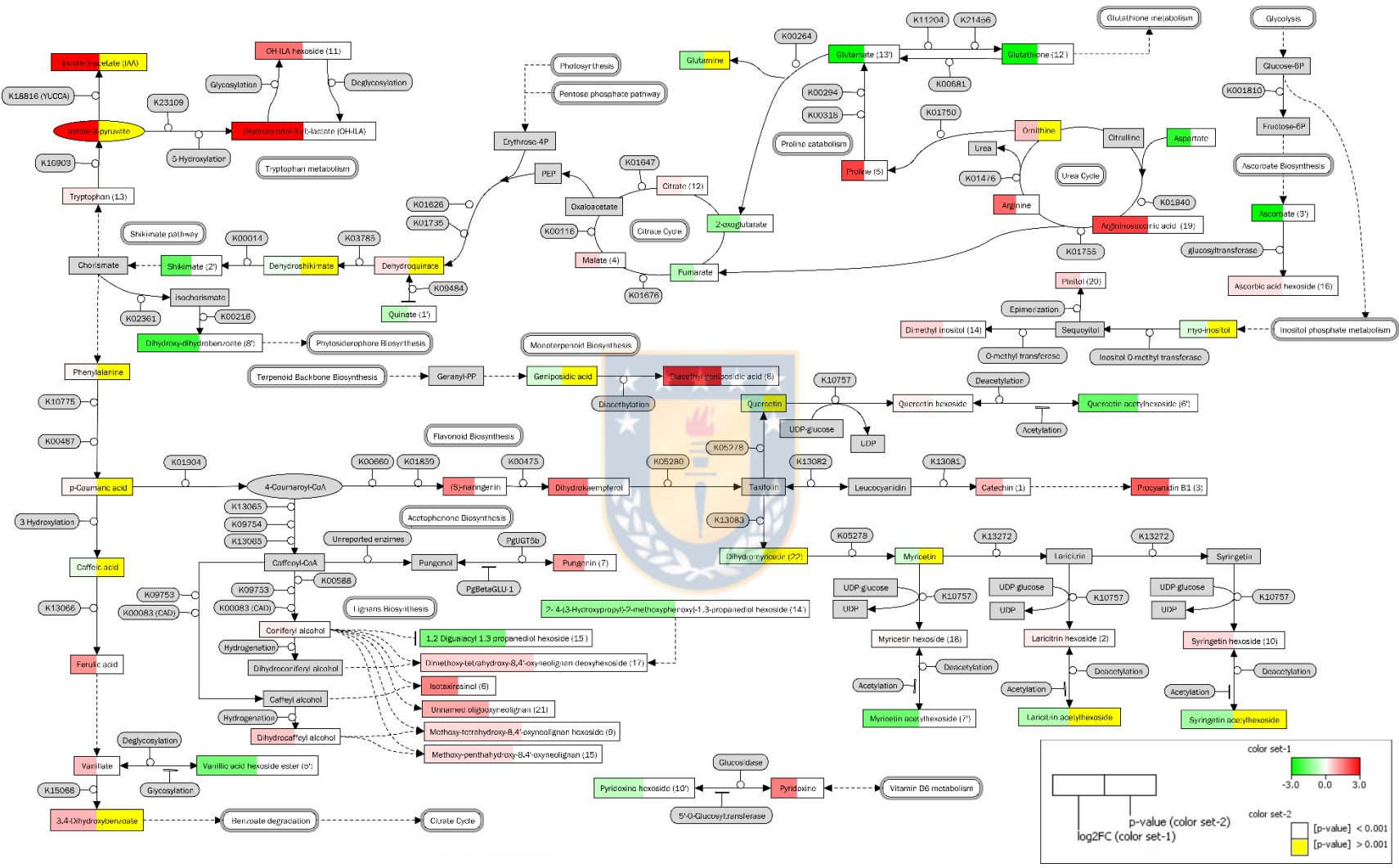


*Figure 7-2: Scheme for the pathway analysis of changes systemically induced in the metabolome of *P. radiata* needles immediately after infestation by *S. noctilio*. Metabolite nodes are shown as rectangles with annotated names and assigned numbers where available. Colour set-1 refers to expression data according to  $\log_2FC$ , where  $FC = IT/HT$ , and  $IT/HT$  is the average intensity ratio for the metabolite, and with the scale adjusted between -3 and 3 for ease of interpretation. Colour set-2 shows statistical significance in a t-test, where white indicates significant ( $p < 0.001$ ) and yellow not significant ( $p > 0.001$ ). Metabolites filled in grey were not detected. Enzymes involved in specific transformations are shown as rounded rectangles, labeled, if possible, with their KEEG Ortholog number (KO). Downstream transformation pathways are shown as rounded grey rectangles. Dashed lines indicate known metabolic pathways containing several conversion steps or proposed ones.*



Catechin (**1**) and procyanidin B1 (**3**) were significantly overexpressed in needles throughout the infestation with 1.75-fold and 3.80-fold at T1 and 1.33-fold and 2.49-fold at T2, respectively (Figure 7-2 and Table S1). However, they were among the metabolites most strongly down-regulated in wood at T2 (Figure 6-2**c,d**). According to the mechanism of *S. noctilio* pathogenicity in *P. radiata*, large areas of dried sapwood are forming around a fungus-infested area, which is in turn surrounded by a polyphenol barrier mainly formed by stilbenes like pinosylvin. No evidence of such barrier was detected in trees that did not survive the infestation, which is attributed to the translocation failure through the trunk vascular tissues (Coutts, 1969a, 1969b; Hillis and Inoue, 1968). In our case, all monitored infested trees died 33 weeks after the first sampling, suggesting such translocation impediment as the reason for the dropping levels of **1** and **3** in the wood. Although pinosylvin along with other stilbenes were detected in the wood metabolome, their levels were not significantly changed throughout the infestation (Table S1-2 and Fig. S9-2).

However, the role of **1** and **3** seems to be other than transport into the wood to overcome the fungal infection, most of all because spreading of fungal colonization is rather unlikely at the infestation onset. In a physiological and proteomic integrated response study in needles to extreme UV radiation

conducted in *P. radiata* seedlings, Pascual and co-workers described the increased expression of key enzymes for flavan-3-ols biosynthesis, suggesting their photoprotective function (Pascual et al., 2017b). These were the Flavone 3-Hydroxylase (F3H, K00475) involved in the conversion of naringenin to dihydrokaempferol (Figure 7-2), and the Anthocyanidin Reductase (ANR) that convert cyanidin into epicatechin. Coincidentally, catechins accumulation was also found 3.72-fold increased after such UV exposure.

Although **1** and **3** absorb maximally at 279 nm and therefore offer protection against high energy UV radiation, the collected data from local climate stations registered a significant decrease in mean daily maximum UVB intensity (280-315 nm) from 3.20 kW h m<sup>2</sup> at T1 to 1.53 kW h m<sup>2</sup> at T2. Thus, their accumulation in needles can be explained as a response to the progressive loss of photosynthetic pigments (chlorosis) caused by the woodwasp venom (Donaldson & Williams, 2018), attenuating the penetration of solar UVB radiation into sensitive tissues, and reducing oxidative damage due to the generation of reactive oxygen species (ROS) (Agati & Tattini, 2010).

The other three flavonols (**2**, **10**, **18**) may be involved, at least partially, in the same mechanism of photoprotection, although they seem to be generated from the cleavage of corresponding phytoanticipins. The levels in needles of **2**

(1.16-fold), **10** (1.36-fold), **18** (1.05-fold), and even that of quercetin hexoside (1.11-fold), were increased in parallel with deacetylation of their acetyl derivatives laricitrin acetylhexoside (0.55-fold), syringetin acetylhexoside (0.48-fold), **7'** (0.31-fold), and **6'** (0.29-fold), respectively (Figure 7-2 and Table S1-2). Presumably, this group of acetyl derivatives is present in pine needles as phytoanticipins, which are converted to more polar substances after infestation to facilitate their transport to target tissues. However, these flavonols maximally absorb at about 355 nm, which means that they are not UVB but UVA-absorbing pigments. The potential function of them during an infestation, besides their well-known antioxidant properties (Note S1), may be related to the ample evidence supporting the role of flavonols as endogenous regulators of auxin transport in plants (Jacobs & Rubery, 1988; Peer & Murphy, 2007; Agati & Tattini, 2010; Buer et al., 2010). They act similarly to naphthylphthalamic acid (NPA), inhibiting polar auxin transport (PAT) by binding to the NPA-receptor in the plasma membrane, which blocks the polar efflux step and causes net auxin accumulation in transporting cells (Jacobs & Rubery, 1988). Together with flavonols **2**, **10**, and **18**, naringenin was also up-regulated (2.75-fold) at the beginning of infestation (Figure 7-2, Table S1-2). It is a precursor of flavonoids that was, in addition, reported affecting the auxin

transport levels when sprayed onto the shoot apex of *Arabidopsis transparent testa* mutant (*tt4*) seedlings lacking chalcone synthase (CHS, K00660), a key enzyme for flavonoid biosynthesis (Peer *et al.*, 2004). Three months later, none of them were highly significant, although **2**, **10**, and naringenin remain slightly up-regulated in needles (Table S1-2).

The function of flavonols as endogenous PAT regulators during the infestation responds to the need to control the transport of the high auxins content accumulated in needles at T1. This includes indole-3-acetate (IAA, 11.0-fold), the potential auxin (hydroxy indole-3-yl)-lactate (OH-ILA, 11.4-fold), and its glycoside **11** (3.14-fold) (Figure 7, Table S1) and is consistent with the previous suggestion that flavonols affect PAT in apical tissues by modulating the amount of auxin loaded into the long-distance PAT stream (Peer & Murphy, 2007). All these could therefore be interpreted as a tolerance mechanism compensating for the chlorosis and premature senescence of needles observed as initial symptoms in infested *P. radiata* trees, promoting faster development of new shoots and young needles.

It seems that the role of auxins in plant tolerance is obvious; nevertheless, in this case, several interesting correlations were found between them that deserve attention. After three months of long-term infestation, IAA remains at nearly



identical levels of 11.1-fold up-regulated, whereas the accumulation in needles of **11** and its isomer (**25**) nearly doubled, from 3.14-fold at T1 to 6.0-fold at T2, and from 3.46-fold at T1 to 6.6-fold at T2, respectively. This, together with the decrease in OH-ILA by almost half, from 11.4-fold at T1 to 5.8-fold at T2 (Table S1), may suggest inactivation of the latter by glycosylation. Further studies are needed to help understand the specific physiological function and regulation of this potential auxin, as well as why its levels decline while those of the major auxin, IAA, remain the same.

Regarding tolerance against premature senescence, an apparent link to proline (**5**) metabolism was found. Proline was classified as one of the most prominent up-regulated metabolites at T1, over-expressed by 4.72-fold (Figure 7, Table S1). After three months of infestation at T2, its levels dropped by almost half (2.54-fold) (Table S1-2), being no more significant. This may suggest that proline catabolism occurs at T2, where it is oxidized to glutamate, which enters to tricarboxylic acid cycle (TCA). Indeed, glutamate (**13'**) still appears to be significantly down-regulated at T2 (Figure 6-2d), although its level appears double from a 10-fold decrease at T1 to a 5-fold decrease at T2, in proportion to the decrease in proline (Table S1). Increased levels at T2 were also found for glutathione (**12'**) (in 14.9-fold), glutamine (in 4.5-fold), fumarate

(in 0.6-fold), and malate (4) (in 0.49-fold) (Table S1-2). Coincidentally, cut roses (*Rosa hybrida*) have previously been reported to have elevated proline levels during senescence, followed by a 50% decrease when petals are fully aged (Kumar *et al.*, 2009). Consequently, 5 mM proline was applied exogenously, observing the extent of the vase life by 30% due to delaying senescence of petals (Kumar *et al.*, 2010), which have been suggested to occur by preventing ATP depletion (Zhang & Becker, 2015).

Unlike flowers, leaves obtain energy from photosynthesis, even in the last stages of senescence. Proline is therefore not originally needed as an energy source, so its oxidation occurs for other reasons. Oxidation of proline is catalyzed by two mitochondrial enzymes, flavin-dependent proline dehydrogenase (PRODH, K00318) and NAD<sup>+</sup>-dependent 1-pyrroline-5-carboxylate dehydrogenase (P5CDH, K00294), yielding about 30 ATP units through coupling to the mitochondrial electron transport chain (Zhang & Becker, 2015). More recently, the role of proline oxidation during senescence has been investigated, suggesting that glutamate and energy generation occur to be then exported to tissues and sink organs, finding additional evidence that suggested proline as an alternative substrate for mitochondrial respiration (Launay *et al.*, 2019). All this is quite consistent with our case, since chlorotic

needle cells in infested trees still have an energy demand that cannot be fully supplied by degraded photosynthetically active chloroplasts, being alternatively supplied by proline oxidation in mitochondria. Thus, it can be thought that the up-regulation of proline represents a tolerance mechanism that prolongs the life of infested trees, allowing them to maintain important biochemical processes in needles while the photosynthetic systems are progressively degraded.

Together with the auxin pathway activation, additional and dramatic changes in needles metabolome simultaneously happened, which most likely compromised trees long-term survival. The most dramatic decrease in the level of any metabolite in needles after infestation was for ascorbate (**3'**). Its content decreased more than 90-fold compared with the original value in healthy trees at T1 (Table S1-2). This is a clear indicator of the magnitude of oxidative stress that trees are likely to encounter during an infestation, which is particularly severe at the very beginning of the *S. noctilio* attack. One would therefore expect to detect at least some increase in the concentration of substances that are products of ascorbate oxidation, such as dehydroascorbate (DHA) (Heber *et al.*, 1996; Smirnoff, 2018). Although not comparable to the magnitude of the observed ascorbate down-regulation, DHA levels in needles at T1 increased 1.47-fold. In parallel, ascorbate hexoside (**16**) was among the significantly up-

regulated metabolites at T1 (1.25-fold) (Figure 7-2, Table S1-2). This is intriguing because it is not an oxidation product of ascorbate, but a derivative that stabilizes ascorbate against oxidation (Smirnoff, 2018).

Such a marked decrease in ascorbate concentration in needles at the beginning of infestation may be partly due to the need to remove  $H_2O_2$  generated not only by photosynthetic electron transport and photorespiration but also by the previously mentioned proline catabolism in mitochondria. Proline catabolism generates  $H_2O_2$  as a by-product that activates antioxidant signaling pathways (Zhang & Becker, 2015). Additionally, it also seems consistent that progressive loss of chlorophylls and desiccation in chlorotic needles may cause damage to photosystems through inactivation of the oxygen-evolving complex. Consequently, the incorporation of ascorbate present in the thylakoid lumen into the electron transport chain of photosystems is induced, thus offsetting water deficiency and harnessing its well-known electron donor property (Tóth et al., 2009, 2011). Three months after the beginning of infestation, a replenished trend of ascorbate levels in needles was observed, dropping in this case by only 3.13-fold (Table S1-2). However, this observation must be interpreted with caution, because at this time in most of the monitored trees the vast part of the old leaves had already been lost due to premature

senescence and desiccation, and thus the collected samples consisted at this time only of the remaining younger greenish needles.

In addition to ascorbate, glutathione levels (**12'**) also suffered a drastic drop among infested trees at T1 (by 17.5-fold) (Figure 7-2, and Table S1). As premature senescence in *P. radiata* infested tree has been explained as a physiological response to toxin removal from woodwasp venom (Fong & Crowdent, 1973b), glutathione consumption can be primarily understood as part of such detoxification mechanism. It is known that through the action of glutathione-S transferases, glutathione in plants can conjugate with xenobiotic substances to detoxify them (Gullner et al., 2018a; Heldt & Piechulla, 2021). However, further evidence is needed to uncover a potential conjugation between glutathione and some components of the woodwasp venom capable of migrating from the *S. noctilio* oviposition site in the trunk through the xylem to the needles, for example, the glycopeptide noctilisin (Bordeaux et al., 2014b).

Additionally, the acute decrease in glutathione levels at T1 may indicate, once again, the magnitude of the oxidative stress faced by the infested trees at the beginning of the infestation. Metabolite **12'** is a reduced form of glutathione (GSH), which normally functions as an antioxidant in plant cells, where it is oxidized to its disulfide derivative (GSSG) to quench ROS or even reduce DHA

to regenerate ascorbate (Gullner et al., 2018; Heldt and Piechulla 2021; Noctor et al., 2012). After three months of infestation (T2), a glutathione deficit persists, although this appears to have been replenished in 14.9-fold (Table S1). However, this fact must be interpreted with caution because the same reasons as stated above for the ascorbate case may influence this result. Either way, this is a clear indication that GSH-GSSG balance was never restored after infestation, which may have dire consequences for redox homeostasis. Moreover, the role of glutathione in plant development is also well understood (Noctor *et al.*, 2012), so the survival of infested trees under its permanent deficit for an extended period seems quite unlikely.

There were also changes in the pine metabolome that suggested a resistant response. It is explained by the overexpression of lignans **6**, **9**, **15**, **17**, and **21** in needles of infested trees at T1 (Figure 7-2), which may be associated with a direct defense response against fungal infection. In a previous phylogenetic study conducted on *Populus trichocarpa*, the expression of five cinnamyl alcohol dehydrogenase (CAD/CAD-like) genes were significantly induced in stem or leaves after inoculation with three fungal pathogens of different lifestyle and pathogenicity (Bagniewska-Zadworna *et al.*, 2014). CAD enzymes (K00083) catalyze the conversion of various cinnamaldehyde to their

corresponding alcohols, a key final step in lignan biosynthesis (Figure 7-2), as well as the formation of lignin bound to secondary cell walls (Möller *et al.*, 2006). Despite the obvious importance of CADs on plant development, the up-regulation of lignans **6**, **9**, **15**, **17**, and **21** after infestation by *S. noctilio*, which also includes colonization of woody tissues by the fungal symbiont *A. areolatum*, may add evidence for a further defensive function of CADs in *P. radiata*.

After three months of infestation, oxyneolignans **9** (1.42-fold), **15** (1.47-fold), **17** (1.65-fold), and **21** (2.86-fold) remain up-regulated in needles, the last being the most significant, increased nearly 1.0-fold. This compound has the highest molecular weight ( $m/z$  617.2593 [M-H]<sup>-</sup>), which may indicate a tendency toward polymerization, although it is still an oxyneolignan. These metabolites could function as antifungal agents, with the ability to form a physical barrier that could block the spread of *A. areolatum* in the wood if transported from needles to affected tissues, or at least synthesized *in-situ*. However, lignans very similar to **17** and **15**, but with pentose instead of a deoxyhexose (**17'**), and glycosylated with pentose (**19'**), respectively, were found significantly down-regulated in wood at T2 (Figure 5-2 **c,d** and Table 1-2). This may indicate that they are metabolized into other undetected

substances. However, this, together with the fact that none of the oxyneolignans synthesized in the needles were up-regulated in the wood, reiterates the aforementioned and previously suggested lack of translocation in non-resistant trees (Coutts, 1969a, 1969b; Hillis and Inoue, 1968). The evidence presented here may therefore suggest that such a polyphenol barrier observed in the wood of resistant trees, maybe formed mainly by oxyneolignans or their transformed derivatives rather than by stilbenes.

## 6. CONCLUSIONS

This work evidenced the usefulness of metabolomics for revealing the fundamental role of plant chemical defense that determines their interactions with insects. Metabolomics approach based on LC-MS dataset used in this case for the study of pine response to the woodwasp *S. noctilio* infestation, uncovered for the first time the ultimate induced downstream products of the cellular biochemical function expressed in needles and wood tissues. The adopted research strategy provided direct evidence for the expression of specific upstream gene products involved in most relevant metabolic processes described for primary and specialized metabolism. Upon infestation, the phenylpropanoid pathway is immediately activated, supplying the necessary precursors for flavonoids biosynthesis, especially to overexpress catechins that



may protect needles from the damage of UVB radiation given the progressive chlorophylls losses caused by the woodwasp injected venom. The huge overexpression of auxins registered in needles throughout the infestation suggested a tolerance process in response to the premature senescence induced in most foliage by the woodwasp venom. Accordingly, a role of polar auxin transport endogenous regulator was attributed to the overexpressed flavonols at the beginning of the infestation, given the need for inhibiting auxin efflux from transporting cells and promoting development in affected needles. In the same line, trees accumulated proline in the first stage of infestation to presumably be then catabolized to fuel mitochondrial respiration, supplying the energy demand in chlorotic needles that may not be fully provided by degraded chloroplasts, delaying the final senescence. However, such a tolerance deployed mechanism is apparently countered by the critical oxidative stress that trees must face throughout the infestation. This prevented replenishing the levels of key antioxidants such as ascorbate and glutathione in the long term, which could negatively impact redox homeostasis, compromising tree survival. Revealing the whole picture of the biochemical response in pine to the woodwasp infestation is essential for understanding this interaction, pointing to new targets for innovation in breeding programs for resistant plant production. Therefore,

future breeding programs may take advantage of findings reported in this study for genotype selection with the highest possible capability of tolerating infestation by *S. noctilio*.


## 7. EXPERIMENTAL

### 9.306 General experimental procedures

Metabolomics analysis was performed by LC-MS/MS on an ultra-high performance liquid chromatography system (Elute UHPLC, Bruker Daltonik GmbH, Bremen, Germany) equipped with a diode array detector (Elute DAD) and coupled in tandem with a quadrupole-time-of-flight mass spectrometer equipped with an atmospheric pressure electrospray ion source (Compact ESI-QTOF, Bruker Daltonik GmbH, Bremen, Germany). Chromatographic separation was performed on a Kinetex C18 UHPLC column (100 mm length × 3 mm id, 1.7 μm particle size, Phenomenex) using a SecurityGuard Ultra Cartridge UHPLC C18 3.0 mm length pre-column and maintained at 30°C. Acetonitrile hypergrade for LC-MS, water LC-MS grade, methanol gradient grade, formic acid MS-grade (98-100%), and chloroform for liquid chromatography were purchased from Merck (Darmstadt, Germany). Compass HyStar 4.1 software (Bruker Daltonik GmbH, Germany) was used for data

acquisition. MetaboScape 3.0 software (Compass, Bruker Daltonik GmbH, Germany) was used for data processing, bucket table generation, and statistical model interactive visualization. Grounding of plant material and homogenization, and metabolome extraction, was performed in a ball mill Retsch MM-400 (GmbH, Haan, Germany). Solvents were evaporated in a vacuum centrifuge (Concentrator plus, Eppendorf, Hamburg, Germany).

## **7.2 Origin of plant material and sampling.**



Plant material was collected from a 14-year-old unmanaged stand of *Pinus radiata* D. Don (Pinaceae) belonging to commercial plantations of Forestal Mininco Co. It was located in an area of *S. noctilio* high incidence (Ide et al., 2018a), in the central valley of Chile, north of San Nicolas city, in the Ñuble Region (36°26'18.0"S 72°14'32.0"W). Identification of trees in the early stage of infestation by *S. noctilio* was confirmed by visual inspection of the main reported symptoms, which usually appear two weeks after the attack. These include several oviposition holes in the trunk with oleoresin exudation and wilting chlorotic needles in the crown (Fig. S1-2) (Bordeaux & Dean, 2012b). Ten infested trees (IT) were randomly selected within the stand, together with

another ten healthy trees (HT) (without such symptoms throughout the period of this study) as closely as possible to each IT. These two groups were used to compare their metabolomes at each sampling point, three months apart. Thus, significant metabolic changes in Its can be attributed to a direct response to infestation, rather than to climatic or seasonal changes.

The first sampling, T1, was conducted on April 12 (fall) 2018. April marks the end of *S. noctilio* flight season in Chile, ensuring that HTs remain without attack throughout the sampling period. The second sampling (T2) was performed on July 12 (winter) 2018, when IT individuals still maintained greenish needles in their foliage. Finally, all monitored infested trees died after 33 weeks of the first sampling (T1). The climatic condition details of sampling days/months are reported in Methods S1-2.

Approximately 200 g of needles, representative of the upper third foliage, were collected from each tree with a pruning pole. Only alive needles were considered for Its. Wood samples containing vascular tissues were also collected from the trunk of each tree at a height of 1.5 m using an incremental borer. Immediately after collection, samples were immersed in liquid nitrogen, transported to the lab, and stored at  $-80^{\circ}\text{C}$  until needed.

### 7.3 Sample preparation and metabolome extraction.

Sample preparation and metabolome extraction for analysis was performed according to a previously described protocol with minor modifications (Valledor et al., 2014b). Briefly, frozen fresh samples (FFS) of needle and wood samples were cryogenically ground to a fine powder and homogenized using a ball mill at 30 Hz for 5 min. Before extraction, moisture content was determined for each sample by a thermogravimetric method to normalize its weight before the extraction. Samples were processed in triplicate within a complete randomized block for one sampling time (T1 or T2). For metabolome extraction, 800  $\mu$ l of cold (4°C) MeOH/H<sub>2</sub>O/CHCl<sub>3</sub> (2.5:0.5:1) were added to 100 mg (dry weight basis) of powdered FFS contained in a 2 ml microcentrifuge tube and shaken for 60 s at 30 Hz. A blank, consisting only of extraction solvent, in triplicate, was treated in the same manner and included in randomized blocks. Samples were then centrifuged at 13300 g for 10 min at 4°C and 600  $\mu$ l of the supernatants were transferred to new tubes for liquid-liquid extraction by adding more water and CHCl<sub>3</sub>, 400  $\mu$ l each, and shaking for 30 s at 20 Hz. After centrifuging at 13300 g for 5 min at 4°C, the two phases were clearly defined with a sharp interface. Hydrophilic (top layer) fractions were transferred to new

tubes, 600 µl each, and dried in a vacuum centrifuge, while bottom lipophilic fractions containing pigments and other lipophilic substances were discarded. Dried extracts were stored at -80°C until needed. In this way, ten biological replicates were considered per group (IT or HT) with three technical replicates per individual sample, resulting in a total of sixty extracts for analysis per randomized block (T1 or T2).

#### **7.4 LC-MS metabolomics analysis.**

Immediately before analysis, dried extracts and blanks were resuspended in 600 µl of cold (4°C) 80% methanol (in water, v/v), shaken for 30 s at 30 Hz, and centrifuged for 10 min at 13300 g and 4°C. Aliquots of 100 µl per sample were collected to form a pooled quality control (QC) sample. Blank, QC, and plant extract samples were then transferred to 200 µl inserts contained in 1.5 ml amber vials and placed in a liquid chromatography autosampler maintained at 4°C according to the predetermined random sequence. This started with three blank samples followed by six QC samples, and another QC sample after every ten plant extracts.

Metabolomics analyses were carried out by LC-MS/MS using a mobile phase consisting of solvent A (0.1% formic acid in Milli-Q water, v/v) and solvent B (0.1% formic acid in acetonitrile hypergrade, v/v) at a flow rate of 0.4 ml min<sup>-1</sup>

<sup>1</sup>. Gradient elution began with 2.0 min of column equilibration at 5% B and continued as follows: 0.0 – 20.0 min, 5 – 60% B linear; 20.0 – 20.5 min, 60 – 95% B linear; 20.5 – 24.0 min, maintained at 95% B; 24.0 – 24.5 min, 95 – 5% B linear. The injection volume was 2.0  $\mu\text{l}$ . DAD was operated in the wavelength range from 194 to 600 nm at a data acquisition rate of 10.0 Hz.

The mass spectrometer was operated in negative and positive ESI modes in data-dependent auto-MS/MS acquisition. MS parameters were set as follows: mass range 50 – 1500  $m/z$ ; scan cycle time 0.2 s; drying temperature 200°C; capillary voltage 3.5 kV (–ESI) and 4.5 kV (+ESI); endplate offset 0.5 kV for both modes; desolvation gas flow 9.0  $\text{l min}^{-1}$  ( $\text{N}_2$ ); nebulizer pressure 4.0 bar. MS/MS spectra were acquired from each scan, subjecting ions (maximum 2) to collision-induced dissociation (CID) if their absolute intensities exceeded 1000 counts per 0.2 s cycle, with variable collision energy in the range of 20 – 50 eV. Active exclusion of the precursor ion was applied after 1 spectrum, and fragmentation was reconsidered if its intensity was at least equal to the previously measured one. For internal reference, sodium formate solution (10 mM in iso-PrOH/ $\text{H}_2\text{O}$ , 1:1, v/v) was pumped continuously at a rate of 1  $\mu\text{l min}^{-1}$  through a six-port valve, so that 20  $\mu\text{l}$  of it was delivered to the mass spectrometer just before each analysis.

## 7.5 Data processing and statistics.

The raw LC-MS data were first processed in MetaboScape software by selecting the algorithm Time aligned Region complete eXtraction (T-ReX 3D). It integrates a stepping workflow, including mass recalibration, retention time (Rt) alignment, feature extraction ( $m/z$  – Rt pairs), adducts and neutral losses handling, whole region feature extraction, import of MS/MS spectra, and generation of Bucket Tables where features are assigned to Buckets ( $m/z$  – Rt pairs and intensity) across samples with recursive extraction of missed peaks for improved statistics. The parameters used for bucket table generation through T-ReX 3D algorithm were set as follow: intensity threshold, 400 counts; minimum spectrum peak length, 5; minimum recursive peak length, 5; minimum number of recursive features to be extracted, if present in 1/3 of a group; feature in a minimum number of analysis, present in 1/3 of a group; mass range, 50 – 1500  $m/z$ ; retention time range, 0.5 – 20.0 min; MS/MS import, average.

Generated bucket tables were first manually curated using exploratory statistics in MetaboScape and then exported to MetaboAnalyst 5.0 for a high-throughput analytical pipeline for metabolomics (Chong et al., 2019; Pang et



al., 2021). After uploading, data were Pareto-scaled and then examined by applying principal component analysis (PCA) for reducing data dimensionality and uncovering the inherent clusters pattern in the data (Worley & Powers, 2013a). Orthogonal Projection to Latent Structures Discriminant Analysis (OPLS-DA) was then applied to the datasets. This is a supervised modeling method that was applied to the dataset to discover features correlated with systemic response in needles and wood of *P. radiata* after infestation by *S. noctilio*, using HT level for healthy and IT for infested. However, the OPLS-DA model aggressively enforces the separation of these two classes, thus causing a risk of over-fitting the model to the data. To avoid this, validation was performed to ensure model reliability by using a combined random permutation test of class labels with internal leave-*n*-out cross-validation. The parameters of a measure of internal consistency between the original and cross-validated predicted data ( $Q^2$ ) and the measure of model fit to the original data ( $R^2Y$ ), were used to assess statistical quality (Worley & Powers, 2013a, 2016a).

## **7.6 Biomarker model evaluation.**

Features relevant to class discrimination according to the OPLS-DA model were further evaluated for their usefulness as biomarkers of early infestation. For this purpose, a receiver operating characteristic (ROC) curve-based approach was used, where in addition to individual features, the ability of their combination to predict classes for new unlabeled samples was evaluated. Such assessment is based on the ability to give a positive test in the case of *S. noctilio* infestation (sensitivity) and a negative test in the absence of infestation (specificity), which is ultimately indicated by the value of the area under the curve (AUC), where the closer to 1.0, the better the metabolite or set of them as a biomarker of infestation (Chong et al., 2019). The ROC models were also validated using a random permutation test, considering the predictive accuracy of the biomarker model created as a measure of performance.

### **7.7 Metabolite annotation.**

The chemical nature of significant metabolites was determined using an integrated workflow in MetaboScape for manual annotation. The first step includes the SmartFormula task to determine molecular formulas based on accurate mass and isotopic patterns information for the extracted feature.

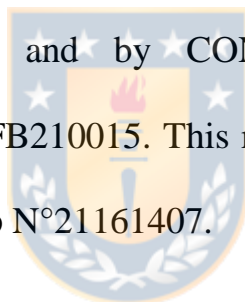
Elements such as C, H, N, O, P, and S, were considered in the calculations, with a tolerance of 5 ppm. SmartFormula 3D calculations are also applied in this step for all features with available MS/MS spectra, improving the quality of the calculated molecular formula. This is an intelligent interface for the annotation of all monoisotopic peaks in the MS/MS spectrum. Thus, for each possible explanation of the  $m/z$  of the precursor and isotopic pattern of a feature, SmartFormula 3D determined which ion formulas best explained the monoisotopic peak and isotopic pattern of the MS/MS fragment spectrum and ranked them according to MS/MS fragment explanation and intensity coverage. In the next step, the Compound Crawler tool searches possible structures that fit the first ranked formula, sending queries for a given molecular formula to databases such as ChEBI, ChemSpider, and PubChem, and returns results that can be used to annotate compounds. The selection of correct structure was then performed using the MetFrag algorithm, as multiple structure candidates were typically found in Compound Crawler for a given elemental composition. Using the MS/MS fragment spectrum, MetFrag searches for ions matching with *in-silico* fragmentation of possible candidates given by Compound Crawler and ranks them according to explained fragment peaks and intensity coverage (Ruttkies *et al.*, 2016). Finally, the selection of the best candidate for a given

feature is refined by the MS/MS Library Search tool, which compares the MS/MS spectrum of a given feature with spectra of known compounds contained in Spectral Libraries previously imported in MetaboScape, such as Bruker MetaboBASE Plant Library and Vaniya/Fiehn Natural Products Library of the MassBank of North America (MoNA). SIRIUS 4.0, a freely available web service integrating high-resolution isotopic pattern analysis and fragmentation trees for structural elucidation, was also used to improve annotation (Dührkop *et al.*, 2019).

In addition, retention times match with that of chemical standards, where available, were checked for final structure confirmation and higher annotation level (A). The complete metabolite data are presented in Table 1-2.

## 8. ACKNOWLEDGMENTS

We thank Dr. Miguel Castillo, chief of the Plant Protection Area at the forestry company MININCO S.A., for his assistance in locating pine stands and identifying the presence of woodwasp. This work was supported by projects ANID/CONICYT FONDECYT Regular 1181915, ANID/CONICYT FONDEF/CONCURSO IdeA I+D FONDEF/CONICYT 2019 ID19I10206, FONDEQUIP EQM170023, and by CONICYT PIA/APOYO CCTE AFB170007, ANID BASAL FB210015. This research was also supported by CONICYT doctoral fellowship N°21161407.



## 9. DATA AVAILABILITY STATEMENT

Data associated with this paper, including LC-MS raw data (.d/.mzXML files), processed bucket tables, and any other required materials, are freely available upon request to the corresponding author (Andy J. Pérez: [aperezd@udec.cl](mailto:aperezd@udec.cl)).

*Table 1-2: Annotation of significant metabolites that changed their levels in P. radiata needles and/or wood during S. noctilio infestation.*

No	Rt (min)	Metabolite identification	Metabolite class	Mol. Formula	- ESI Theor m/z	- ESI Found m/z	+ ESI Theor m/z	+ ESI Found m/z	m/z error (ppm) <sup>a</sup>	MS/MS ESI (-) m/z (rel. int.)	MS/MS ESI (+) m/z (rel. int.)	UV/Vis (nm)	InChI-Key	Ident. Level (A-D)
Up-regulated metabolites in needles and wood of <i>P. radiata</i> following infestation by <i>S. noctilio</i> at T1 and/or at T2														
1	4.64	Catechin	Flavan-3-ol	C <sub>15</sub> H <sub>14</sub> O <sub>6</sub>	289.0718	289.0708 [M-H] <sup>-</sup>	291.0863	291.0862 [M+H] <sup>+</sup>	3.39, 0.26	289.1 (84), 245.1 (100), 203.1 (52), 151 (38), 123.0 (61), 109.0 (73)	207.0 (21), 147.0 (21), 139.0 (100), 123.0 (74)	279	PFTAWBLQP ZVEMU- HIFRSBDPSA- N	A <sup>n-T1-T2</sup> *
2	7.56	Laricitrin hexoside	Flavonol glycoside	C <sub>22</sub> H <sub>22</sub> O <sub>13</sub>	493.0988	493.0970 [M-H] <sup>-</sup> , 315.1226 <sup>b</sup>	495.1133	495.1125 [M+H] <sup>+</sup> , 317.1378 <sup>b</sup>	3.53, 1.66	493.1 (98), 330 (43), 315.0 (100), 287.0 (33)	333.0 (100) 318.0 (13)	281, 353	ODXINVOINF DDDD- CLXWZIMCS A-N	B <sup>n-T1</sup>
3	4.43	Procyanidin B1	Proanthocyanidin	C <sub>30</sub> H <sub>26</sub> O <sub>12</sub>	577.1351	577.1339 [M-H] <sup>-</sup>	579.1497	579.1487 [M+H] <sup>+</sup>	2.09, 1.70	577.1 (75), 451.1 (27), 425.1 (100), 407.1 (87), 289.1 (98), 125.0 (78)	479.1 (18), 427.1 (69), 409.1 (40), 289.1 (100), 127.0 (76)	278	XFZJEEAOW LFHDH- UKWJTHFES A-N	A <sup>n-T1-T2</sup> *
4	1.16	Malic acid	Dicarboxylic acid	C <sub>4</sub> H <sub>6</sub> O <sub>5</sub>	133.0142	133.0144 [M-H] <sup>-</sup>	n.d.	n.d.	1.0, n.d.	115.0 (100)	n.d.	n.d.	BJEPYKJPYR NKOW- UHFFFAOYS A-N	A <sup>n-T1-T2</sup>
5	1.06	Proline	Amino acid	C <sub>5</sub> H <sub>9</sub> NO <sub>2</sub>	n.d.	n.d.	116.0706	116.0704 [M+H] <sup>+</sup>	n.d., 1.63	n.d.	116.1 (100)	n.d.	ONIBWKKTO POVIA- BYPYZUCNS A-N	A <sup>n-T1</sup>
6	7.48	Isotaxiresinol	Lignan	C <sub>19</sub> H <sub>22</sub> O <sub>6</sub>	345.1344	345.1332 [M-H] <sup>-</sup>	317.1384 <sup>b</sup>	317.1378 <sup>b</sup> [M+H] <sup>+</sup>	3.26, 1.73	327.1 (28), 315.1 (100), 300.1 (14)	299.1 (29), 271.1 (69), 175.1 (42), 165.1 (47), 151.1 (50), 137.1 (100)	n.d.	GQLVRVYXA HDDL- PJFSTORSA- N	B <sup>n-T1</sup>
7	3.02	Pungenin	Acetophenone glycoside	C <sub>14</sub> H <sub>18</sub> O <sub>8</sub>	313.0929	313.0925 [M-H] <sup>-</sup>	n.d.	n.d.	1.41, n.d.	313.1 (7), 151.0 (15), 107.1 (100)	n.d.	n.d.	AOXMCWFZP ZRDPE- RKQHYHRCS A-N	B <sup>n-T1</sup>
8	7.74	Diacetyl derivative of geniposidic acid	Iridoid glycoside	C <sub>19</sub> H <sub>26</sub> O <sub>10</sub>	413.1453	413.1443 [M-H] <sup>-</sup>	437.1418	437.1408 [M+Na] <sup>+</sup>	2.46, 2.33	413.1 (100), 163.0 (16), 135.0 (73), 129.1 (15), 121.0 (88)	415.2 (5), 267.1 (52), 249.1 (35), 105.0 (100)	282, 320	MHPLKAPNU FHKRF- SLHLPCJXSA- N	B <sup>n-T1</sup>
9	7.6	Methoxy-tetrahydroxy-8,4'-oxyneolignan hexoside	Oxyneolignan glycoside	C <sub>25</sub> H <sub>34</sub> O <sub>11</sub>	509.2028	509.2016 [M-H] <sup>-</sup>	n.d.	n.d.	2.41, n.d.	509.2 (25), 491.2 (28), 473.2 (13), 461.2 (16), 367.1 (24), 313.1 (50), 179.1 (100), 167.1 (24), 146.0 (35), 134.0 (19)	n.d.	n.d.	BUSMKRODP AQUMM- NAPQKZHS A-N	B <sup>n-T1</sup>
10	8.43	Syringetin hexoside	Flavonol glycoside	C <sub>23</sub> H <sub>24</sub> O <sub>13</sub>	507.1144	507.1127 [M-H] <sup>-</sup>	347.0761 <sup>b</sup>	347.0755 <sup>b</sup> [M+H] <sup>+</sup>	3.39, 1.87	507.1 (100), 344.1 (24), 329.0 (16) 301.0 (29), 287.0 (13), 273.0 (44), 258.0 (16), 242.0 (21)	347.1 (100), 163.1 (29), 137.1 (85), 122.0 (26), 94.0 (14)	263, 357	JMFWYRWPJ VEZPV- WKRUDVTBS A-N	B <sup>n-T1</sup>

Chapter 2

11	4.76	(Hydroxyindol-3-yl)-lactate hexoside	Indole glycoside	C <sub>17</sub> H <sub>21</sub> NO <sub>9</sub>	382.1143	382.1135 [M-H] <sup>-</sup>	406.1109	406.1103 [M+Na] <sup>+</sup>	1.42, 1.43	382.1 (100), 249.1 (26), 237.1 (18), 220.1 (16), 202.1 (78), 158.1 (67), 132.0 (29)	222.1 (100), 176.1 (86), 158.1 (89), 130.1 (26)	279	-	B <sup>n-T1-T2</sup>
12	1.25	Citric acid	Tricarboxylic acid	C <sub>6</sub> H <sub>8</sub> O <sub>7</sub>	191.0197	191.0191 [M-H] <sup>-</sup>	193.0343	193.0345 [M+H] <sup>+</sup>	3.04, 1.08	191.1 (17), 129 (9), 111.0 (100)	193.0 (100)	276	KRKNYBCHX YNGOX- UHFFFAOYS A-N	A <sup>n-T1</sup>
13	3.68	Tryptophan	Amino acid	C <sub>11</sub> H <sub>12</sub> N <sub>2</sub> O <sub>2</sub>	203.0826	203.0819 [M-H] <sup>-</sup>	205.0972	205.0966 [M+H] <sup>+</sup>	1.04, 3.27	203.1 (44), 186.1 (35), 142.1 (50), 116.1 (100)	188.1 (61), 146.1 (100), 115.1 (45), 91.1 (18)	282, 303	QIVBCDIJAJ PQS- VIFPVBQESA -N	A <sup>n-T1-T2</sup>
14	1.09	Dimethyl-inositol	Sugar alcohol	C <sub>8</sub> H <sub>16</sub> O <sub>6</sub>	n.d.	n.d.	209.1020	209.1017 [M+H] <sup>+</sup>	n.d., 1.39	n.d.	141.1 (30), 109.0 (100), 98.0 (24)	n.d.	DYQWYDOD KPTUPA- YNJOCIMMS A-N	B <sup>n-T1</sup>
15	7.06	Methoxy-pentahydroxy-8,4'-oxyneolignan	Oxyneolignan	C <sub>19</sub> H <sub>24</sub> O <sub>7</sub>	363.1449	363.1437 [M-H] <sup>-</sup>	n.d.	n.d.	3.45, n.d.	179.1 (45), 167.1 (100), 149.0 (27), 134.0 (21), 121.0 (25)	n.d.	280	KMYQEVOSR SCASE- UHFFFAOYS A-N	B <sup>n-T1</sup>
16	1.13	Ascorbic acid hexoside	Aldonic acid lactone glycoside	C <sub>12</sub> H <sub>18</sub> O <sub>11</sub>	337.0776	337.0767 [M-H] <sup>-</sup>	339.0922	339.0920 [M+H] <sup>+</sup>	2.69, 0.57	337.1 (100), 277.1 (24), 191.1 (10), 174.0 (10)	n.d.	n.d.	MLSJBGYKD YSOAE- DCWMUDTN SA-N	B <sup>n-T1</sup>
17	7.87	Dimethoxy-tetrahydroxy-8,4'-oxyneolignan deoxyhexoside	Oxyneolignan glycoside	C <sub>26</sub> H <sub>36</sub> O <sub>11</sub>	523.2185	523.2169 [M-H] <sup>-</sup>	n.d.	n.d.	3.05, n.d.	523.0 (57), 475.2 (100), 327.1 (23), 195.1 (23), 165.1 (55), 149.0 (51), 133.0 (22)	n.d.	280	BAVLMBOW TIUCML- QPMGRVRES A-N	B <sup>n-T1</sup>
18	6.6	Myricetin hexoside	Flavonol glycoside	C <sub>21</sub> H <sub>20</sub> O <sub>13</sub>	479.0831	479.0816 [M-H] <sup>-</sup>	481.0977	481.0967 [M+H] <sup>+</sup>	3.08, 1.93	479.1 (100), 316.0 (90), 287.0 (31), 271.0 (53)	319.1 (100)	260, 355	FOHXFLPXB UAOJM- LIBJPBHASA- N	B <sup>n-T1</sup>
19	1.12	Arginin-succinic acid	Amino acid	C <sub>10</sub> H <sub>18</sub> N <sub>4</sub> O <sub>6</sub>	289.1154	289.1146 [M-H] <sup>-</sup>	291.1299	291.1289 [M+H] <sup>+</sup>	2.63, 3.43	n.d.	291.1 (100), 232.1 (19), 175.1 (64)	n.d.	KDZOASGQN OPSCU- WDSKDSINS A-N	B <sup>n-T1</sup>
20	1.03	Pinitol	Sugar alcohol	C <sub>7</sub> H <sub>14</sub> O <sub>6</sub>	n.d.	n.d.	195.0863	195.0862 [M+H] <sup>+</sup>	n.d., 0.48	n.d.	127.0 (33), 109.0 (100), 97.0 (16)	n.d.	DSCFFEYYQ KRSRV- FEPQRWDDS A-N	B <sup>n-T1</sup>
21	10.40	Unnamed oligoxyneolignan	Oxyneolignan	C <sub>32</sub> H <sub>42</sub> O <sub>12</sub>	617.2604	617.2593 [M-H] <sup>-</sup>	619.2749	619.2747 [M+H] <sup>+</sup>	1.75, 0.27	617.3 (100), 587.2 (16), 380.2 (57), 362.2 (70), 308.2 (20), 239.1 (79)	619.3 (100), 482.2 (14), 452.2 (61), 408.2 (35), 285.1 (35)	277, 383	FDGLTYXSIL TPCR- UHFFFAOYS A-N	B <sup>n-T1-T2</sup>
22	6.23	Dihydromyricetin	Flavanonol	C <sub>15</sub> H <sub>12</sub> O <sub>8</sub>	319.0459	319.0452 [M-H] <sup>-</sup>	321.0605	321.0589 [M+H] <sup>+</sup>	2.30, 4.81	301.0 (6), 257.0 (16), 215.0 (15), 193.0 (100), 179.0 (37) 175.0 (35), 151.0 (21), 125.0 (48)	n.d.	291	KJXSIXMJHK AJOD- LSDHHAUSA -N	B <sup>w-T2</sup>
23	4.43	Sebacic acid	Dicarboxylic acid	C <sub>10</sub> H <sub>18</sub> O <sub>4</sub>	201.1132	201.1124 [M-H] <sup>-</sup>	n.d.	n.d.	4.15, n.d.	201.1 (100), 183.1 (16), 139.1 (6), 127.1 (6), 111.1 (7)	n.d.	-	CXMXRPHRN RROMY- UHFFFAOYS A-N	B <sup>w-T2</sup>

Chapter 2

24	1.18	Mannitol	Sugar alcohol	C <sub>6</sub> H <sub>14</sub> O <sub>6</sub>	181.0718	181.0711 [M-H] <sup>-</sup>	n.d.	n.d.	3.79, n.d.	89.1 (100)	n.d.	n.d.	FBPFZTCFMR RESA- KVTDDHHQDS A-N	B <sup>w-T2</sup>
25	4.40	Isomer of 11	Indole glycoside	C <sub>17</sub> H <sub>21</sub> NO <sub>9</sub>	382.1143	382.1147 [M-H] <sup>-</sup>	222.0761 <sup>b</sup>	222.0748 <sup>b</sup> [M-H-Hex] <sup>+</sup>	1.00, 5.91	382.1 (100), 249.1 (18), 237.1 (18), 220.1 (13), 202.1 (72), 158.1 (62), 132.0 (31)	176.1 (100), 158.1 (66), 130.1 (91), 103.1 (51)	284	-	B <sup>n-T2</sup>
26	1.73	Unknown	Unknown	C <sub>9</sub> H <sub>15</sub> NO	n.d.	n.d.	154.1226	154.1226 [M+H] <sup>+</sup>	n.d., 0.21	n.d.	154.1 (61), 108.1 (36), 95.1 (100)	n.d.	-	D <sup>n-T2</sup>
Down-regulated metabolites in needles and wood of <i>P. radiata</i> following infestation by <i>S. noctilio</i> at T1 and/or at T2														
1'	1.05	Quinic acid	Cyclitol carboxylic acid	C <sub>7</sub> H <sub>12</sub> O <sub>6</sub>	191.0561	191.0557 [M-H] <sup>-</sup>	193.0707	193.0704 [M+H] <sup>+</sup>	2.26, 1.26	191.1 (100), 173.0 (4), 127.0 (5), 93.0 (5)	157.0 (12), 147.1 (19), 139.0 (24), 129.1 (31), 121.0 (10), 111.0 (100) 95.1 (41)	n.d.	AAWZDTNXL SGCEK- LNVDRNJUS A-N	B <sup>n-T1-T2, w-T2</sup>
2'	1.13	Shikimic acid	Cyclitol carboxylic acid	C <sub>7</sub> H <sub>10</sub> O <sub>5</sub>	173.0455	173.0445 [M-H] <sup>-</sup>	197.0420	197.0420 [M+Na] <sup>+</sup>	1.33, 0.44	155.0 (6), 137.0 (43), 115.0 (56), 111.0 (22), 93.0 (100)	141.0 (30), 129.0 (22), 113.0 (40), 111.0 (72), 97.0 (40), 95.0 (100)	n.d.	JXOHGGNKM LTUBP- HSUXUTPPSA -N	A <sup>n-T1-T2</sup>
3'	1.15	Ascorbic acid	Aldonic acid lactone	C <sub>6</sub> H <sub>8</sub> O <sub>6</sub>	175.0248	175.0241 [M-H] <sup>-</sup>	177.0394	177.0390 [M+H] <sup>+</sup>	4.31, 2.23	137.0 (22), 115.0 (100), 93.0 (61)	141.0 (8), 129.0 (20), 111.0 (12), 95.0 (100)	n.d.	CIWBSHSHK KDKBQ- JLAZNSOCSA -N	A <sup>n-T1-T2</sup>
4'	4.92	Isobutyl malic acid hexoside	Dicarboxylic acid glycoside	C <sub>14</sub> H <sub>24</sub> O <sub>10</sub>	397.1351	397.1340 [M+HCOO H-H] <sup>-</sup>	375.1262	375.1258 [M+Na] <sup>+</sup>	2.79, 0.92	221.1 (7), 189.1 (100), 157.0 (21), 129.0 (39), 115.0 (41), 113.1 (36)	375.1 (18), 213.1 (100)	277	RLSITCAUHU NHRO- BGWRNRDFS A-N	B <sup>n-T1-T2</sup>
5'	2.85	Vanillic acid hexoside ester	Hydroxybenzoate glycoside	C <sub>14</sub> H <sub>18</sub> O <sub>9</sub>	329.0878	329.0868 [M-H] <sup>-</sup>	169.0495 <sup>b</sup>	169.0490 <sup>b</sup> [M+H] <sup>+</sup>	3.09, 3.13	167.0 (100), 152.0 (36), 123.0 (16), 108.0 (58)	151.0 (77), 110.0 (100), 93.0 (38)	285	YROOZUQRT LHXIO- DIACKHNES A-N	B <sup>n-T1</sup>
6'	8.62	Quercetin acetylhexoside	Flavonol glycoside	C <sub>23</sub> H <sub>22</sub> O <sub>13</sub>	505.0988	505.0972 [M-H] <sup>-</sup>	507.1133	507.1121 [M+H] <sup>+</sup>	3.12, 2.49	505.1 (93), 300.0 (100), 271.0 (72), 255.0 (30), 243.0 (14)	303.0 (100), 187.1 (10)	268, 355	IGLUNMMND NWZOA- LNNZMUSMS A-N	B <sup>n-T1-T2</sup>
7'	7.49	Myricetin acetylhexoside	Flavonol glycoside	C <sub>23</sub> H <sub>22</sub> O <sub>14</sub>	521.0937	521.0919 [M-H] <sup>-</sup>	523.1082	523.1072 [M+H] <sup>+</sup>	3.35, 1.97	521.1 (95), 316.0 (100), 287.0 (32), 271.0 (48)	319.0 (100) 187.1 (9) 127.0 (5)	266, 355	SVRJGKAZQ HHOSZ- UHFFFAOYS A-N	B <sup>n-T1</sup>
8'	1.14	Dihydroxy-dihydrobenzoic acid	2,3-Dihydroxy benzoate	C <sub>7</sub> H <sub>6</sub> O <sub>4</sub>	155.0350	155.0342 [M-H] <sup>-</sup>	139.0390	139.0385 [M- H <sub>2</sub> O+H] <sup>+</sup>	5.20, 3.61	n.d.	139.0 (15), 121.0 (19), 111.0 (100), 95.0 (10)	n.d.	INCSWYKICI YAHB- WDSKDSINS A-N	B <sup>n-T1-T2</sup>
9'	1.00	Unknown	Unknown	C <sub>6</sub> H <sub>6</sub> N <sub>2</sub> O <sub>7</sub>	n.d.	n.d.	219.0248	219.0255 [M+H] <sup>+</sup>	n.d., 3.27	n.d.	156.0 (50), 143.0 (97), 97.0 (100), 85.0 (70)	n.d.	-	D <sup>n-T1-T2</sup>
10'	1.22	Pyridoxine hexoside	Hydroxymethyl pyridine glycoside	C <sub>14</sub> H <sub>21</sub> NO <sub>8</sub>	330.1194	330.1182 [M-H] <sup>-</sup>	332.1340	332.1333 [M+H] <sup>+</sup>	3.71, 1.98	283.2 (69), 269.0 (40), 195.0 (56), 150.1 (83), 136.0 (59), 97.0 (100)	332.1 (100), 314.1 (93), 170.1 (15), 152.1 (91), 134.1 (20), 124.1 (39), 108.1 (90)	278	MDLTWTOQ CHCLSZ- RGCYKPLRS A-N	B <sup>n-T1</sup>



Chapter 2

11'	1.03	3-Hydroxy-3-methyl glutaric acid	Dicarboxylic acid	C <sub>6</sub> H <sub>10</sub> O <sub>5</sub>	207.0510	207.0509 [M+HCOO H-H] <sup>-</sup>	163.0601	163.0598 [M+H] <sup>+</sup>	0.71, 1.94	207.1 (100), 147.0 (5), 129.0 (7), 109.0 (5), 99.0 (5)	127.0 (71), 103.0 (73), 99.0 (100)	n.d.	NPOAOTPXW NWTSH- UHFFFAOYS A-N	B <sup>n-T1-T2</sup>
12'	1.23	Glutathione	Oligopeptide	C <sub>10</sub> H <sub>17</sub> N <sub>3</sub> O <sub>6</sub> S	306.0765	306.0772 [M-H] <sup>-</sup>	308.0911	308.0911 [M+H] <sup>+</sup>	2.05, 0.03	306.1 (14), 272.1 (17), 254.1 (21), 179.0 (14), 143.0 (100), 128.0 (95), 115.0 (25), 99.0 (13)	233.1 (28), 291.1 (14), 179.0 (100), 162.0 (91), 130.0 (29), 116.0 (27)	n.d.	RWSXRVC GQZWBV- WDSKDSINS A-N	B <sup>n-T1</sup>
13'	1.02	Glutamic acid	Amino acid	C <sub>5</sub> H <sub>9</sub> NO <sub>4</sub>	146.0459	146.0455 [M-H] <sup>-</sup>	148.0604	148.0606 [M+H] <sup>+</sup>	2.81, 1.24	n.d.	84.0 (100)	n.d.	WHUUTDBJX JRKMK- VKHMYHEAS A-N	B <sup>n-T1-T2</sup>
14'	4.76	2-[4-(3-Hydroxypropyl)-2-methoxyphenoxy]-1,3-propanediol hexoside	Phenylpropanoid glycoside	C <sub>19</sub> H <sub>30</sub> O <sub>10</sub>	463.1821	463.1810 [M+HCOO H-H] <sup>-</sup>	441.1731	441.1721 [M+Na] <sup>+</sup>	2.40, 2.27	463.2 (9), 417.2 (52), 235.1 (10), 181.1 (100), 166.1 (60), 121.0 (9)	419.2 (8), 257.1 (31), 183.1 (25), 165.1 (51), 137.1 (100), 133.1 (37), 105.1 (24)	n.d.	LRRKTNFBBS NZEN- UHFFFAOYS A-N	B <sup>n-T1</sup>
15'	3.27	1,2-Diguaiacyl-1,3-propanediol hexoside	Lignan glycoside	C <sub>23</sub> H <sub>30</sub> O <sub>11</sub>	481.1715	481.1704 [M-H] <sup>-</sup>	n.d.	n.d.	2.36, n.d.	319.1 (28), 271.1 (100), 256.1 (63), 241.1 (56)	n.d.	276	SUJSUXUCRO GYLL- HDKVOMASS A-N	B <sup>n-T1</sup>
16'	1.23	Trehalose	Disaccharide	C <sub>12</sub> H <sub>22</sub> O <sub>11</sub>	341.1089	341.1085 [M-H] <sup>-</sup>	343.1235	343.1221 [M+H] <sup>+</sup>	1.20, 4.16	341.1 (100), 179.1 (96), 119.0 (90)	n.d.	n.d.	HDTRYLNUV ZCQOY- LIZSDCNHSA -N	B <sup>w-T2, n-T2</sup>
17'	6.30	Dimethoxy-tetrahydroxy-8,4'-oxyneolignan pentoside	Oxyneolignan glycoside	C <sub>25</sub> H <sub>34</sub> O <sub>11</sub>	555.2083	555.2066 [M+HCOO H-H] <sup>-</sup>	533.1993	533.1969 [M+Na] <sup>+</sup>	3.17, 4.54	555.2 (11), 377.2 (100), 329.1 (34), 314.1 (10), 195.1 (6)	533.2 (100), 401.2 (37), 335.1 (23), 204.1 (37)	279	WKWOMGUC NMHNP- CFCXQZMHS A-N	B <sup>w-T2</sup>
18'	1.25	Glyceroheptosyl-dihexoside	Trisaccharide	C <sub>19</sub> H <sub>34</sub> O <sub>17</sub>	533.1723	533.1720 [M-H] <sup>-</sup>	n.d.	n.d.	0.63, n.d.	191.1 (100)	n.d.	n.d.	KGHSEEBNC XPOMY- SNJCTUIQSA- N	B <sup>w-T2, n-T2</sup>
19'	5.94	Methoxy-pentahydroxy-8,4'-oxyneolignan pentoside	Oxyneolignan glycoside	C <sub>24</sub> H <sub>32</sub> O <sub>11</sub>	495.1872	495.1858 [M-H] <sup>-</sup>	519.1837	519.1811 [M+Na] <sup>+</sup>	2.89, 4.90	495.2 (5), 363.1 (43), 315.1 (13), 179.1 (37), 167.1 (100)	519.2 (100), 387.1 (45)	279	XBHWAKRD NVCHEC- UHFFFAOYS A-N	B <sup>w-T2</sup>
20'	4.46	Feruloyl-hexose	Hydroxycinnamic acid glycoside	C <sub>16</sub> H <sub>20</sub> O <sub>9</sub>	355.1035	355.1026 [M-H] <sup>-</sup>	379.0999	379.0979 [M+Na] <sup>+</sup>	2.45, 5.39	193.1 (100), 178.0 (16), 149.1 (21), 134.0 (54)	379.1 (100)	286, 315	JWRQVQWB NRGGPK- PMQCXRHVS A-N	B <sup>w-T2</sup>
21'	1.28	Unknown	Trisaccharide	C <sub>19</sub> H <sub>32</sub> O <sub>16</sub>	515.1618	515.1610 [M-H] <sup>-</sup>	n.d.	n.d.	1.57, n.d.	515.2 (10), 341.1 (100), 173.0 (70), 93.0 (8)	n.d.	n.d.	-	D <sup>w-T2, n-T2</sup>
22'	6.98	Taxifolin hexoside	Flavanonol	C <sub>21</sub> H <sub>22</sub> O <sub>12</sub>	465.1038	465.1027 [M-H] <sup>-</sup>	n.d.	n.d.	2.46, n.d.	465.1 (100), 437.1 (19), 303.1 (12), 285.0 (10), 152.0 (12), 125.0 (23)	n.d.	286	FVQOMEDMF UMIMO- UTZHSPHRSA -N	B <sup>w-T2</sup>

<sup>a</sup>: Mean accurate mass error for negative and positive ESI acquisition modes, respectively; <sup>b</sup>: in-source fragmented; <sup>n</sup>: metabolite found in needles; <sup>w</sup>: metabolite found in wood; <sup>T1</sup>: up- or down-regulated during first sampling time; <sup>T2</sup>: up- or down-regulated during second sampling time; n.d.: not detected; \*: metabolite also down-regulated in wood at T2; Hex: hexosyl; UV/Vis: absorbance maxima; InChi-Key: IUPAC international identifier for chemicals according to PubChem; Level of identification (A-D): A-standard or NMR, B-MS/MS, C-MS<sup>E</sup>, D-MS only.



## 8 REFERENCES

- Agati, G., Tattini, M., 2010. Multiple functional roles of flavonoids in photoprotection. *New Phytol.* 186, 786–793. <https://doi.org/10.1111/j.1469-8137.2010.03269.x>
- Bagniewska-Zadworna, A., Barakat, A., Łakomy, P., Smoliński, D.J., Zadworny, M., 2014. Lignin and lignans in plant defence: Insight from expression profiling of cinnamyl alcohol dehydrogenase genes during development and following fungal infection in *Populus*. *Plant Sci.* 229, 111–121. <https://doi.org/10.1016/j.plantsci.2014.08.015>
- Beèche, M., Lanfranco, D., Zapata, M., Ruiz, C., 2012. Surveillance and control of the Sirex woodwasp: The Chilean experience, in: Slippers, B., de Groot, P., Wingfield, M.J. (Eds.), *The Sirex Woodwasp and Its Fungal Symbiont: Research and Management of a Worldwide Invasive Pest*. Springer, Dordrecht Heidelberg London New York, pp. 229–245.
- Bordeaux, J.M., Dean, J.F.D., 2012. Susceptibility and response of pine to *Sirex noctilio*, in: Slippers, B., de Groot, P., Wingfield, M.J. (Eds.), *The Sirex Woodwasp and Its Fungal Symbiont: Research and Management of a Worldwide Invasive Pest*. Springer, Dordrecht Heidelberg London New York, pp. 31–50.
- Bordeaux, J.M., Lorenz, W.W., Johnson, D., Badgett, M.J., Glushka, J., Orlando, R., Dean, J.F.D., 2014. Noctilisin, a venom glycopeptide of *Sirex noctilio* (Hymenoptera: Siricidae), causes needle wilt and defense gene responses in pines. *J. Econ. Entomol.* 107, 1931–1945. <http://dx.doi.org/10.1603/EC14151>
- Buer, C.S., Imin, N., Djordjevic, M.A., 2010. Flavonoids: New roles for old molecules. *J. Integr. Plant Biol.* 52, 98–111. <https://doi.org/10.1111/j.1744-7909.2010.00905.x>
- Celedon, J.M., Bohlmann, J., 2019. Oleoresin defenses in conifers: chemical diversity, terpene synthases and limitations of oleoresin defense under climate change. *New Phytol.* 224, 1444–1463. <https://doi.org/10.1111/nph.15984>
- Chong, J., Wishart, D.S., Xia, J., 2019. Using MetaboAnalyst 4.0 for comprehensive and integrative metabolomics data analysis. *Curr. Protoc. Bioinform.* 68, e86. <https://doi.org/10.1002/cbi.86>
- Clough, S., McLaughlin, S., Murray, S., 2019. *National Exotic Forest Description*, 36<sup>th</sup> ed. Ministry for Primary Industries New Zealand, Wellington.

- Coutts, M.P., 1969a. The mechanism of pathogenicity of *Sirex noctilio* on *Pinus radiata*. I. Effects of the symbiotic fungus *Amylostereum* sp. (Thelophoraceae). *Aust. J. Biol. Sci.* 22, 915–924.
- Coutts, M.P., 1969b. The mechanism of pathogenicity of *Sirex noctilio* on *Pinus radiata*. II. Effects of *S. noctilio* mucus. *Aust. J. Biol. Sci.* 22, 1153–1161.
- Donaldson, L., Williams, N., 2018. Imaging and spectroscopy of natural fluorophores in pine needles. *Plants* 7, 1–16. <https://doi.org/10.3390/plants7010010>
- Dührkop, K., Fleischauer, M., Ludwig, M., Aksenov, A.A., Melnik, A. V., Meusel, M., Dorrestein, P.C., Rousu, J., Böcker, S., 2019. SIRIUS 4: a rapid tool for turning tandem mass spectra into metabolite structure information. *Nat. Methods* 16, 299–302. <https://doi.org/10.1038/s41592-019-0344-8>
- Eckenwalder, J.E., 2018. Conifer. *Encyclopedia Britannica*. <https://www.britannica.com/plant/conifer/> (accessed 10 December 2021).
- Evans, E.D., Duvallat, C., Chu, N.D., Oberst, M.K., Murphy, M.A., Rockafellow, I., Sontag, D., Alm, E.J., 2020. Predicting human health from biofluid-based metabolomics using machine learning. *Sci. Rep.* 10, 1–13. <https://doi.org/10.1038/s41598-020-74823-1>
- Ferrer, J.-L., Austin, M.B., Stewart, C., Noel, J.P., 2008. Structure and function of enzymes involved in the biosynthesis of phenylpropanoids. *Plant Physiol. Biochem.* 46, 356–370. <https://doi.org/10.1016/j.plaphy.2007.12.009>
- Fong, L.K., Crowdent, R.K., 1973. Physiological effects of mucus from the wood wasp, *Sirex noctilio* F., on the foliage of *Pinus radiata* D. Don. *Aust. J. Biol. Sci.* 26, 365–378.
- Forestry Corporation, 2016. Radiata pine “the remarkable pine”. Forest Fact No 04. [https://www.forestrycorporation.com.au/\\_data/assets/pdf\\_file/0017/420920/forest-fact-radiata-pine.pdf](https://www.forestrycorporation.com.au/_data/assets/pdf_file/0017/420920/forest-fact-radiata-pine.pdf) (accessed 10 December 2021).
- Fraga-Corral, M., Carpena, M., Garcia-Oliveira, P., Pereira, A.G., Prieto, M.A., Simal-Gandara, J., 2020. Analytical metabolomics and applications in health, environmental and food science. *Crit. Rev. Anal. Chem.* 1–23. <https://doi.org/10.1080/10408347.2020.1823811>
- Gullner, G., Komives, T., Király, L., Schröder, P., 2018. Glutathione S-Transferase enzymes in plant-pathogen interactions. *Front. Plant Sci.* 9, 1–19. <https://doi.org/10.3389/fpls.2018.01836>

- Gysling Caselli, A.J., Álvarez González, V.D.C., Soto Aguirre, D.A., Pardo Velasquez, E.J., Poblete Hernandez, P.A., Kahler González, C., 2019. Chilean statistical yearbook of forestry, N° 168. Ed, Anuario Forestal INFOR. Forestry Institute (INFOR), Santiago. <https://doi.org/ISBN:978-956-318-098-5>
- Hao, D.C., Gu, X.-J., Xiao, P.G., 2015. Taxus medicinal resources: a comprehensive study, Medicinal Plants. Elsevier Ltd. <https://doi.org/10.1016/b978-0-08-100085-4.00003-7>
- Heber, U., Miyake, C., Mano, J., Ohno, C., Asada, K., 1996. Monodehydroascorbate radical detected by electron paramagnetic resonance spectrometry is a sensitive probe of oxidative stress in intact leaves. *Plant Cell Physiol.* 37, 1066–1072. <https://doi.org/10.1093/oxfordjournals.pcp.a029055>
- Heldt, H.-W., Piechulla, B., 2021. Glutathione serves the cell as an antioxidant and is an agent for the detoxification of pollutants, in: *Plant Biochemistry*. Elsevier, pp. 314–318.
- Hillis, W.E., Inoue, T., 1968. The formation of polyphenols in trees-IV. The polyphenols formed in *Pinus radiata* after *Sirex* attack. *Phytochemistry* 7, 13–22.
- Ide, S., Beeche, M., Sandoval, A., Opazo, A., Velazquez, P., Schafer, M., Aravena, J.C., Barrientos, C., Sievert, H., Gonzalez, M., Valenzuela, J., Peragallo, M., Muñoz, C., Gallardo, R., 2018. Programa control biológico de *Sirex noctilio* F. (Hymenoptera: Siricidae): 2006-2017. Servicio Agrícola y Ganadero, Ministerio de Agricultura, Gobierno de Chile. [http://www.sag.cl/sites/default/files/control\\_biologico\\_sirex.pdf](http://www.sag.cl/sites/default/files/control_biologico_sirex.pdf) (accessed 10 December 2021)
- Jacobs, M., Rubery, P.H., 1988. Naturally occurring auxin transport regulators. *Science* 241, 346–349. <https://doi.org/10.1126/science.241.4863.346>
- Klapwijk, M.J., Bylund, H., Schroeder, M., Björkman, C., 2016. Forest management and natural biocontrol of insect pests. *Forestry* 89, 253–262. <https://doi.org/10.1093/forestry/cpw019>
- Kumar, N., Pal, M., Singh, A., SaiRam, R.K., Srivastava, G.C., 2010. Exogenous proline alleviates oxidative stress and increase vase life in rose (*Rosa hybrida* L. 'Grand Gala'). *Sci. Hortic.* 127, 79–85. <https://doi.org/10.1016/j.scienta.2010.09.009>
- Kumar, N., Pal, M., Srivastava, G.C., 2009. Proline metabolism in senescing rose petals (*Rosa hybrida* L. 'First Red'). *J. Hortic. Sci. Biotechnol.* 84, 536–540. <https://doi.org/10.1080/14620316.2009.11512562>

- Kumar, R., Bohra, A., Pandey, A.K., Pandey, M.K., Kumar, A., 2017. Metabolomics for plant improvement: Status and prospects. *Front. Plant Sci.* 8, 1302. <https://doi.org/10.3389/fpls.2017.01302>
- Lantschner, M.V., Villacide, J.M., Garnas, J.R., Croft, P., Carnegie, A.J., Liebhold, A.M., Corley, J.C., 2014. Temperature explains variable spread rates of the invasive woodwasp *Sirex noctilio* in the Southern Hemisphere. *Biol. Invasions* 16, 329–339. <https://doi.org/10.1007/s10530-013-0521-0>
- Launay, A., Cabassa-Hourton, C., Eubel, H., Maldiney, R., Guivarc'h, A., Crilat, E., Planchais, S., Lacoste, J., Bordenave-Jacquemin, M., Clément, G., Richard, L., Carol, P., Braun, H.-P., Lebreton, S., Savouré, A., 2019. Proline oxidation fuels mitochondrial respiration during dark-induced leaf senescence in *Arabidopsis thaliana*. *J. Exp. Bot.* 70, 6203–6214. <https://doi.org/10.1093/jxb/erz351>
- Mead, D.J., 2013. Sustainable management of *Pinus radiata* plantations. FAO Forestry Paper No. 170, Rome.
- Möller, R., Koch, G., Nanayakkara, B., Schmitt, U., 2006. Lignification in cell cultures of *Pinus radiata*: Activities of enzymes and lignin topochemistry. *Tree Physiol.* 26, 201–210. <https://doi.org/10.1093/treephys/26.2.201>
- New York Invasive Species Information, 2019. *Sirex Woodwasp*. [http://nyis.info/invasive\\_species/sirex-woodwasp/](http://nyis.info/invasive_species/sirex-woodwasp/) (accessed 10 December 2021).
- Noctor, G., Mhamdi, A., Chaouch, S., Han, Y., Neukermans, J., Marquez-Garcia, B., Queval, G., Foyer, C.H., 2012. Glutathione in plants: An integrated overview. *Plant Cell Environ.* 35, 454–484. <https://doi.org/10.1111/j.1365-3040.2011.02400.x>
- Pang, Z., Chong, J., Zhou, G., De Lima Morais, D.A., Chang, L., Barrette, M., Gauthier, C., Jacques, P.É., Li, S., Xia, J., 2021. MetaboAnalyst 5.0: narrowing the gap between raw spectra and functional insights. *Nucleic Acids Res.* 49, W388–W396. <https://doi.org/10.1093/nar/gkab382>
- Pascual, J., Canal, M.J., Escandon, M., Meijon, M., Weckwerth, W., Valledor, L., 2017. Integrated physiological, proteomic, and metabolomic analysis of ultra violet (UV) stress responses and adaptation mechanisms in *Pinus radiata*. *Mol. Cell. Proteomics* 16, 485–501. <https://doi.org/10.1074/mcp.M116.059436>

- Peer, W.A., Bandyopadhyay, A., Blakeslee, J.J., Makam, S.N., Chen, R.J., Masson, P.H., Murphy, A.S., 2004. Variation in expression and protein localization of the PIN family of auxin efflux facilitator proteins in flavonoid mutants with auxin transport in *Arabidopsis thaliana*. *Plant Cell* 16, 1898–1911. <https://doi.org/10.1105/tpc.021501>
- Peer, W.A., Murphy, A.S., 2007. Flavonoids and auxin transport: modulators or regulators? *Trends Plant Sci.* 12, 556–563. <https://doi.org/10.1016/j.tplants.2007.10.003>
- Ralph, S.G., Yueh, H., Friedmann, M., Aeschliman, D., Zeznik, J.A., Nelson, C.C., Butterfield, Y. s. N., Kirkpatrick, R., Liu, J., Jones, S. j. M., Marra, M.A., Douglas, C.J., Ritland, K., Bohlmann, J., 2006. Conifer defence against insects: microarray gene expression profiling of Sitka spruce (*Picea sitchensis*) induced by mechanical wounding or feeding by spruce budworms (*Choristoneura occidentalis*) or white pine weevils (*Pissodes strobi*) reveals large-scale. *Plant Cell Environ.* 29, 1545–1570. <https://doi.org/10.1111/j.1365-3040.2006.01532.x>
- Ruttkies, C., Schymanski, E.L., Wolf, S., Hollender, J., Neumann, S., 2016. MetFrag relaunched: Incorporating strategies beyond in silico fragmentation. *J. Cheminformatics* 8, 3. <https://doi.org/10.1186/s13321-016-0115-9>
- Ryan, K., Hurley, B.P., 2012. Life history and biology of *Sirex noctilio*, in: Slippers, B., de Groot, P., Wingfield, M.J. (Eds.), *The Sirex woodwasp and its fungal symbiont: Research and management of a worldwide invasive Pest*. Springer, Dordrecht Heidelberg London New York, pp. 15–30.
- Sharma, K., Sarma, S., Bohra, A., Mitra, A., Sharma, N.K., Kumar, A., 2018. Plant metabolomics: An emerging technology for crop improvement, in: Celik, Ö. (Eds.), *New Visions in Plant Science*. IntechOpen. <https://doi.org/10.5772/intechopen.76759>
- Slippers, B., Hurley, B.P., Wingfield, M.J., 2015. *Sirex* woodwasp: A model for evolving management paradigms of invasive forest pests. *Annu. Rev. Entomol.* 60, 601–619. <https://doi.org/10.1146/annurev-ento-010814-021118>
- Smirnoff, N., 2018. Ascorbic acid metabolism and functions: A comparison of plants and mammals. *Free Radic. Biol. Med.* 122, 116–129. <https://doi.org/10.1016/j.freeradbiomed.2018.03.033>

- Spradbery, J.P., Kirk, A.A., 1978. Aspects of the ecology of siricid woodwasps (Hymenoptera: Siricidae) in Europe, North Africa and Turkey with special reference to the biological control of *Sirex noctilio* F. in Australia. *Bull. Entomol. Res.* 68, 341–359.
- Tóth, S.Z., Nagy, V., Puthur, J.T., Kovács, L., Garab, G., 2011. The physiological role of ascorbate as photosystem II electron donor: Protection against photoinactivation in heat-stressed leaves. *Plant Physiol.* 156, 382–392. <https://doi.org/10.1104/pp.110.171918>
- Tóth, S.Z., Puthur, J.T., Nagy, V., Garab, G., 2009. Experimental evidence for ascorbate-dependent electron transport in leaves with inactive oxygen-evolving complexes. *Plant Physiol.* 149, 1568–1578. <https://doi.org/10.1104/pp.108.132621>
- Valledor, L., Escandón, M., Meijón, M., Nukarinen, E., Cañal, M.J., Weckwerth, W., 2014. A universal protocol for the combined isolation of metabolites, DNA, long RNAs, small RNAs, and proteins from plants and microorganisms. *Plant J.* 79, 173–180. <https://doi.org/10.1111/tpj.12546>
- Wang, T., Zhao, M., Rotgans, B.A., Ni, G., Dean, J.F.D., Nahrung, H.F., Cummins, S.F., 2016. Proteomic analysis of the venom and venom sac of the woodwasp, *Sirex noctilio* – Towards understanding its biological impact. *J. Proteomics* 146, 195–206. <https://doi.org/10.1016/j.jprot.2016.07.002>
- Warren, R.L., Keeling, C.I., Yuen, M.M., Saint, Raymond, A., Taylor, G.A., Vandervalk, B.P., Mohamadi, H., Paulino, D., Chiu, R., Jackman, S.D., Robertson, G., Yang, C., Boyle, B., Hoffmann, M., Weigel, D., Nelson, D.R., Ritland, C., Isabel, N., Jaquish, B., Yanchuk, A., Bousquet, J., Jones, S.J.M., Mackay, J., Birol, I., Bohlmann, J., 2015. Improved white spruce (*Picea glauca*) genome assemblies and annotation of large gene families of conifer terpenoid and phenolic defense metabolism. *Plant J.* 83, 189–212. <https://doi.org/10.1111/tpj.12886>
- Whitehill, J.G.A., Yuen, M.M.S., Henderson, H., Madilao, L., Kshatriya, K., Bryan, J., Jaquish, B., Bohlmann, J., 2019. Functions of stone cells and oleoresin terpenes in the conifer defense syndrome. *New Phytol.* 221, 1503–1517. <https://doi.org/10.1111/nph.15477>
- Worley, B., Powers, R., 2016. PCA as a predictor of OPLS-DA model reliability. *Current Metabolomics* 4, 97–103. <https://doi.org/10.2174/2213235X04666160613122429.PCA>
- Worley, B., Powers, R., 2013. Multivariate analysis in metabolomics. *Curr. Metabolomics* 1, 92–107. <https://doi.org/10.2174/2213235x130108>



Xu, Q., Sun, X., Lu, P., Luo, Y., Shi, J., 2019. Volatile profiles of three tree species in the northeastern China and associated effects on *Sirex noctilio* activity. *J. Plant Interact.* 14, 334-339. <https://doi.org/10.1080/17429145.2019.1629035>

Zhang, L., Becker, D.F., 2015. Connecting proline metabolism and signaling pathways in plant senescence. *Front. Plant Sci.* 6, 552. <https://doi.org/10.3389/fpls.2015.00552>



## 9 SUPPORTING INFORMATION

Article title: ***Sirex noctilio* infestation led to inevitable pine death despite activating pathways involved in tolerance.**

Authors: Sebastián Riquelme<sup>a</sup>, Jasna V. Campos<sup>a</sup>, Łukas Pecio<sup>c</sup>, Rosa Alzamora<sup>d,e</sup>, Claudia Mardones<sup>a,b</sup>, Ana M. Simonet<sup>f</sup>, Luis E. Arteaga-Pérez<sup>g</sup>, Rafael Rubilar<sup>e,h</sup>, Oliver Fiehn<sup>i</sup>, Andy J. Pérez<sup>a,b,\*</sup>

<sup>a</sup> Departamento de Análisis Instrumental, Facultad de Farmacia, Universidad de Concepción, Concepción, Chile.

<sup>b</sup> Unidad de Desarrollo Tecnológico, UDT, Universidad de Concepción, Coronel, Chile.

<sup>c</sup> Department of Biochemistry and Crop Quality, Institute of Soil Science and Plant Cultivation, State Research Institute, ul. Czartoryskich 8, 24-100 Puławy, Poland.

<sup>d</sup> Departamento Manejo de Bosques y Medio Ambiente, Facultad de Ciencias Forestales, Universidad de Concepción, Concepción, Chile.

<sup>e</sup> Centro UC de Innovación en Madera, Pontificia Universidad Católica de Chile, Santiago, Chile.

<sup>f</sup> Allelopathy Group, Department of Organic Chemistry, Institute of Biomolecules (INBIO), Campus de Excelencia Internacional (ceiA3), School of Science, University of Cadiz, Puerto Real, Cadiz, Spain.

<sup>g</sup> Laboratory of Thermal and Catalytic Processes (LPTC), Department of Wood Engineering, University of Bío-Bío, Chile.

<sup>h</sup> Cooperativa de Productividad Forestal, Departamento de Silvicultura, Facultad de Ciencias Forestales, Universidad de Concepción, Concepción, Chile.

<sup>i</sup> NIH West Coast Metabolomics Center, UC Davis Genome Center, University of California, Davis, CA 95616, USA.

\* Corresponding author E-mail: [aperezd@udec.cl](mailto:aperezd@udec.cl). Phone: + 56 41 220 3027

The following Supporting Information is available for this article:

**Fig. S1** Photos showing the symptoms in *P. radiata* trees after the infestation by *S. noctilio*.

**Fig. S2** OPLS-DA models validation.

**Fig. S3** Individual ROC curve analysis for each significant metabolite.

**Fig. S4** Quantitative data for up-regulated metabolites in *P. radiata* needles at T1.

**Fig. S5** Quantitative data for down-regulated metabolites in *P. radiata* needles at T1.

**Fig. S6** Quantitative data for up-regulated metabolites in *P. radiata* needles at T2.

**Fig. S7** Quantitative data for down-regulated metabolites in *P. radiata* needles at T2.

**Fig. S8** Quantitative data for up and down-regulated metabolites in *P. radiata* wood at T2.

**Fig. S9** Quantitative data for the metabolite Pinosylvin in wood at T2.

**Table S1** Expression data of metabolites in needles and wood at T1 and at T2.

**Method S1** Climatic conditions during sampling.

**Note S1** Antioxidant hypothesis for the up-regulated flavonols in needles.

**Note S2** Additional systemic defense triggered in foliage after *S. noctilio* infestation.

Figure S1-2: Original photos of *P. radiata* trees from the sampling place, showing the visual symptoms of infestation by *S. noctilio*. The black arrow shows a hole drilled by a female woodwasp in the act of oviposition (a). Oleoresin exudation as droplets in drilling sites of a tree being under attack (b). Wilting and chlorotic needles in the whole foliage (c) and in the crown (d) of two infested trees. Holes left in the trunk of an already dead tree by the emergence of woodwasp adults approximately after a year from the oviposition I.

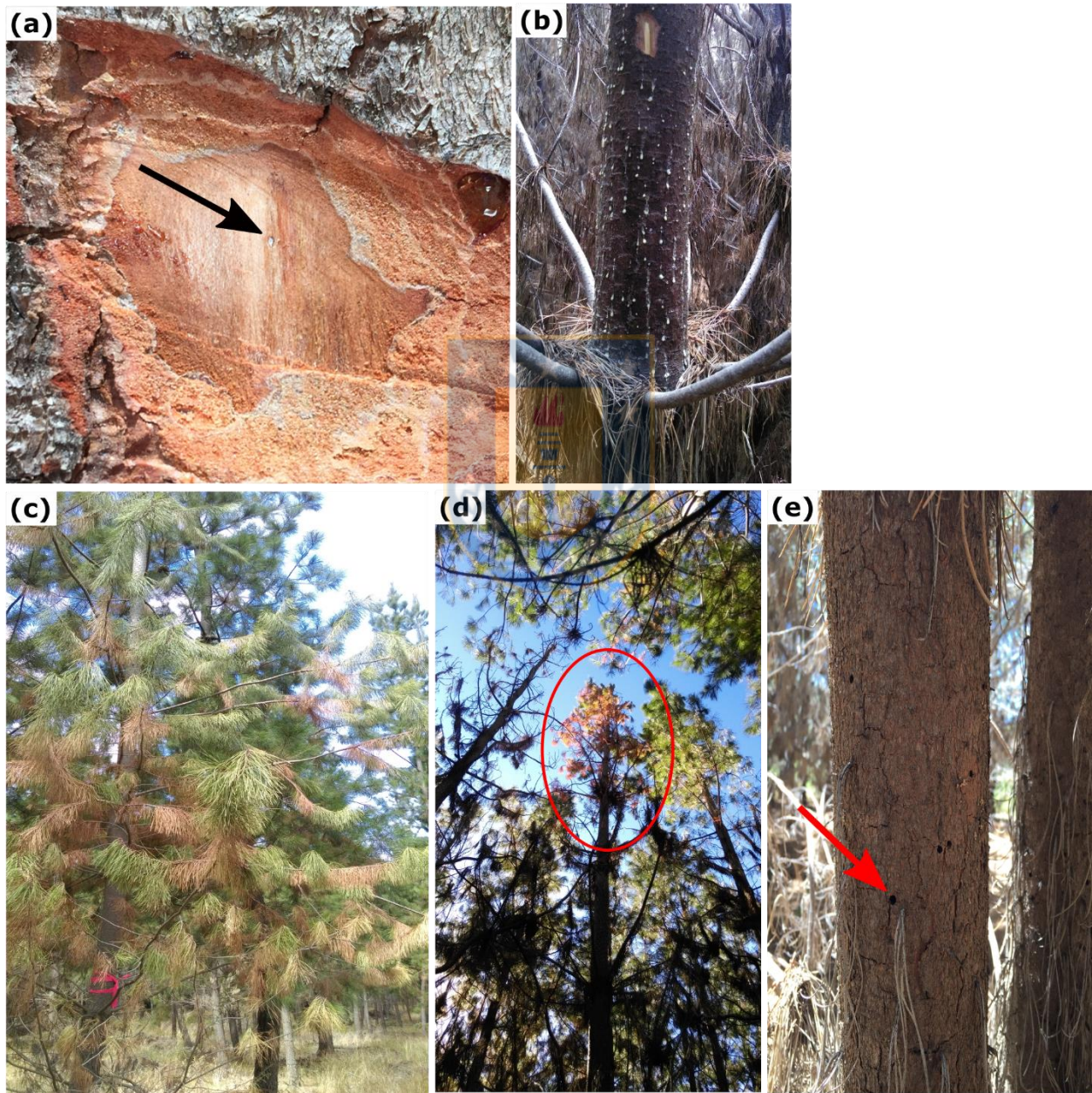


Figure S2-2 Validation of OPLS-DA models based on LC-MS dataset by random permutation test of class membership with 1000 permutations, showing the observed and cross-validated  $R^2Y$  and  $Q^2$  coefficients for needles at T1 in  $-ESI$  (a) and  $+ESI$  (b), for wood at T2 in  $-ESI$  (c) and  $+ESI$  (d), and for needles at T2 in  $-ESI$  (e) and  $+ESI$  (f).

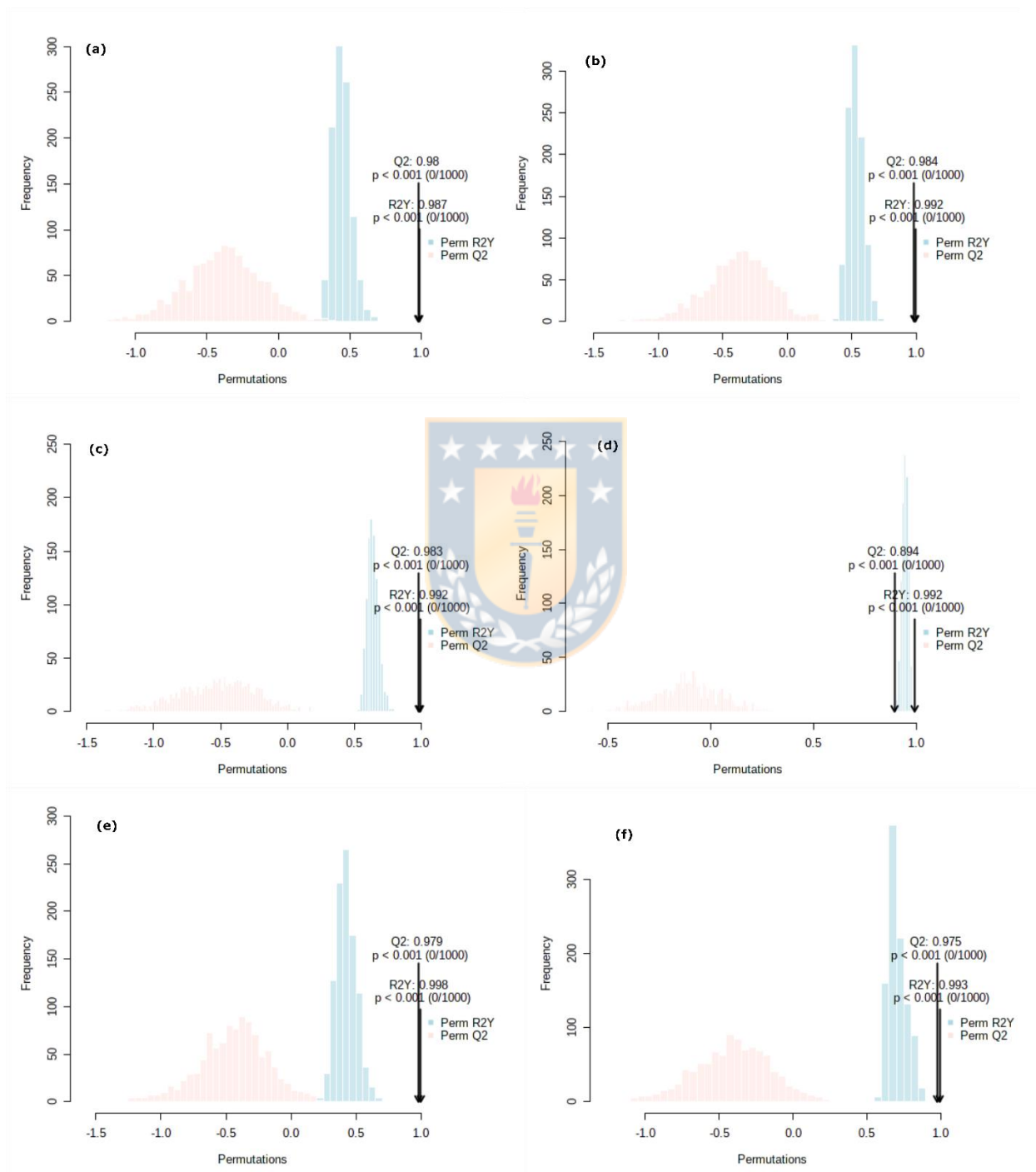
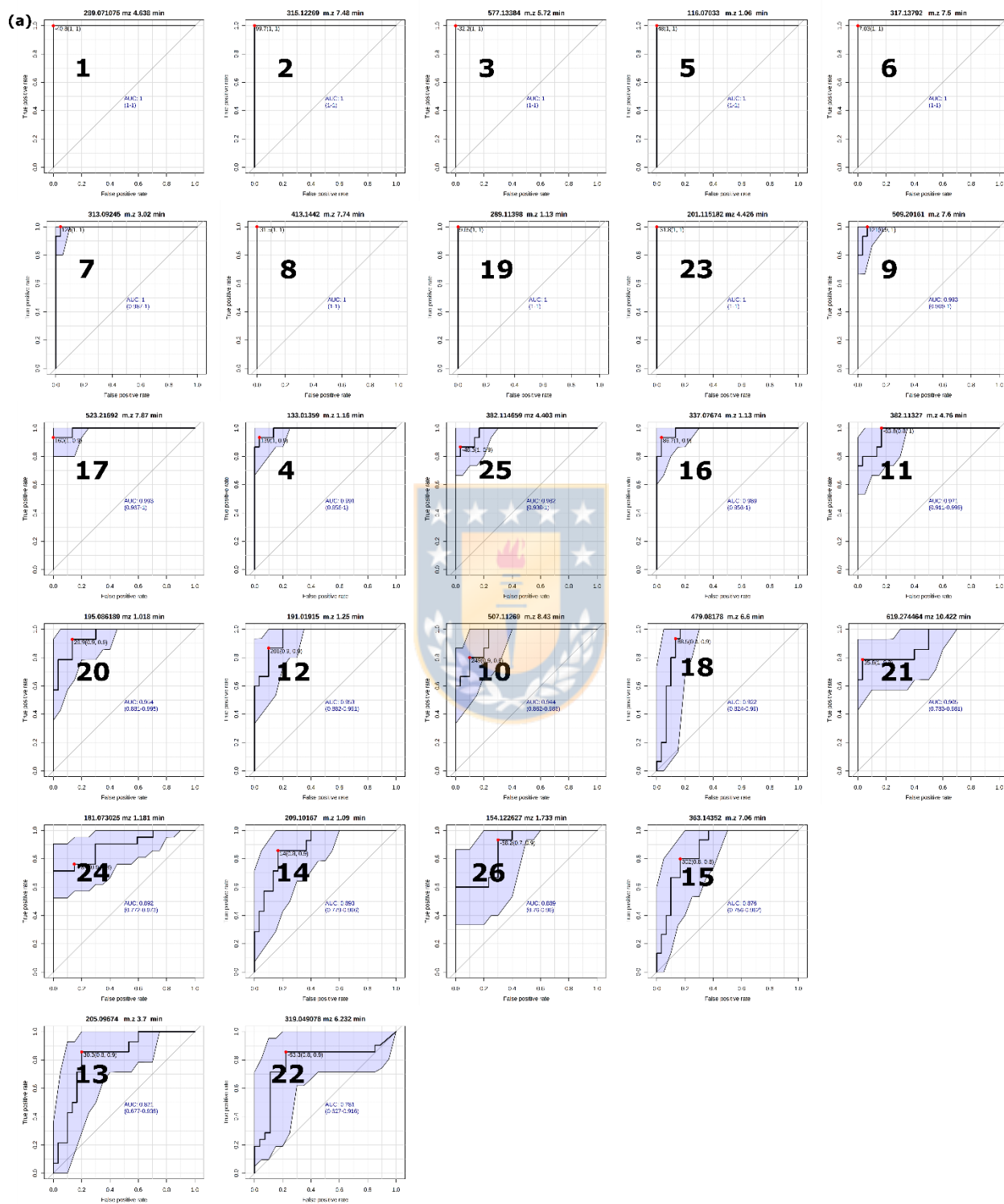
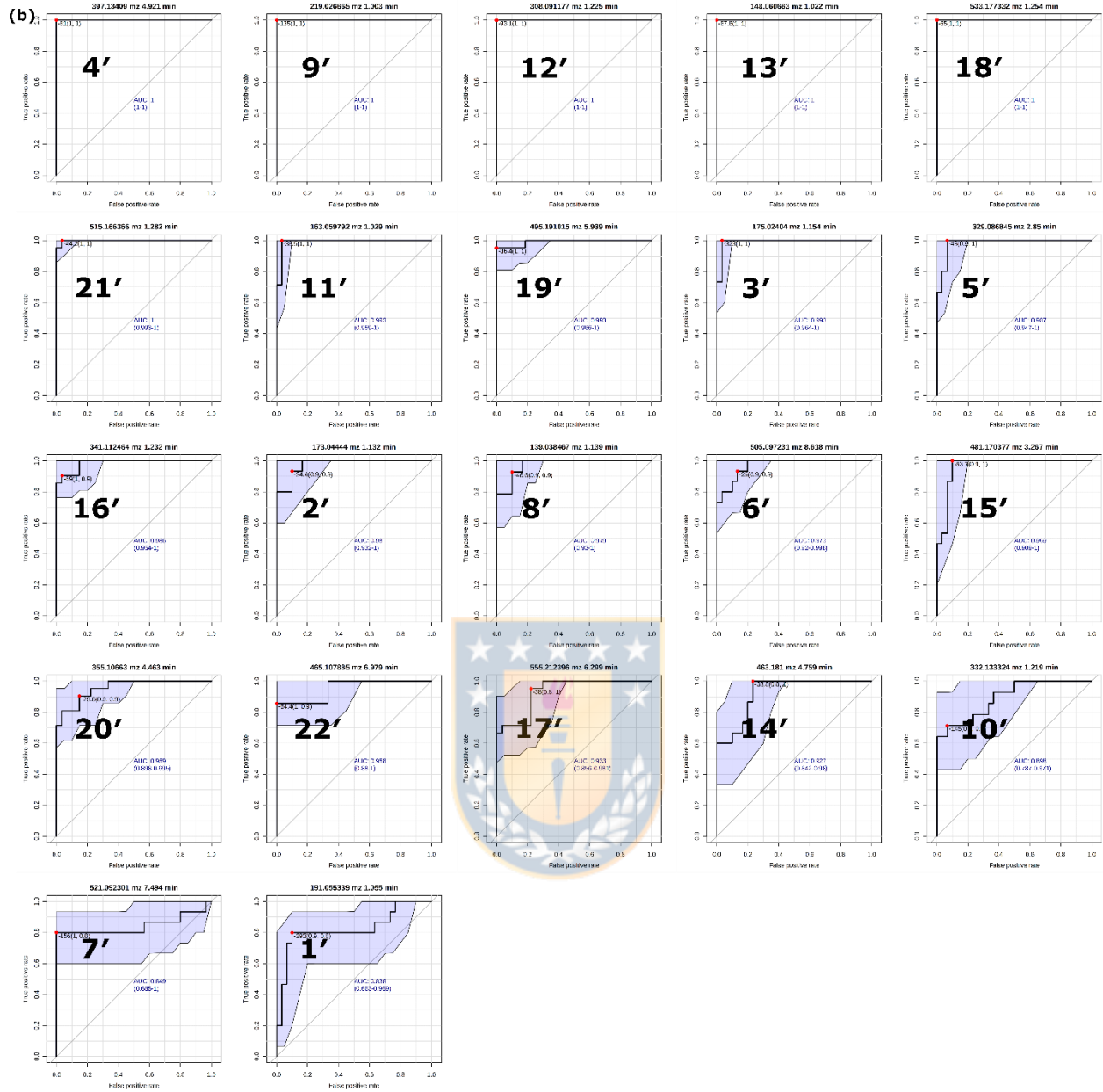


Figure S3-2: ROC curves obtained for each individual metabolite up-regulated (a) and down-regulated (b) in needles at T1, sorted in descending order of their AUC value.



Chapter 2



*Figure S4-2: Quantitative data for metabolites significantly overexpressed in the needles of P. radiata infested trees at T1. Per each compound, box-and-whisker plots on the left show the original values of peak intensities in healthy (HT, blue) and infested trees (IT, red). The plots on the right summarize the normalized values. In each box plot, black dots represent the actual concentration (intensity) of the given metabolite in each analysed sample, the notch indicates the 95% confidence interval around the median of each group, and the yellow diamond indicates the mean concentration of each group.*





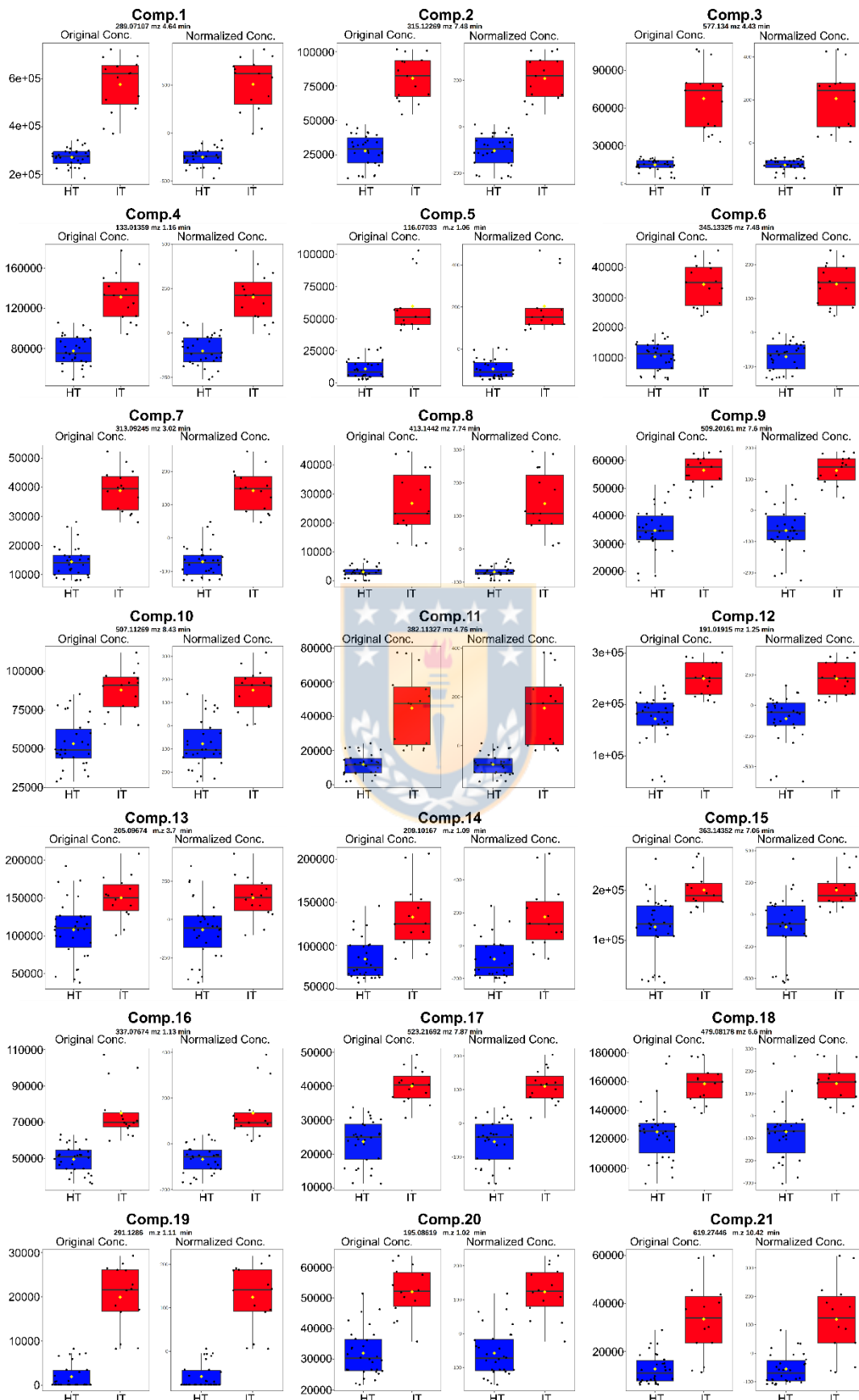


*Figure S5-2: Quantitative data for metabolites significantly 146rabidopsi in the needles of P. radiata infested trees at T1. Per each compound, box-and-whisker plots on the left show the original values of peak intensities in healthy (HT, blue) and infested trees (IT, red). The plots on the right summarize the normalized values. In each box plot, black dots represent the actual concentration (intensity) of the given metabolite in each analysed sample, the notch indicates the 95% confidence interval around the median of each group, and the yellow diamond indicates the mean concentration of each group.*



Chapter 2

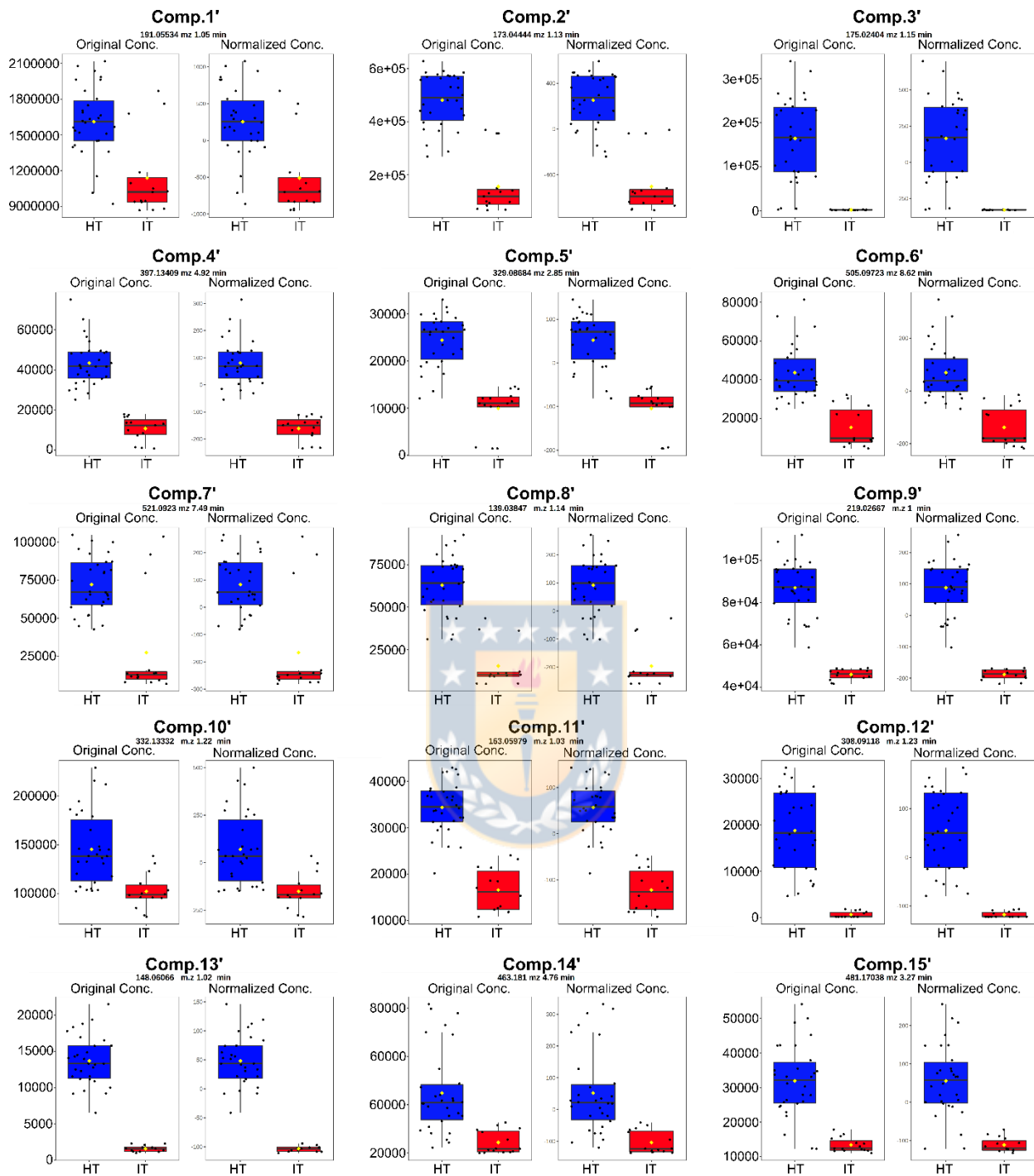


Figure S6-2: Quantitative data for metabolites significantly overexpressed in the needles of *P. radiata* infested trees at T2. Per each compound, box-and-whisker plots on the left show the original values of peak intensities in healthy (HT, blue) and infested trees (IT, red). The plots on the right summarize the normalized values.

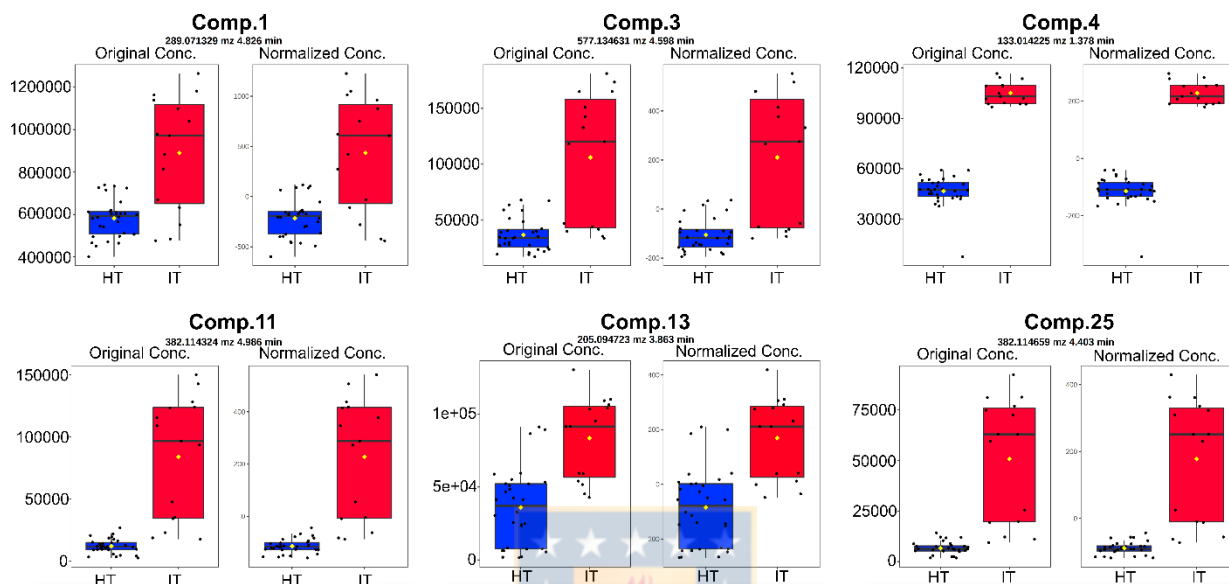


Figure S7-2: Quantitative data for metabolites significantly 149rabidopsi in the needles of *P. radiata* infested trees at T2. Per each compound, box-and-whisker plots on the left show the original values of peak intensities in healthy (HT, blue) and infested trees (IT, red). The plots on the right summarize the normalized values.

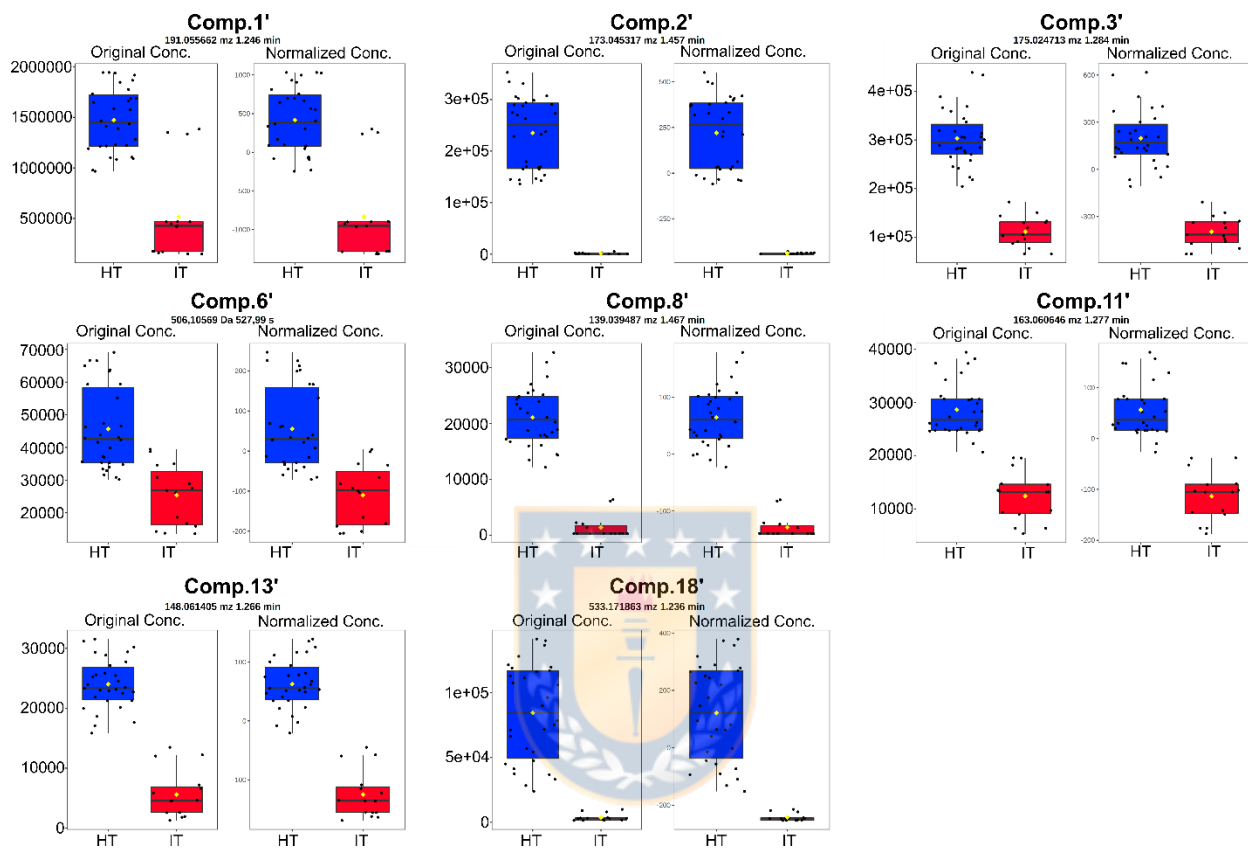


Figure S8-2: Quantitative data for metabolites significantly up and down-regulated in wood of *P. radiata* infested trees at T2. Per each compound, box-and-whisker plots on the left show the original values of peak intensities in healthy (HT, blue) and infested trees (IT, red). The plots on the right summarize the normalized values.

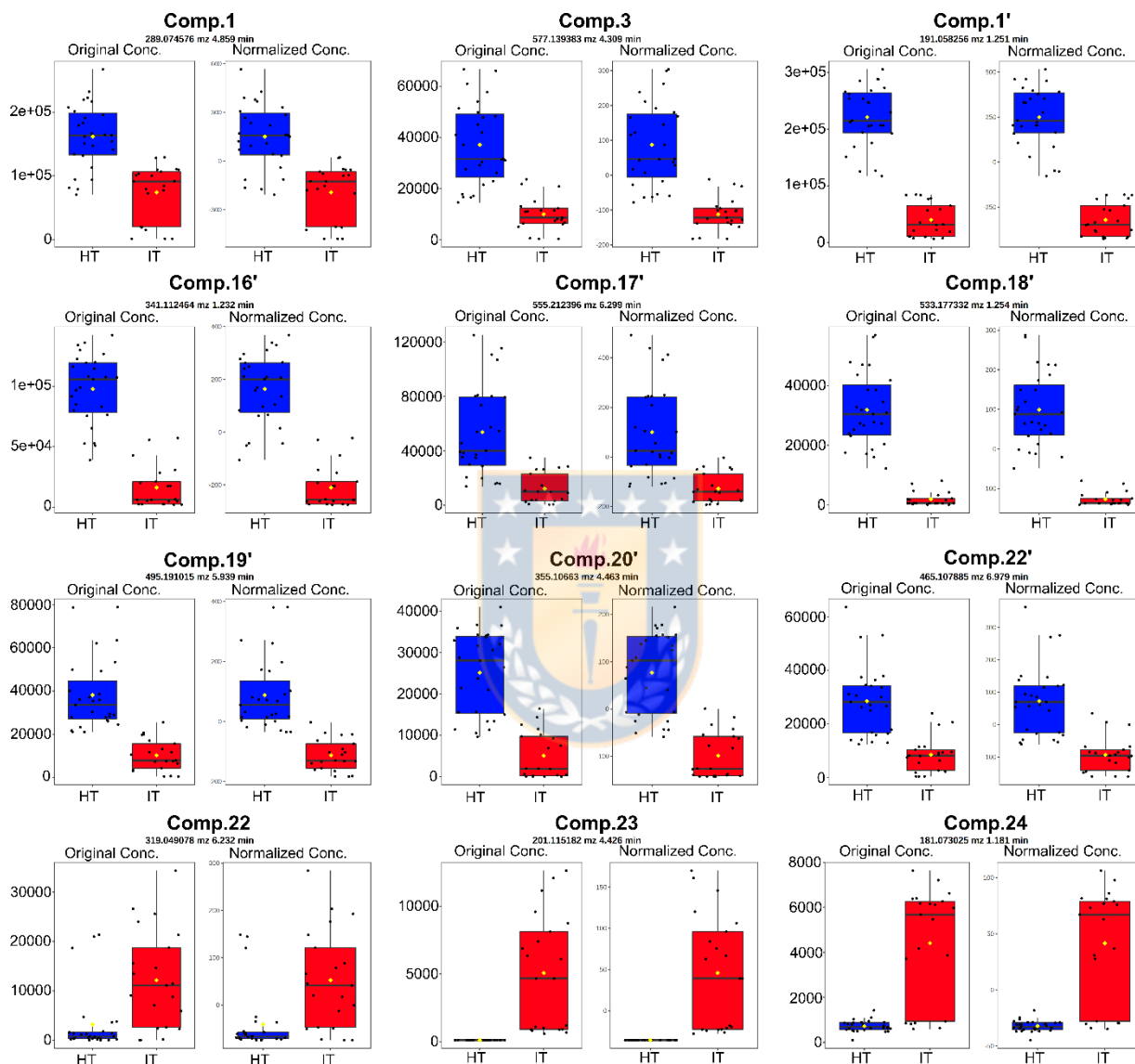


Figure S9-2: Quantitative data for the metabolite Pinosylvin found not significantly changed in the wood of *P. radiata* trees at T2. Box-and-whisker plots on the left show the original values of peak intensities in healthy (HT, blue) and infested trees (IT, red). The plots on the right summarize the normalized values.

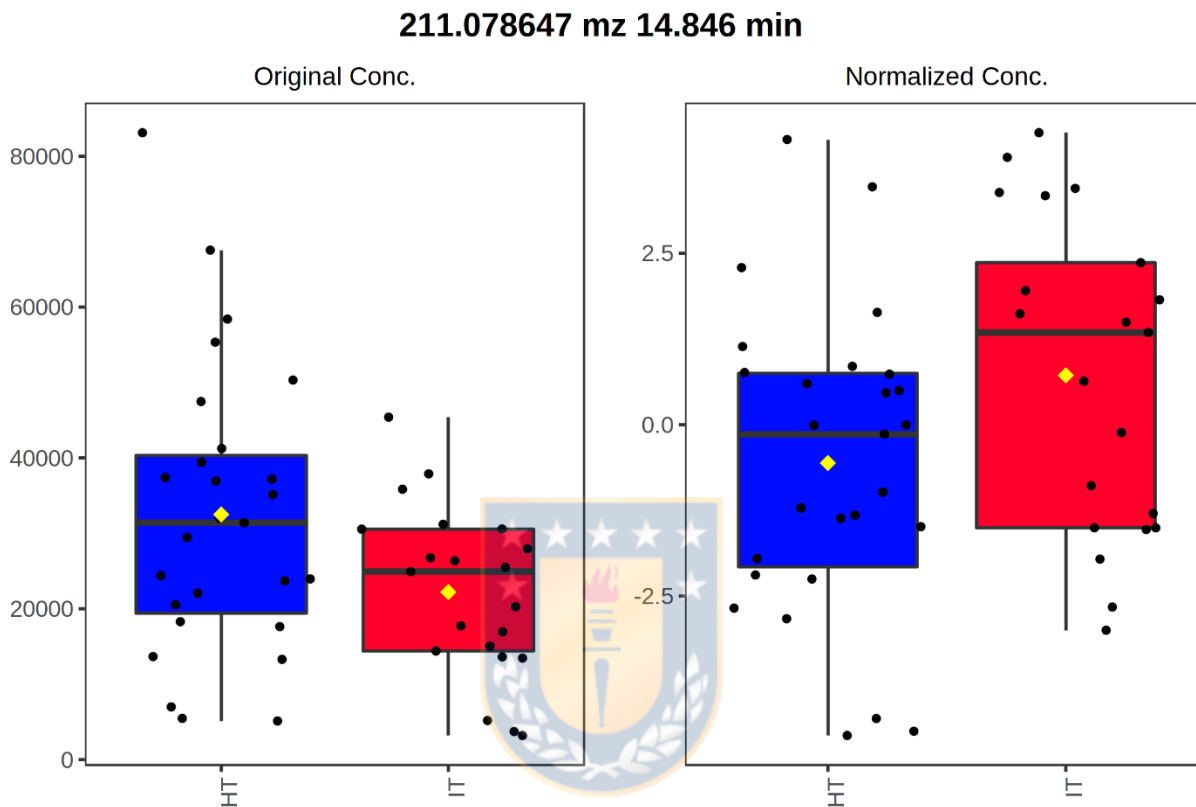


Table S1-2.: Expression data of metabolites in needles and wood at T1 and at T2.

NEEDLES AT T1							
Compound number/name	Identifier	System code	Fold Change "IT/ HT"	log2FC	p-value	Type	
1	CHEBI:15600	Ce	1,749	0,8065	0	Metabolomics	
2	44259475	Cpc	1,156	0,2091	0	Metabolomics	
3	HMDB29754	Ch	3,8	1,9260	0,000001	Metabolomics	
4	CHEBI:30797	Ce	1,4	0,4854	0	Metabolomics	
5	CHEBI:17203	Ce	4,715	2,2373	0	Metabolomics	
6	9841162	Cpc	2,726	1,4468	0	Metabolomics	
7	12314759	Cpc	2,224	1,1532	0	Metabolomics	
8	MHPLKAPNUFHKRF-SLHLPCJXSA-N	Ik	6,189	2,6297	0,000001	Metabolomics	
9	BUSMKRODPAQUUMM-NAPQKZHBSA-N	Ik	1,339	0,4212	0	Metabolomics	
10	20056942	Cpc	1,359	0,4425	0	Metabolomics	
11	NUEVO11	Ik	3,14	1,6508	0,000027	Metabolomics	
12	CHEBI:16947	Ce	1,202	0,2654	0	Metabolomics	
13	CHEBI:16828	Ce	1,215	0,2810	0,000131	Metabolomics	
14	7099087	Cpc	1,394	0,4792	0,000098	Metabolomics	
15	KMYQEVSORSASE-UHFFFAOYSA-N	Ik	1,302	0,3807	0,000011	Metabolomics	
16	CHEBI:81685	Ce	1,248	0,3196	0,000005	Metabolomics	
17	101791981	Cpc	1,393	0,4782	0	Metabolomics	
18	CHEBI:75813	Ce	1,047	0,0663	0	Metabolomics	
19	CHEBI:15682	Ce	4,778	2,2564	0	Metabolomics	
20	CHEBI:28548	Ce	1,428	0,5140	0	Metabolomics	
21	139310259	Cpc	1,959	0,9701	0,000118	Metabolomics	
22	CHEBI:28429	Ce	0,667	-0,5842	0,368279	Metabolomics	
25	NA		3,463	1,7920	0,0000037		
1'	CHEBI:29751	Ce	0,584	-0,7760	0,00011	Metabolomics	
2'	CHEBI:16119	Ce	0,267	-1,9051	0	Metabolomics	
3'	CHEBI:29073	Ce	0,011	-6,5064	0	Metabolomics	
4'	10521921	Cpc	0,207	-2,2723	0	Metabolomics	
5'	14132344	Cpc	0,335	-1,5778	0	Metabolomics	
6'	HMDB0037366	Ch	0,288	-1,7959	0	Metabolomics	
7'	101068307	Cpc	0,314	-1,6712	0,00014	Metabolomics	
8'	CHEBI:48968	Ce	0,202	-2,3076	0	Metabolomics	
10'	CHEBI:17382	Ce	0,611	-0,7108	0,000005	Metabolomics	
11'	1662	Cpc	0,416	-1,2653	0	Metabolomics	
12'	CHEBI:16856	Ce	0,057	-4,1329	0	Metabolomics	
13'	CHEBI:14321	Ce	0,1	-3,3219	0	Metabolomics	
14'	131752798	Cpc	0,449	-1,1552	0,000001	Metabolomics	
15'	11465803	Cpc	0,347	-1,5270	0	Metabolomics	
	Naringenin CHEBI:17846	Ce	2,746	1,4573	0,000009	Metabolomics	
	Dihydrokaempferol CHEBI:15401	Ce	3	1,5850	0	Metabolomics	
	Myricetin CHEBI:18152	Ce	0,703	-0,5084	0,278323	Metabolomics	
	Laricitrin acetylglucoside 44259481	Cpc	0,553	-0,8546	0,008362	Metabolomics	
	Syringetin acetylglucoside 44259495	Cpc	0,475	-1,0740	0,010146	Metabolomics	
	Quercetin CHEBI:16243	Ce	0,623	-0,6827	0,068034	Metabolomics	
	Quercetin glucoside CHEBI:68352	Ce	1,111	0,1519	0,000591	Metabolomics	
	Coniferyl alcohol CHEBI:17745	Ce	1,16	0,2141	0,000157	Metabolomics	
	Piceatannol hexoside (trans-Astringin) CHEBI:2899	Ce	0,913	-0,1313	0,268066	Metabolomics	
	Phenylalanine CHEBI:68528	Ce	1,083	0,1150	0,160999	Metabolomics	
	p coumaric acid CHEBI:36090	Ce	1,115	0,1570	0,648952	Metabolomics	
	2-oxoglutarate CHEBI:16810	Ce	0,453	-1,1424	0,000009	Metabolomics	
	Glutamine CHEBI:18050	Ce	0,451	-1,1488	0,00262	Metabolomics	
	Fumarate CHEBI:29806	Ce	0,583	-0,7784	0,000044	Metabolomics	
	Ornithine CHEBI:15729	Ce	1,636	0,7102	0,010935	Metabolomics	
	Aspartate CHEBI:17053	Ce	0,18	-2,4739	0	Metabolomics	
	Arginine CHEBI:16467	Ce	3,349	1,7437	0,000357	Metabolomics	
	Dehydroquininate CHEBI:32364	Ce	1,257	0,3300	0,024812	Metabolomics	
	Dehydroshikimate CHEBI:16630	Ce	0,881	-0,1828	0,69581	Metabolomics	
	myo-Inositol CHEBI:17268	Ce	0,76	-0,3959	0,456215	Metabolomics	
	Geniposidic acid CHEBI:5301	Ce	0,714	-0,4860	0,15543	Metabolomics	
	Indole-3-acetate 802	Cpc	11,054	3,4665	0,004737	Metabolomics	
	Vanillate CHEBI:16632	Ce	1,718	0,7807	0	Metabolomics	
	Caffeic acid CHEBI:16433	Ce	0,849	-0,2362	0,778845	Metabolomics	
	Ferulic acid CHEBI:17620	Ce	2,341	1,2271	0	Metabolomics	
	3,4-Dihydroxybenzoate CHEBI:36062	Ce	1,822	0,8655	0,013696	Metabolomics	
	Pyridoxine CHEBI:16709	Ce	2,839	1,5054	0	Metabolomics	
	Indole-3-pyruvate CHEBI:29750	Ce	10,591	3,40	0,006486	Metabolomics	
	Hydroxyindol-3-lactate CHEBI:36665	Ce	11,407	3,51	0,000016	Metabolomics	
	Dihydrocaffeyl-alcohol 11217464	Cpc	1,551	0,63	0,000205	Metabolomics	



NEEDLES AT T2							
Compound number/name	identifier	System code	Fold Change "IT/ HT"	log2FC	p-value	Type	
1	CHEBI:15600	Ce	1,328	0,41	0,000558	Metabolomics	
2	44259475	Cpc	1,126	0,17	0,000727	Metabolomics	
3	HMDB29754	Ch	2,494	1,32	0,000412	Metabolomics	
4	CHEBI:30797	Ce	1,892	0,92	0	Metabolomics	
5	CHEBI:17203	Ce	2,544	1,35	0,000433	Metabolomics	
6	9841162	Cpc	1,002	0,00	0,001663	Metabolomics	
7	12314759	Cpc	2,182	1,13	0	Metabolomics	
9	BUSMKRODPAQUMM-NAPQKZHBSA-N	Ik	1,421	0,51	0,000007	Metabolomics	
10	20056942	Cpc	1,114	0,16	0,010547	Metabolomics	
11	NUEVO11	Ik	5,99	2,58	0,000053	Metabolomics	
12	CHEBI:16947	Ce	1,087	0,12	0,000162	Metabolomics	
15	KMYQEVSRSRSCASE-UHFFFAOYSA-N	Ik	1,472	0,56	0,001198	Metabolomics	
16	CHEBI:81685	Ce	1,88	0,91	0,00001	Metabolomics	
17	101791981	Cpc	1,652	0,72	0,000072	Metabolomics	
18	CHEBI:75813	Ce	1,042	0,06	0,008469	Metabolomics	
21	139310259	Cpc	2,864	1,52	0,000078	Metabolomics	
25	NA		6,604	2,72	0,000065	Metabolomics	
3'	CHEBI:29073	Ce	0,319	-1,65	0	Metabolomics	
12'	CHEBI:16856	Ce	0,393	-1,35	0	Metabolomics	
13'	CHEBI:14321	Ce	0,209	-2,26	0	Metabolomics	
2-oxoglutarate	CHEBI:16810	Ce	0,476	-1,07	0	Metabolomics	
5-Hydroxyindol-3-lactate	CHEBI:36665	Ce	5,795	2,53	0,000016	Metabolomics	
Arginine	CHEBI:16467	Ce	9,93	3,31	0,000364	Metabolomics	
Coniferyl alcohol	CHEBI:17745	Ce	1,268	0,34	0,003431	Metabolomics	
Dihydrocaffeoyl-alcohol	11217464	Cpc	1,345	0,43	0,00179	Metabolomics	
Fumarate	CHEBI:29806	Ce	0,888	-0,17	0,732092	Metabolomics	
Glutamine	CHEBI:18050	Ce	2,281	1,19	0,007796	Metabolomics	
Indole-3-acetate	802	Cpc	11,074	3,47	0,001633	Metabolomics	
Indole-3-pyruvate	NA		13,184	3,72	0,002499	Metabolomics	
Naringenin	CHEBI:17846	Ce	1,335	0,42	0,011594	Metabolomics	

WOOD AT T2							
Compound number/name	identifier	System code	Fold Change "IT/ HT"	log2FC	p-value	Type	
6	9841162	Cpc	0,661	-0,5973	0,004398	Metabolomics	
22	CHEBI:28429	Ce	3,483	1,8003	0,000319	Metabolomics	
23	5192	Cpc	19,775	4,3056	0	Metabolomics	
24	6251	Cpc	4,997	2,3211	0,000007	Metabolomics	
22'	NA		0,409	-1,2898	0		
Piceatannol hexoside (trans-Astringin)	CHEBI:2899	Ce	1,303	0,3818	0,141763	Metabolomics	
Resveratrol	CHEBI:27881	Ce	2,042	1,0300	0,001533	Metabolomics	
Piceatannol	CHEBI:28814	Ce	1,032	0,0454	0,961404	Metabolomics	
Pinosylvin	CHEBI:17323	Ce	1,06	0,0841	0,85015	Metabolomics	
Pinoembrin	CHEBI:28157	Ce	0,739	-0,4364	0,114992	Metabolomics	
Salicylic acid	CHEBI:16914	Ce	2,75	1,4594	0,002109	Metabolomics	
Quercetin	CHEBI:16243	Ce	0,985	-0,0218	0,879948	Metabolomics	
Taxifolin	CHEBI:17948	Ce	1,296	0,3741	0,221807	Metabolomics	
Dihydrokaempferol	CHEBI:15401	Ce	1,047	0,0663	0,83742	Metabolomics	
Naringenin	CHEBI:17846	Ce	1,242	0,3127	0,175739	Metabolomics	
Coniferyl alcohol	CHEBI:17745	Ce	3,775	1,9165	0,008144	Metabolomics	

\*NA: The metabolite identifier is not available

**Method S1** Climatic conditions during sampling time, T1 and T2.

Weather conditions in April 2018 (T1) according to the nearest available stations of the Chilean Meteorological Department, located at Chillán (36°35'8.99"S 72°2'11.99"W) (code 360011) and Concepción (36°46'49.99"S 73°3'58.99"W) (code 360019), were as follow: mean maximum and minimum temperatures of 19.7 °C and 6.0 °C, respectively; accumulated rainfall of 60.8 mm, with 21.6 mm accumulated only in the day before sampling; a daily average of the UVB (280-315 nm) maximum radiation intensity was 3.2 kWh m<sup>-2</sup>; and relative humidity mean of 82.5%, with 79.9% for the day of sampling. During the second sampling (T2) on July 2018, weather conditions were as follows: mean maximum and minimum temperatures of 12.7 °C and 2.4 °C, respectively; accumulated rainfall of 80.2 mm, with 0.0 mm on the day before sampling; daily average of the UVB (280-315 nm) maximum radiation intensity was 1.53 kWh m<sup>-2</sup>; and relative humidity mean of 90.4%, with 97.9% for the day of sampling.

**Note S1** Antioxidant hypothesis for the up-regulated flavonols (**2**, **10** and **18**) in needles of *P. radiata* infested trees.

It is well known that quercetin is a more effective antioxidant than kaempferol, and luteolin than apigenin, and given that their structural differences consist only in an additional hydroxyl group in the B-ring in the case of the former (Agati & Tattini, 2010), we can hypothesize that the more hydroxyl groups are attached to the same ring, the higher antioxidant capacity they achieve. This is the case of myricetin, laricitrin, and syringetin, which are aglycones of **18**, **2**, and **10**, respectively, having a trihydroxylated B-ring. In this scenario, these flavonols could potentially function as ROS-quenching antioxidants and, together with **1** and **3**, represent the plant's photoprotective response to progressive chlorosis caused by *S. noctilio* infestation.

**Note S2** Additional systemic defense triggered in foliage after *S. noctilio* infestation.

An additional indication of *P. radiata* defense was the significant up-regulation of pungenin (**7**) in needles at T1 (2.22-fold) and T2 (2.18-fold) (Fig. **5**, Table S1). It is a glycosyl derivative of pungenol, acetophenone usually associated with a defense response in white spruce (*Picea glauca*) against the budworm *Choristoneura fumiferana* (Delvas et al., 2011; Mageroy et al., 2015, 2017). Pungenin, along with another acetophenone glycosyl derivative (picein), accumulates in white spruce leaves that, upon budworm herbivory, are hydrolyzed by the action of  $\beta$ -glucosidase (Pg $\beta$ GLU-1), releasing the corresponding toxic aglycones, pungenol and piceol (Mageroy et al., 2015, 2017). In our case, only the inactive form (pungenin) was up-regulated in needles of infested *P. radiata* trees, which leads us to think that it is a systemic response that, upon reaching target tissues or upon foliar damage, can be cleaved to fight the threat. Neither pungenin nor pungenol was up-regulated in wood at any time during the infestation, even though is in wood that *S. Noctilio* larvae form galleries during feeding and development for nearly a year before adult emergence. This may be due to the aforementioned impediment to translocation unless it is a nonspecific response triggered in the Pinaceae family after any biotic stress to protect foliage from some opportunistic organisms or herbivores.

## Reference

- Agati G, Tattini M. 2010. Multiple functional roles of flavonoids in photoprotection. *New Phytologist* 186: 786–793.
- Delvas, N., Bauce, É., Labbé, C., Ollevier, T., Bélanger, R., 2011. Phenolic compounds that confer resistance to spruce budworm. *Entomologia Experimentalis et Applicata* 141, 35–44. <https://doi.org/10.1111/j.1570-7458.2011.01161.x>
- Mageroy, M.H., Jancsik, S., Yuen, M.M. Saint, Fischer, M., Withers, S.G., Paetz, C., Schneider, B., Mackay, J., Bohlmann, J., 2017. A conifer udp-sugar dependent glycosyltransferase contributes to acetophenone metabolism and defense against insects. *Plant Physiology* 175, 641–651. <https://doi.org/10.1104/pp.17.00611>
- Mageroy, M.H., Parent, G., Germanos, G., Giguère, I., Delvas, N., Maaroufi, H., Bauce, É., Bohlmann, J., Mackay, J.J., 2015. Expression of the  $\beta$ -glucosidase gene Pg $\beta$ glu-1 underpins natural resistance of white spruce against spruce budworm. *Plant Journal* 81, 68–80. <https://doi.org/10.1111/tpj.12699>



### 3. CHAPTER N°3

**Lipidomics analysis reveals the effect of *Sirex noctilio* infestation on the lipid metabolism in *Pinus radiata* needles**



## **Lipidomics analysis reveals the effect of *Sirex noctilio* infestation on the lipid metabolism in *Pinus radiata* needles**

Sebastián Riquelme<sup>1</sup>, Valentina Campos<sup>1</sup>, Rosa Alzamora<sup>2</sup>, Oliver Fiehn<sup>3</sup> Andy J. Pérez<sup>1,4,\*</sup>

<sup>1</sup> Departamento de Análisis Instrumental, Facultad de Farmacia, Universidad de Concepción, Concepción, Chile.

<sup>2</sup> Departamento Manejo de Bosques y Medio Ambiente, Facultad de Ciencias Forestales, Universidad de Concepción, Concepción, Chile.

<sup>3</sup> UC Davis Genome Center, University of California, Davis, CA, USA

<sup>4</sup> Unidad de Desarrollo Tecnológico, UDT, Universidad de Concepción, Coronel, Chile.

\* Corresponding author E-mail: [aperezd@udec.cl](mailto:aperezd@udec.cl). Phone: + 56 41 220 3027



## 1. SUMMARY

The *Sirex noctilio*'s climatic adaption and rapid proliferation have caused *Pinus* mortality worldwide. The infestation combines the early effect of female *S. noctilio* gland secretion that causes crown foliage wilting with premature needle abscission. The spreading symbiotic fungus *Amylostereum areolatum* causes a water deficit in the crown. The water deficit caused by the fungus, along with the defoliation of the tree crown induced by the secretion of sirex, gradually weakens the tree until its death.

Lipid signals in plant-pathogen interactions occur at multiple levels in plant metabolism, from communicating virulence factors to activating plant host defence responses. 'Lipidomics' is the study of all non-water-soluble components of the metabolome. Most of these non-water-soluble compounds correspond to lipids which can provide information about a biological activity, an organelle, an organism, or a disease. Using HPLC-MS/MS based lipidomics, 122 lipids were identified in *P. radiata* needles during *S. noctilio* infestation. Twenty fatty acids (FA) were detected in the early infestation and seventeen in the prolonged infestation. In addition, phosphatidic acids (PA), N- acylethanolamines (NAE), and phosphatidylinositol-ceramides (PI-cer) accumulated in IT suggest a high level of phospholipases (PLs) activity. The

phosphatidylcholines (PC) were the most down-regulated species during infection, suggesting that this compound may be used as a substrate for up-regulated lipids. The accumulation of very long-chain fatty acids (VLCFA) and long-chain fatty acids (LCFA) during the infestation could imply the tree defence response to create a barrier in the drilled zone to avoid larvae development and fungus proliferation. On the other hand, the growth arrest phase of the trees during the prolonged infestation suggests a resistance response of the trees, regulated by the accumulation of NAE, potentially shifting the tree energy to respond to the infestation.

**Keywords:** Lipidomics, *Pinus radiata*, *Sirex noctilio*, glycerolipids, pathogenesis.





## 2. INTRODUCTION

The woodwasp, *Sirex noctilio* Fabricius (Hymenoptera: Siricidae), is one of the most damaging invasive forest pests causing several economic losses in commercial conifer stands (Klapwijk et al., 2016b). The good *S. noctilio* climate adaptation and its relatively fast spread hinder plague management causing high mortality in *Pinus* plantations worldwide (Lantschner et al., 2014b; Xu et al., 2019b). The lethality of the infestation combines the early effect of the female *S. Noctilio* gland secretion (injected in the oviposition) that induces foliage wilting at the crown with premature abscission and yellowing of the needles. Subsequently, the spreading symbiotic fungus *Amylostereum areolatum* in wood tissue causes a prolonged water deficit in the crown, killing the trees (Coutts, 1969b,c). The alteration of *P. radiata* metabolome by *S. noctilio* infestation as a catechin accumulation to avoid UV-light damage in chlorotic needles, auxins accumulation to develop new needles after abscission and the catabolism of glutathione as a substitute respiration substrate in a prolonged infestation are reported (Riquelme et al., 2022). However, the alterations of pine lipidome against *S. noctilio* infection have not been reported.

Plants constantly exposed to environmental pathogens have evolved complex mechanisms to identify and protect themselves (Rojas *et al.*, 2014). Cell membrane disruptions and alterations allow plants to detect environmental stimuli, and biotic/abiotic stresses can alter the structure and composition of cell membranes

(Beccaccioli *et al.*, 2019). Lipids are related to the primary metabolism of plants and compose 30–70 % of the membrane structures (Li-beisson, 2016). Phosphoglycerides and glycosylglycerides are higher plants' most abundant lipids specie (Schmid, 2016a). Membrane phospholipids can act as co-factor for membrane enzymes, precursors for second messengers activating ion channels, receptor kinases, or receptor-activated effector enzymes (Munnik *et al.*, 1998). Lipids signals in plant-pathogen interactions act at several levels in plant metabolism extending from the communication of virulence factors to the activation and implementation of plant host immune defences (Mehta *et al.*, 2021). Most plant-membranes consist of lipids with a hydrophilic, polar head attached to a glycerol backbone and a hydrophobic tail composed of two FA. Lipids form a hydrophobic barrier between cells and organelles and the surrounding environment. The fundamental constituent of FA is a hydrocarbon chain with an attached carboxyl group (-COOH). FA are classified according to their chain length as follows: short-chain (aliphatic tails of up to 5 or 7 carbons), medium-chain (aliphatic tails of 8 to 14 carbons), long-chain (aliphatic tails of 14 to 22 carbons), and very-long-chain (aliphatic tails longer than 22 carbons) (Reszczyńska & Hanaka, 2013). The plant biosynthesis of Fas has been widely reported. In plastids, Fas species are synthesized de novo from acetyl-coenzyme A (CoA) and malonyl-CoA, due to the joint activity of acetyl-CoA carboxylase (ACC) and fatty acid synthase (FAS) involving more than 30 enzymatic

reactions (Ohlrogge & Browse, 1995). FA build the acyl chains of all glycerolipids. FA are dynamic molecules whose degree of unsaturation can vary. Saturated FA becomes unsaturated via desaturase enzymes regulated by fatty acid desaturase genes (van der Hoeven & Steffens, 1995). Critical steps in fatty acid biosynthesis are the desaturation of the FA 18:0 to FA 18:1 catalyzed by the stearoyl-desaturase (Lightner *et al.*, 1994). Two acylation reactions transfer fatty acids to glycerol-3-phosphate to form phosphatidic acid during the initial stages of glycerolipid synthesis. Diacylglycerol (DG) is produced from phosphatidic acid (PA) by a specific phosphatase; alternatively, the cytidine 5'-diphosphate (CDP)-DG is produced from the reaction of PA with cytidine 5'-triphosphate (CTP). CDP-choline, CDP-ethanolamine, and CDP-methylethanolamine can serve as substrates for phospholipid synthesis using DG as substrate, UDP-galactose and UDP-sulfoquinovose serve as substrates for monogalactosyldiacylglycerol (MGDG) and sulfoquinovosyldiacylglycerol (SQDG) respectively. Digalactosyl-diacylglycerol (DGDG) is synthesized from MGDG. CDP-DG act as a substrate reacting with myoinositol, serine, and glycerol-3-phosphate to produce phosphatidylinositol (PI), phosphatidylserine (PS), and phosphatidyl glycerol (PG) respectively (Ohlrogge & Browse, 1995). The primary storage lipid TG is produced from DG by two key processes, acyl-CoA dependent and independent reactions catalyzed by a

diacylglycerol acyltransferase (DGAT) and diacylglycerol acyltransferase (PDAT), respectively (Li-beisson, 2016).

In chloroplast, glycerolipids such as MGDG, DGDG, SQDG, PG form the lipid bilayer of the thylakoid membrane, which has a specific role in the biogenesis and maintenance of the photosynthetic machinery (Kobayashi & Wada, 2016). In the extra-chloroplastic membrane, PC and PE are prevalent over other lipids species. PC is the central intermediate for TG production (Correa *et al.*, 2020). The accumulation of TG and DG is the primary mechanism for lipids fuel storage in plant tissue (Schmid, 2016b). TG formation is crucial to sequester FA, PA and DG into lipid droplets protecting cells from lipotoxic death (Ding *et al.*, 2017).

Plants under stress can mobilise chloroplast lipids via the glyoxylate cycle as respiration substitutes. In pathogen-plant interaction, lipids signalling plays an essential role in pathogen detection and the forward defensive cascade responses. N-acylethanolamines (NAE) are a functionally varied class of signalling lipids. NAE consist of a FA linked by an amide bond to ethanolamine (Teaster *et al.*, 2007). The synthesis NAE species activates phenylalanine ammonia-lyase (PAL) expression at a sub-micromolar level acting as elicitors (Tripathy *et al.*, 1999). PAL is a crucial enzyme of the phenylpropanoid pathway for supplying the basic structures to produce polyphenolic compounds that act as defensive compounds against fungi, insects, and viruses (Dixon & Paiva, 1995; Ferrer *et al.*, 2008a).

‘Lipidomics’ is the broad analysis of all non-water-soluble components in the metabolome, although in practice commonly involves a wide number of class lipids giving helpful knowledge about a biological process, organelle, entire organism or/and pathological state of interest (Kenwood & Merrill, 2016). Comprehensive lipidomics analysis, validation of the methodology, and the increment of lipids coverage (Tobias *et al.*, 2013), made feasible the identification of thousand lipids compounds in the biological samples (Cajka & Fiehn, 2014, 2016; Cajka *et al.*, 2017). Applying lipidomics to *P. radiata* trees infected with *S. noctilio* it is possible to know the alterations in the lipidome caused by the infection by noctilio. Understanding these alterations can help focus pinus breeding programs selection.

### **3. EXPERIMENTAL PROCEDURES**

#### **3.1 Origin of plant material and collection**

Unmanaged Stand of *Pinus radiata* D. Don with 14-year-old belonging to commercial plantations of the forestry company MININCO S.A. was selected. The plantation was in a high-incidence area of *S. noctilio* (36°26’18.0”S 72°14’32.0”W) (Ide *et al.*, 2018). Early *S. noctilio* infestation was confirmed by visual inspection of the main reported symptoms (Bordeaux & Dean, 2012c). Ten infested trees (IT) with several *S. noctilio* oviposition holes in the tree trunk and wilting needles at the crown

were randomly selected. Also, ten healthy trees (HT) without visual symptoms of *S. noctilio* attack as closely as possible to each (IT) were chosen as control.

The lipidome analysis was focused on two infestation states. The first period (early infestation) was chosen to study the lipidome changes of *P. radiata* related to the *S. noctilio* venom. The early infestation sampling (T1) was performed on April 12, 2018 (fall). April marks the end of the *S. noctilio* flight season in Chile, safeguarding that (HT) remain without attack throughout the experiment. The second sampling (T2) was performed on July 12, 2018.

Approximately 200 g of needles from the upper third of each tree was harvested. Only green needles from infected trees were considered to prevent advanced senescence symptoms. Immediately after collection, samples were quenched in liquid nitrogen and transported to the lab. Samples were kept at -80 °C until their analysis.

### **3.2 Sample preparation and lipidome extraction**

Sample preparation for the analysis was performed for metabolome/lipidome extraction with minor modifications (Valledor et al., 2014c). Needles frozen-fresh samples (FFS) were cryogenically ground to a fine powder employing a ball mill at 30 Hz for 5 min (Retsch MM-400, GmbH, Haan, Germany). The moisture content of each FFS was determined by a thermogravimetric method to normalize the weight

for extraction. In an independent 167rabidopsi block, samples were processed in triplicate for each sampling time (T1 or T2). For the extraction, 800  $\mu\text{l}$  of cold ( $4^{\circ}\text{C}$ )  $\text{MeOH}/\text{H}_2\text{O}/\text{CHCl}_3$  (2.5:0.5:1) were added to 100 mg (dry weight basis) of powdered FFS contained in a 2 ml microcentrifuge tube and shaken for 60 s at 30 Hz. Then, samples were centrifuged at 13300 g for 10 min at  $4^{\circ}\text{C}$ . Next, 600  $\mu\text{l}$  of the supernatants were transferred to new tubes, and 400  $\mu\text{l}$  of water and 400  $\mu\text{l}$  of  $\text{CHCl}_3$  were added, shaking for 30 s at 20 Hz. The two phases were centrifuged at 13300 g for 5 min at  $4^{\circ}\text{C}$ . Hydrophilic (top layer) and lipophilic (bottom layer) fractions were transferred to new microcentrifuge tubes, 600  $\mu\text{l}$  each, and dried in a vacuum centrifuge (Eppendorf, Concentrator plus). Dried extracts were stored at  $-80^{\circ}\text{C}$  until needed. Only the lipophilic fractions were used in this study.

### 3.3 LC-MS lipidomics analysis

Dried lipophilic extracts were resuspended in 488  $\mu\text{l}$  of ice-cold (3:10) methanol:methyl tertbutyl ether with quality control mix 22:1 cholesterol ester standard, vortex for 10 sec, and dried for 4 hrs at 1500 rpm in a Centrivap I. Then, 1000  $\mu\text{l}$  of methanol:toluene (9:1 v/v) with 12-[[cyclohexylamino)carbonyl]amino]-dodecanoic acid (50 ng/ml) were added to each sample. The samples were vortexed for 10 sec, sonicated for 5 min, and centrifuged for 2 min at 16000 g. Aliquots of 50

$\mu\text{l}$  per sample were collected for pooled quality control (QC). Two aliquots of 450  $\mu\text{l}$  of each sample were taken separately for positive and negative UPLC-MSMS analysis modes.

Data are acquired by LC-MS/MS on an ultra-high performance liquid chromatography system Agilent 1290 Infinity LC system (Agilent Technologies, Santa Clara, CA, USA) with a pump (G4220A), a column oven (G1316C), and autosampler (G4226A). Lipids were separated on an Acquity UPLC CSH C18 column (100 mm length, 2.1 mm id., 1.7  $\mu\text{m}$ ) coupled to an Acquity CSH C18 VanGuard pre-column (5 mm length, 2.1 mm id., 1.7  $\mu\text{m}$ ) (Waters, Milford, MA, USA). Separations were carried out at 65°C at a flow rate of 0.6 ml/min. The mobile phases consisted of (A) 60:40 (v/v) acetonitrile:water and (B) 90:10 (v/v) isopropanol:acetonitrile, both with ammonium acetate 10 mM for negative mode and both with ammonium formate 10 mM plus 0.1% formic acid for positive mode. The gradient for each mode was: 0 min 15 % (B); 0–2 min 30 % (B); 2–2.5 min 48 % (B); 2.5–11 min 82 % (B); 11–11.5 min 99 % (B); 11.5–12 min 99 % (B); 12–12.1 min 15 % (B); 12.1–15 min 15 % (B).

### **3.4 Data processing and statistics**



Data were converted into open raw files using Reifycs Analysis Base File (ABF) software. Time correction for Lipidblast library annotation was done with a Microsoft excel sheet using the retention time of the standards quality control mixture. General workflow for data processing: data collection, peak detection, deconvolution, identification, adducts and alignment were made in MS-DIAL (Tsugawa et al., 2015b). Generated bucket tables were first manually cured using Microsoft excel for blank subtraction, feature filter using intragroup covariant upper limits of 50%, features present in almost 50% of the biological replicates per group, and signal/noise ratio higher than ten were selected. Potential duplicates, adducts and isotopes were filtered using MS-FLO (DeFelice et al., 2017a). Curated data with only annotated lipids species from (+) and (-) ESI modes were combined in a single dataset used in the subsequent statistical analysis.

Statistical analysis was done in the Metaboanalyst platform. The data was Pareto-scaled and normalized by sum. Then, exploratory statistics were done using principal component analysis (PCA) to reduce data dimensionality and uncover the inherent cluster pattern in the combined data (features in ESI positive and negative mode) (Worley & Powers, 2013b). Also, Orthogonal Projection to Latent Structures Discriminant Analysis (OPLS-DA) was applied for the T1 and T2 data sets. The supervised modelling method was applied to the dataset to discover features correlated with systemic lipids alteration in needles of *P. radiata* after infestation by

*S. noctilio*. Cross-validations and a permutation test of class labels using internal leave-*n*-out cross-validation were done (Worley & Powers, 2013b, 2016c). The VIP score of a variable is calculated as a weighted sum of the squared correlations between the PLS-DA components and the original variable. The most contributory variables in class discrimination are estimated with the highest VIP scores. In the VIP score, each variable corresponds to each identified lipid. Finally, the volcano plot analysis method was used to visualize statistically significant lipids characterizing IT and HT in both early and prolonged infection. The analyses were set at 2.0 Fold-change threshold and 0.01 P-value threshold. Each point corresponds to identified lipids in the volcano plot. The lipids placed at the upper extremities of the volcano plots and further from the centre correspond to the most significant lipids for the model and contribute significantly to the separation of the groups.

## 4. RESULTS

### 4.1 Lipids profile in *P. radiata* needles under *S. noctilio* infestation

One hundred twenty-two lipids were identified in *P. radiata* needles, 90 and 32 compounds using ESI negative and ESI positive mode, respectively (detailed in Table S1-3). The identified lipids correspond to 40 phospholipids, 20 glycolipids and 62 neutral lipids. The identified phospholipids were subdivided into PA: 2 compounds, PG: 4 compounds, PC: 19 compounds, lysophosphatidylcholine (LPC): 4 compounds, PE: 8 compounds, PI: 1 compound, phosphatidylinositol-ceramide (PI-cer): 2 compounds. The identified glycolipids were subdivided into DGDG: 12 compounds, and MGDG: 8 compounds. The identified Neutral lipids were DG: 25 compounds, TG: 2 compounds, NAE: 11 compounds. FA: 24 compounds, and two fatty acyl esters of hydroxy fatty acid (FAHFA).

The lipid library and species were selected considering glycerolipids representing the most abundant class present in higher plants. Sulfoquinovosyl diacylglycerol (SQDG) species were not detected in the analysed data.

### 4.2 Statistical models of *P. radiata* trees upon infestation by *S. noctilio*

Unsupervised statistical analysis by PCA in T1 and T2 was used to evaluate each tree condition's spontaneous differentiation. The results of PCA lipidomic analysis in trees during early and prolonged *S. noctilio* infestation are shown in Fig.

S1-3. The lipidomic response in the score plot during the early infestation (T1) showed a clear separation between healthy HT and infested IT with red and green dots, respectively (Fig. S1-3a). The groups are within their 95% confidence regions with an explained variance of 63.2% for PC1 and 14.6% for PC2 (combined explained variation of 77.8%). On the other hand, a partial separation between groups during prolonged *S. noctilio* infestation (Fig. S1-3b) shows an overlapping of their 95% confidence region. However, the model showed a separation trend between groups, with acceptable variance explained in PC1 of 60.8% and 14.8% for PC2, with a combined explained variation of 75.6%. The separation in the score graphs in the PCA model indicates significant intrinsic differences in the level of the features of each analyzed group (IT and HT). The PCA model can be used as a quality indicator of the subsequent supervised models (Worley & Powers, 2016b). The score plots of the supervised model oPLS-DA to discover features correlated with systemic lipids alteration in needles of *P. radiata* during T1 and T2 infestation by *S. noctilio* showed a clear group separation (Fig. 1-3).

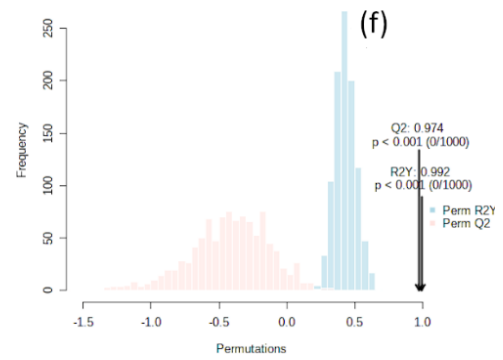
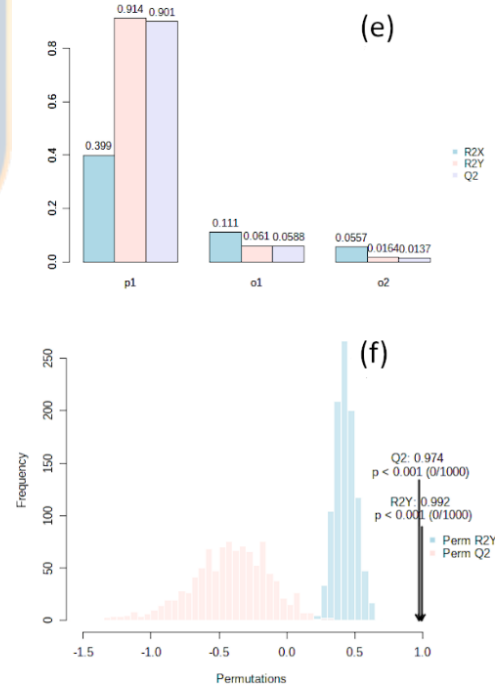
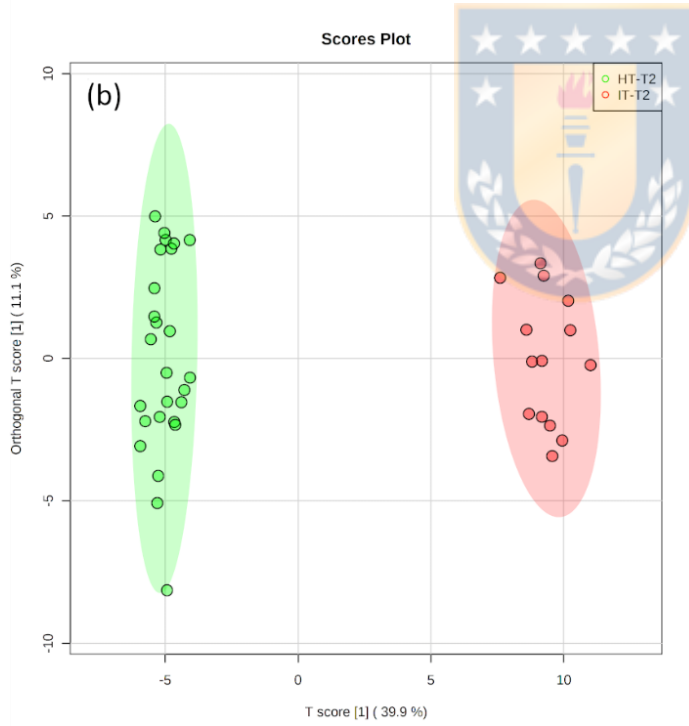
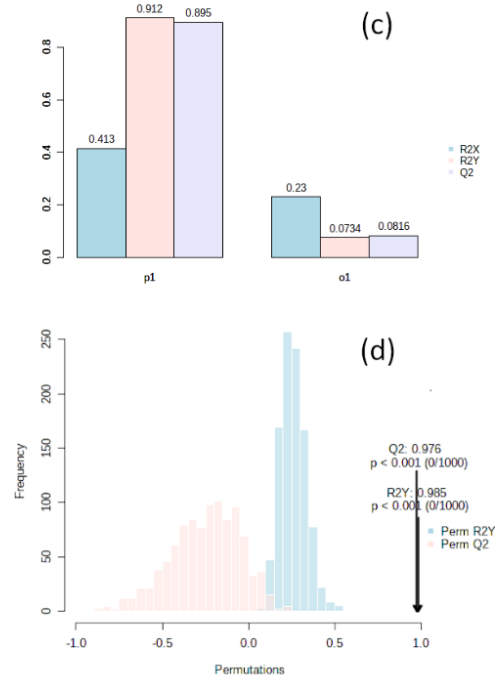
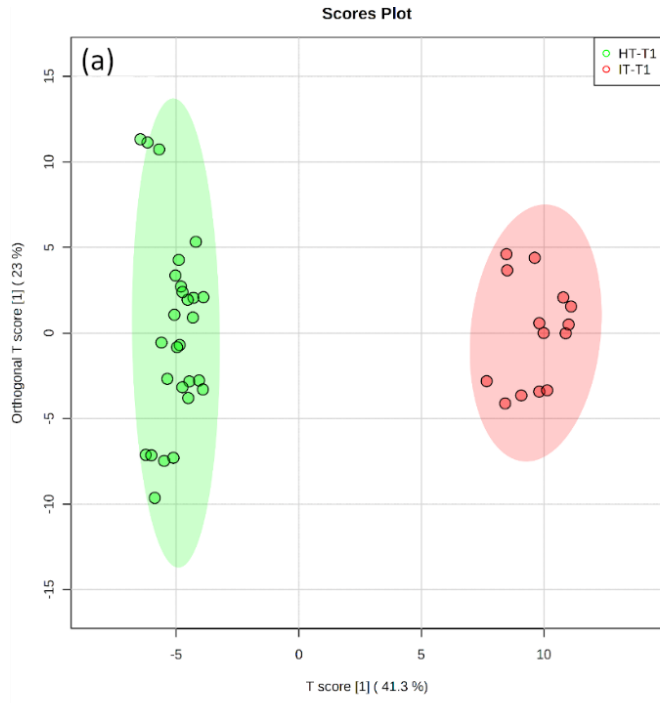


Figure 1-3: Score plot of OPLS-DA models based on combined datasets (+) ESI and (-) ESI among healthy trees (HT, green circles) and infested (IT, red circles), with their 95% confidence regions for (a) T1 (sampling 1) and (b) T2 (sampling 2). Graphics of OPLS-DA predictive model performance by (c) cross-validation, and (d) permutation with 1000 random permutation tests of class membership for T1 and I and (f) T2, respectively.

The supervised model of early *S. noctilio* infestation (Figure 1-3a) revealed a substantial difference in lipid levels between HT (green dots) and IT (red dots) groups, as well as their 95% confidence region. To avoid an overfitted model or biological nonsense feature explanation, the OPLS-DA model was validated using permutation and cross-validation tests (Figure 1-3c) with R2X (explained variance in X) of 0.643 and Q2 (goodness of prediction) of 0.977, as well as the test leave-n-out approach (Figure 1-3d) with Q2: 0.976 and R2Y: 0.985. In the same way, the score plot of prolonged infestation by *S. noctilio* (Figure 1-3b) showed a significant differentiation of HT (green dots) and IT (red dots) groups with their 95% confidence regions. Validation of the oPLS-DA model by permutation (Figure 1-3e) revealed a strong correlation with R2X values of 0.51 and Q2 values of 0.973 (goodness of prediction). In cross-validation (Figure 1-3f), Q2 was 0.74, and R2Y was 0.99. The oPLS-DA results in T1 and T2, presented an excellent statistical performance, demonstrating consistency between projected and original data and good model-to-data fitting quality for both models, confirming statistically significant differences in features between HT and IT during the early and prolonged *S. noctilio* infestation.

### 4.3 The Early effect of *S. noctilio* infestation in lipids of *P. radiata* trees

VIP scores extracted from the oPLS-DA model indicate the contribution of each variable in the separation (Worley & Powers, 2016b). The results of VIP analysis of the leading twenty lipids species with high-score are represented in Fig. S2-3. During the early stage of *S. noctilio* infestation (Fig. S2-3a), the IT group (red square) showed a high correlation with the increase of the concentrations of two fatty acyl ester of hydroxy fatty acid (FAHFA): FAHFA 26:0;O|FAHFA 12:0/14:0;O, and FAHFA 28:0;O|FAHFA 12:0/16:0;O. Likewise, with seven FA: FA 18:3;O, FA 20:0, FA 17:0, FA 18:1, FA 23:0, FA 22:0, and FA 38:6|FA18:2\_20:4. Finally, with one PI: PI 34:3 was correlated with IT. In contrast, HT-related lipids (blue square) with a high VIP value which were in low concentrations in IT during an incipient infestation, thus were consumed or no longer synthesized during this process were mainly PC: PC 36:3 B, PC 38:5 B, PC 40:6|PC 20:3\_20:3, PC 36:3|PC 18:1\_18:2, PC 36:3|PC 18:1\_18:2, PC 38:5 A, PC 34:1, PC 36:5|PC 18:2\_18:3, and PC 38:8, and one saturated PI-Cer 37:0;3O.

On the other hand, using the volcano plot model applied to T1 (Figure 2-3), fifty-nine lipids were identified such as significant lipids in needles of *P. radiata*. Twenty-nine lipids were upregulated (red circles), and thirty lipids were downregulated (blue circles) during early *S. noctilio* infestation. PCs with fifteen significant compounds were the most abundant lipids downregulated, reaching fifty

per cent of the group. The second most abundant type of lipids corresponds to DG with six significant compounds (20%), followed by MGDG with five compounds (17%), PE with three compounds (10%) and PI-cer with 1 compound (3%). In contrast, FA were the most abundant lipid upregulated with 18 significant compounds (69%), followed by DG with four compounds (14%), and LPC and PA with two compounds each (7% each).

The results of the statistical models using volcano plot and VIP score extracted from the oPLS-DA, applied to *P. radiata* needles during the early infestation of *S. noctilio* confirm that the most abundant significant lipid species correspond to FA and PC, up and downregulated, respectively.

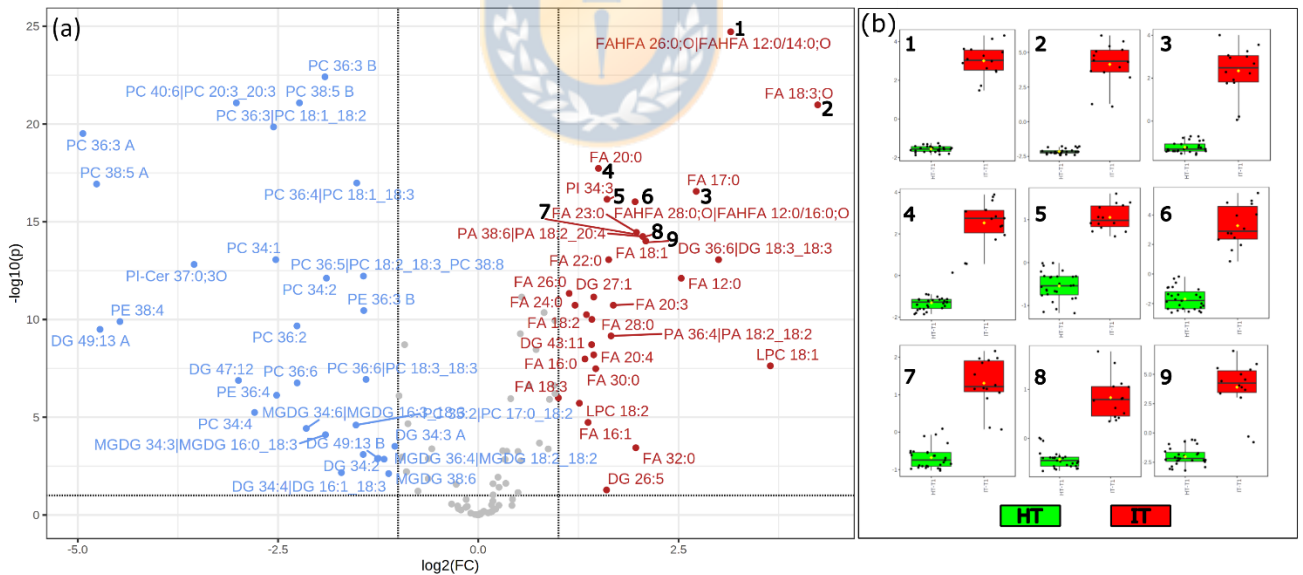


Figure 2-3: Volcano plot of IT vs HT in **T1** from using Fold Change (FC) analysis and T-tests to select significant features based on biological significance and statistical significance of features present in *P. radiata* needles under *S. noctilio* infestation (a) and whisker and box plot of



the first 9 significant feature related with IT plotted by decreasing magnitude order (**b**). (Suggested 2-column fitting image)

#### 4.4 The prolonged effect of *S. noctilio* infestation in lipids of *P. radiata* trees

VIP analysis results during the prolonged stage of *S. noctilio* infestation (Fig. S2-3b) were similar to those obtained during the early stage of infestation. The IT group (red squares) showed an upregulation of two FAHFA: FAHFA 26:0;O|FAHFA 12:0/14:0;O, and FAHFA 28:0;O|FAHFA 12:0/16:0;O. likewise with eight FA: FA 18:1, FA 20:3, FA 17:0, FA 28:0, FA 30:0, FA 12:0, FA 23:0, and FA 20:4. Also, the results showed an increase in the levels of LPC 18:1, and PI-Cer 37:1;3O. On the other hand, lipids present in higher concentrations in HT (blue squares) correspond to four PC: PC 36:3 B, PC 36:3 A, PC 34:2, and PC 36:3|PC 18:1\_18:2. One MGDG: MGDG 34:6|MGDG 16:3\_18: 3 and one PI-cer: PI-Cer 37:1;3O.

Interestingly, upregulation of a PI-cer lipid was associated with HT during the early infestation stage. However, during the prolonged infestation stage, one PI-cer lipid was bound to the Its. It is important to point out that both PI-cers differ in one unsaturation in their aliphatic chain, presenting saturation in IT and unsaturation in HT.



## 5. DISCUSSION

The following discussion focuses on the lipid groups with the most significant number of compounds, particularly those activated in infected trees.

In early infection of *S. noctilio* on *P. radiata* trees, the results of the volcano plot (Figure 2-3a) The most significant lipids in early infestation of *S. noctilio* on *P. radiata* trees correspond to the FA class with 18 FA and 2 FAHFA. FAHFA 26:0;O|FAHFA 12:0/14:0;O was the most upregulated significant lipid (8.8-fold), followed by FA 18:3;O (18.9-fold), FA 17:0 (6.6 fold), FA 20:0 (2.8-fold), FAHFA 28:0;O|FAHFA 12:0/16:0;O (3.8-fold) FA 23:0 (3.9-fold), and FA18:1 (4.2-fold).

FAHFA are a recently discovered class of lipids with attractive biological activity in mammals, highlighting their anti-inflammatory effect. Interesting amounts of FAHFA have been found in foods such as vegetable oils, grains, fruits, and meats. However, its biological activity in the plant has not been investigated. On the other hand, activating phospholipase genes in plants, particularly Fas formation, has been reported as an early signalling mechanism in plant defence responses (Laxalt & Munnik, 2002a). Female *S. noctilio* inject venom gland secretion into their conifer hosts during oviposition. As a result, the mucus must be responsible for the early physiological changes in *P. radiata* detected following *S. noctilio* infection (Coutts, 1969a). Pathogens typically induce nonhost resistance, PTI [pathogen-associated molecular pattern (PAMP)-triggered immunity], and ETI in the host

(effector-triggered immunity). When pathogen-derived elicitors are recognized by the host-encoded pattern-recognition receptors (PRRs), PTI or basal resistance is activated. Induction of PTI reduces the spread of pathogens but cannot prevent it entirely (Lim *et al.*, 2017).

In *Arabidopsis* models, the activation of phospholipases D (PLD) by the accumulation of oleic acid (FA 18:3) was reported. The FA accumulation triggers changes such as water loss, stomatal activity and the generation of ROS. The PLD activity affects mature leaves, which have comparatively higher PLDs than juvenile leaves (Wang & Wang, 2001). *P. radiata* under *S. noctilio* infestation, the early physiological change is the increase of starch in the leaves, and, in some instances, caused photosynthate accumulation in the needles, and chlorophyll begins to decrease, the older needles turn yellow, and yellowing spreads to younger needles (Coutts, 1969b). In the early stage of infestation, apparent symptoms of *S. noctilio* infestation were the needle wilt and senescence of older foliage (see Fig. S3-3). The accumulation of FA is characteristic of natural leaves senescence (Hong *et al.*, 2000). Consequently, it could be suggested that the venom of *S. noctilio* activates PLs that increase the concentration of FA in the needles, promoting their natural senescence. Moreover, the report of glutathione consumption in needles after *S. noctilio* infestation (Riquelme *et al.*, 2022) suggests the senescence could act as a resistance mechanism to the removal of xenobiotic substances by the glutathione S-

transferase (GST) detoxification (Gullner et al., 2018b). However, the specific mechanism of venom-needle interaction remains unclear.

On the other hand, the significant accumulation of LCFA (ten compounds) and VLCFA (nine compounds) produced in needles in the early stage of infestation could suggest a defence response to form a barrier defence in the drilling zone (Raffaele *et al.*, 2009). Besides, the prolonged infestation found a similar activity with seventeen FA. Also, the increase in chain length of VLCFA species could be related to an antifungal defensive response of pine trees, which involves the production of a polyphenolic resinous barrier in the cell wall to prevent the fungi spread (M. P. Coutts & Dolezal, 1966). In this regard, seven VLCFAs with chain lengths between 22 and 32 carbon units were triggered. For the above, the reports of some resistance pines to *S. noctilio* attack with high activity of resin formation were reported (Ryan & Hurley, 2012). In the field experiment in T2, the resin in the oviposition site of *S. noctilio* to form a barrier kept working until the *P. radiata* tree died, even in non-resistance trees (see Fig. S3-3). However, the evidence indicates that polyphenols were not part of the resins in the defence mechanism, possibly due to difficulties with their translocation (Riquelme et al., 2022). In this context, the evidence suggests that the translocation of FA through the resin ducts could be altered but not entirely prevented.

The trigger of unsaturated C18 FAs (UFAs) such as FA 18:3 (2.0, 2.2-fold), FA 18:2 (2.6, 2.4-fold), and FA 18:1 (4.2, 2.6-fold) was observed in the early and prolonged infestation stage, respectively (details shown in table S2-3 and S3-3). FA are precursors of bioactive molecules such as NAEs, oxylipins and jasmonates in responding to biotic and abiotic stresses (He & Ding, 2020). For example, the accumulation in plants of FA 16:0, 16:1, 18:1, 18:2 and 18:3 is associated with resistance to fungus and pathogens, serving as energy sources in the plant defence response. Also, FA C16 and C18 upregulate the R-gene transcription and control the ROS-generating enzyme (Lim et al., 2017). During prolonged infection, metabolic activity associated with C18 FA was maintained, indicating that infected trees were unsuccessfully attempting to respond to *S. noctilio* attack.

During the early stage of infection, the PC group exhibited the ten compounds downregulated (50% of the significant lipids in HT group). PCs are a primary glycerolipid of most plant cell membranes but are virtually absent from the internal plastid membranes. In green tissue senescing, PC begins to diminish, along with PE and PI. Decreased phospholipid levels associated with ageing reduces membrane integrity and allows nutrient leakage (Ferguson & Simon, 1973). At the time of natural leaf senescence, galactolipases and phospholipases release FA from glycerolipids in the chloroplast, endoplasmic reticulum, and other membranes. The

process for lipid turnover feeds the tricarboxylic acids (TCA) cycle, glyoxylate cycle, or the glutamate-glutamine cycle to produce primary metabolites from the senescing leaf to the phloem and sink tissue (Troncoso-Ponce et al., 2013). Chloroplast PC are potential precursors for the manufacture of eukaryotic galactolipids. Galactolipids are produced in the plastid envelope by galactosylation of DG with UDP-galactose. Feeding eukaryotic galactolipid synthesis with DG from the PC requires FAD2-desaturation in the ER and the transfer of lipids from the ER to the chloroplast envelope (Botella et al., 2017). This cycle on PC (the Lands cycle) transiently creates PA and LPC with higher water solubility than PC, which could enhance the transfer of PC across aqueous compartments and membranes (Zhao, 2015). During the early infestation stage, the LPC 18:1 (7.3-fold) and LPC 18:2 (2.9-fold) were triggered, which can be attributed to hydrolysis of the chloroplast membranes, possibly to recycle compounds from chlorotic leaves to sink organs during senescence caused by *S. noctilio*'s venom (Millner & Ekin Atilla-Gokcumen, 2020; Troncoso-Ponce et al., 2013).

Phospholipases A1 (PLA1) and A2 (PLA2) can remove acyl groups from both sn-1 and sn-2 positions of PCs yielding FA and lysophospholipids formation. Plant PLD and PLA1-2 release FA during the host-pathogen interaction (Beccaccioli et al., 2019). Mainly, PLD may regulate the temporal and spatial creation of particular PA, which may serve a specialized role (Wang et al., 2006). For instance, a previous

study demonstrated that PLD and its derivative PA were necessary for the Arabidopsis response to ROS. The absence of PLD makes plants more susceptible to H<sub>2</sub>O<sub>2</sub>-induced cell death (Zhang et al., 2003). In addition, the reduction of PA synthesis by a PLD inhibitor decreased penetration resistance of powdery mildew (Pinosa et al., 2013). PA participate in the ROS response during plant-endophyte contact (Camehl et al., 2011). During the early stage of the infestation, the concentrations of PA 36:4|PA 18:2\_18:2 and PA 38:6|PA 18:2\_20:4, were 3.1-fold and 4.1-fold, respectively. Also, during the prolonged infestation, they were 2.5 and 2.3-fold, suggesting the infected trees maintained PLD activity to combat the *S. noctilio* infection. However, an increase in PA concentration has been reported in plants exposed to UV radiation damage. Considering that *P. radiata* trees synthesize flavonoids to reduce UV radiation damage during chlorosis, it is possible to suggest a relationship in PA signalling with UV-B radiation damage (Dong et al., 2012)

Various PLD produces NAE in plants (Blancaflor et al., 2014). NAE can influencing the expression of defensive genes such as phenylalanine ammonia-lyase (PAL) in plant-pathogen interactions (Tripathy et al., 1999). In addition, NAE metabolism and abscisic acid signalling influence growth regulation in response to abiotic stresses (Teaster et al., 2007). NAE regulate secondary dormancy and growth arrest mediated by the ABA signalling pathway that controls the seed-to-seedling transition (Lopez-Molina et al., 2001). In the early stages of an infestation, no detectable NAE was



induced in IT (Figure 2-3A). In contrast, prolonged *S. noctilio* infestation resulted in a 2.2-fold upregulation of NAE 16:2 (Figure 3-3a). Hence the NAE response could be due to a growth stop to redirect the tree's energy to respond to the infestation.

During the prolonged infestation stage, the upregulation of PI-Cer 37:1;3O could be attributable to the interaction with *A. areolatum* by 185rabidopsis the cell-surface pattern recognition receptor. In 185rabidopsis, the ceramide D (Pi-Cer D) triggers a defence response to the plant pathogenic oomycete *Phytophthora infestans*. Further, PI-Cer 37:0;3O was downregulated in early (0.08-fold) and prolonged infestation (0.24-fold), suggesting a feasible relation in the synthesis of both species.

Finally, DG species showed variable trends in the early infestation with the upregulation of DG 36:6|DG 18:3\_18:3 (8.0-fold), DG 25:5(3-fold), DG 27:1 (2.7-fold), DG 43:1 (2.7-fold), and downregulation of DG 49:13 A (0.038-fold), DG 47:12 (0.12-fold), DG 36:6|DG 18:3\_18:3 (0.3-fold), DG 34:2 (0.41-fold), DG 49:13 B (0.42-fold), DG 34:3 A (0.48-fold). The same trend was observed in the prolonged infestation with the upregulation of DG 36:6|DG 18:3\_18:3 (11.2-fold). However, DG 29:1, and DG 49:13 were upregulated in *P. radiata* needles under the prolonged infestation by *S. noctilio*. Typically, the DG level of plant cells is minimal, and no plant proteins involved in signal transduction have been found. However, it is known that DG levels change in response to numerous developmental and environmental signals. For instance, the accumulation of DG from the PC/PLC route under salinity

stress (Ha & Thompson, 1991), phosphate starvation (Pierrugues et al., 2001), and the conversion of MGDG to DG by PLCs in response to freezing stress (Tan et al., 2018).

## 6. CONCLUSION

The attack of *S. noctilio* on *P. radiata* trees triggers a marked change in the lipid profile of the leaves. The most notable changes in both early and late infection were an increase in FA, being the family of significant compounds triggered in infected trees with high activity in C18 FA with several functions in plant defence and VLCFA with activity in the resin formation (Fett-Neto & Rodrigues-Corrêa, 2012; Lloyd, 1975). Also, FAHFA were upregulated in both infection periods. However, it was not possible to attribute its specific biochemical function. On the other hand, the upregulation of LPC and PA can be observed, suggesting a marked activity of phospholipases (Canonne et al., 2011; Laxalt & Munnik, 2002b; Wang & Wang, 2001; Zhao, 2015). A remarkable decrease in the PC family was observed in early and late infestations. Lipid changes can be attributed to pathogen recognition by the tree, with marked early leaf senescence playing a dominant role in the outcome of infection. In prolonged infection, NAE accumulation could be participating, signalling the arresting growth of infected *P. radiata* trees. Finally, compounds such as PA that interfere with the ROS balance and the direct response

against pathogens suggest that the plant invests energy in a defence mechanism, which is ultimately unsuccessful and culminates in the death of infected individuals (Shiva et al., 2018; Zhao, 2015).

The attack of *S. noctilio* causes a series of alterations in the lipidome of *P. radiata* trees. Our investigation is the first report of alterations in the pine lipidome caused by the infestation of the insect. We believe that the reported results help to understand how the tree responds to the insect attack. Although more studies are necessary to understand the specific mechanisms involved in the plant-insect interaction, we believe that the reported information could help future crop improvement programs.



## 7. ACKNOWLEDGMENTS

We thank Dr. Miguel Castillo, chief of the Plant Protection Area at the forestry company MININCO S.A., for his assistance in locating pine stands and identifying the presence of woodwasp. This work was supported by projects ANID/CONICYT FONDECYT Regular 1181915, ANID/CONICYT FONDEF/CONCURSO IdeA I+D FONDEF/CONICYT 2019 ID19I10206, FONDEQUIP EQM170023, and by CONICYT PIA/APOYO CCTE AFB170007, ANID BASAL FB210015. This research was also supported by CONICYT doctoral fellowship N°21161407.



## 8. SUPPORTING INFORMATION

### Supporting Information

Article title: **Lipidomics analysis reveals the effect of *Sirex noctilio* infestation on the lipid metabolism in *Pinus radiata* needles.**

Authors: Sebastián Riquelme<sup>1</sup>, Jasna V. Campos<sup>1</sup>, Andy J. Pérez<sup>1,5,\*</sup>

#### The following Supporting Information is available for this article:

Fig. S1-3 Principal component analysis (PCA) for unsupervised clustering exploration from combined datasets (+) ESI and (-) ESI.

Fig. S2-3 VIP score plots from oPLS-DA for annotated lipids of combined datasets.

Fig. S3-3: Photographic recorder of *Pinus radiata* under *S. noctilio* early and prolonged infestation

Table S1 Lipids identified in *P. radiata* needles by lipidomics analysis.

Table S2 Volcano plots results of *P. radiata* needles in early *S. noctilio* infestation

Table S3 Volcano plots results of *P. radiata* needles in prolonged *S. noctilio* infestation

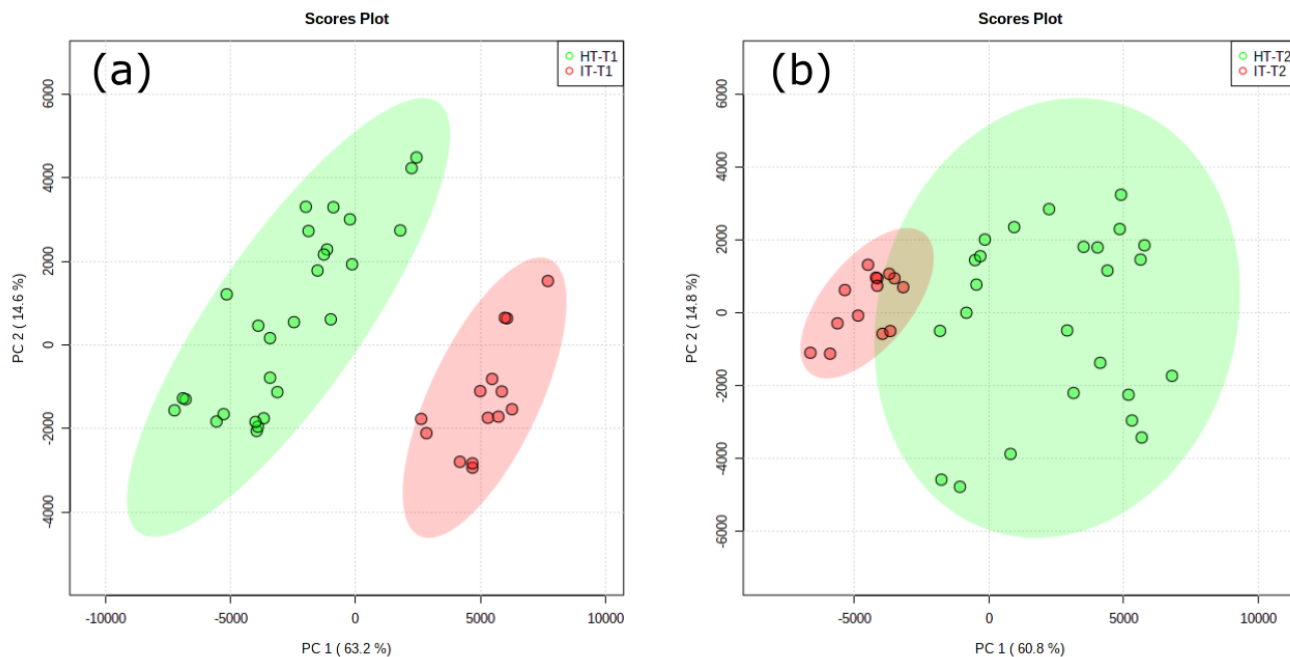


Figure S1-3: Scores plots of PCA models based on combined datasets (+) ESI and (-) ESI, for unsupervised exploration clustering patterns between principal components (PCs) 1 and 2, among healthy trees (HT, green circles) and infested (IT, red circles), with their 95% confidence regions for (a) T1 (sampling 1) and (b) T2 (sampling 2).

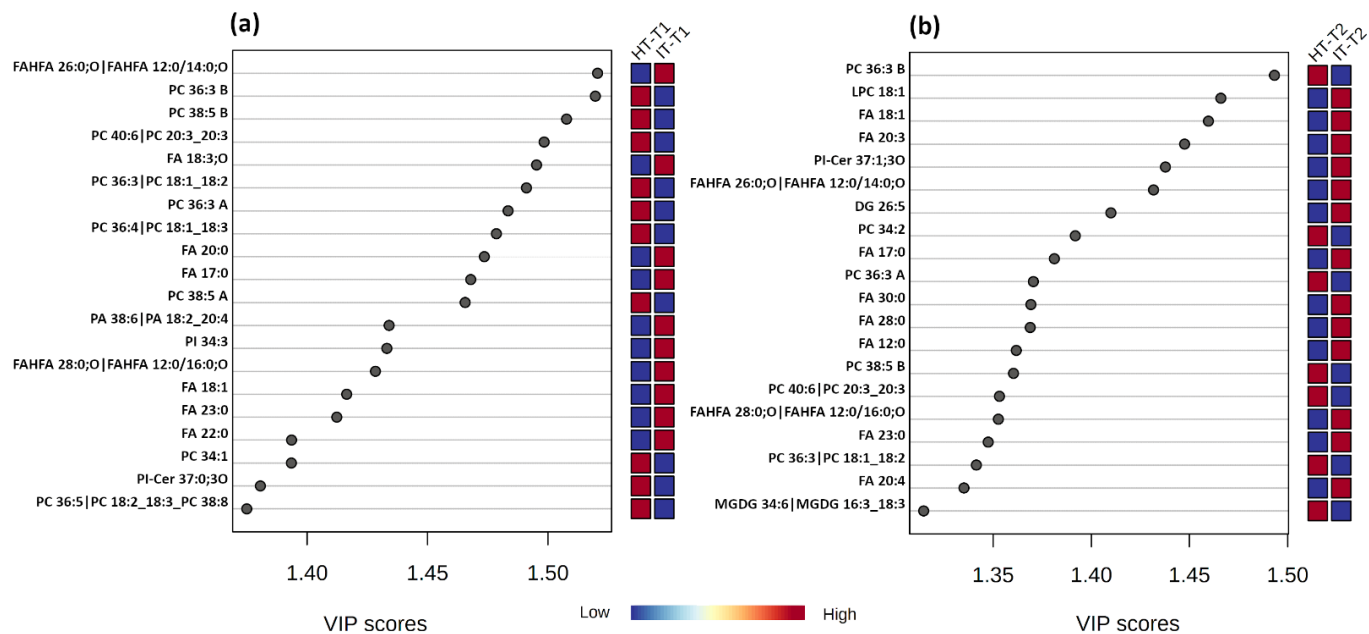
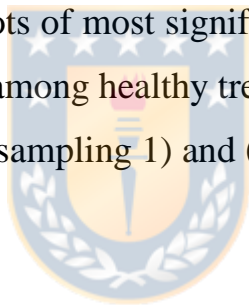


Figure S2-3: VIP-score plots of most significant features based on combined datasets from oPLS-DA models among healthy trees (HT, blue square) and infested trees (IT, red square) for **(a)** T1 (sampling 1) and **(b)** T2 (sampling 2).



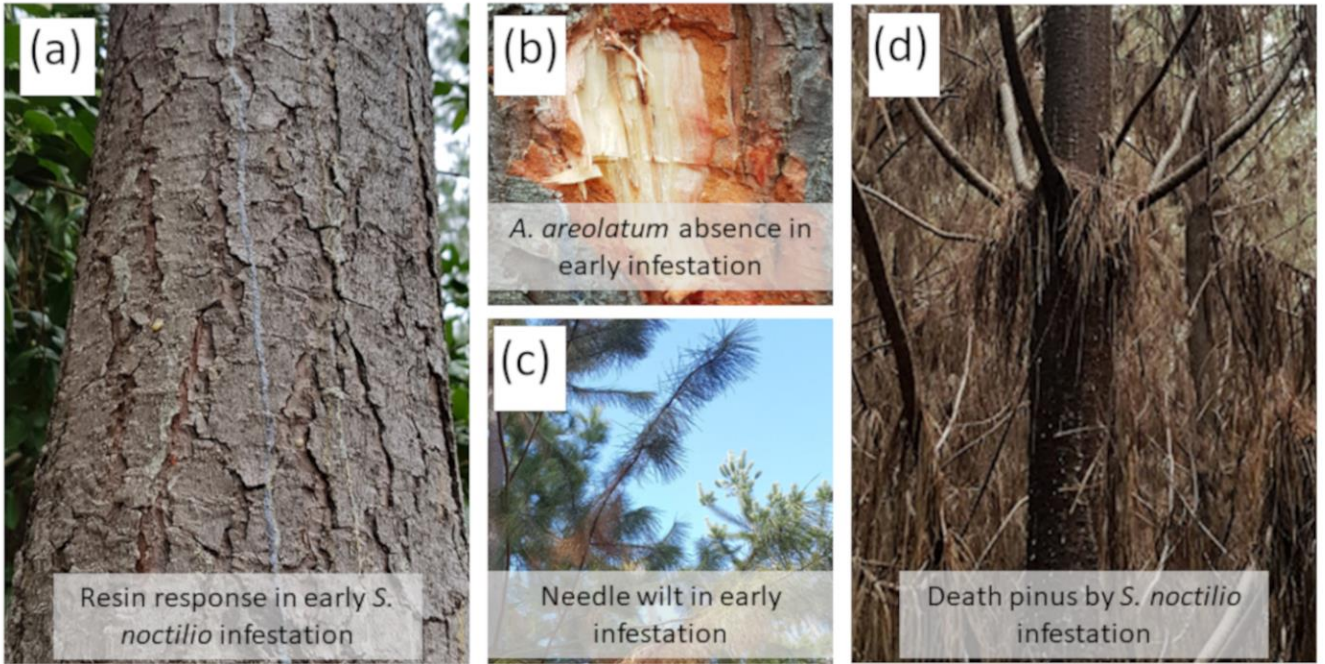


Figure S3-3: *Pinus radiata* under *S. noctilio* early infestation: Resin in *S. noctilio* holes in the tree trunk (a), the visual absence of *A. areolatum* spread in the wood (b), and the needles wilt in the tree crown and early senescence and abscission in older needles (c). Death tree for multiples attack in the tree trunk on the prolonger infestation (d).



**Table S1-3** Annotated lipids present in *P. radiata* needles identified in lipidomics analysis related to *S. noctilio* infestation

Lipids	INCHIKEY	Species (ion)	m/z (dalton)	RT (min)	Total score	*RT similarity	*Dot product
FA 12:0	POULHZVOKOAJMA-UHFFFAOYSA-N	[M-H]-	199,1711	1,012	100	99,9	75
FA 14:0	TUNFSRHWOTWDNC-UHFFFAOYSA-N	[M-H]-	227,2037	1,644	100	99,9	75
FA 16:0	IPCSVZSSVZVIGE-UHFFFAOYSA-N	[M-H]-	255,2335	2,518	100	99,9	75
FA 16:0;O	KMEKMXBMYZGGDT-UHFFFAOYSA-N	[M-H]-	271,2291	0,736	100	99,9	73,4
FA 16:1	SECPZKHBENQXJG-UHFFFAOYSA-N	[M-H]-	253,2187	1,912	100	99,9	72,5
FA 17:0	KEMQGTRYUADPNZ-UHFFFAOYSA-N	[M-H]-	269,2498	2,947	100	99,9	75
FA 18:1	ZQPPMHVWECSIRJ-UHFFFAOYSA-N	[M-H]-	281,2507	2,746	100	99,9	75
FA 18:2	OYHQOLUKZRVURQ-UHFFFAOYSA-N	[M-H]-	279,2353	2,076	100	99,9	75
FA 18:3	DTOSIQBPPRVQHS-UHFFFAOYSA-N	[M-H]-	277,2184	1,599	100	99,9	74,8
FA 18:3;O	NFIYIXFARWVBH-UHFFFAOYSA-N	[M-H]-	293,2133	0,681	100	99,9	16,5
FA 20:0	VKOBVWXKNCXXDE-UHFFFAOYSA-N	[M-H]-	311,2966	3,883	100	99,9	75
FA 20:3	AHANXAKGNAKFSK-UHFFFAOYSA-N	[M-H]-	305,25	2,418	100	99,9	75
FA 20:4	HQPCSDADVLFHHO-UHFFFAOYSA-N	[M-H]-	303,2332	1,867	100	99,9	75
FA 20:5	JAZBEHYOTPTENJ-UHFFFAOYSA-N	[M-H]-	301,2182	2,135	100	99,9	75
FA 20:5	JAZBEHYOTPTENJ-UHFFFAOYSA-N	[M-H]-	301,2195	2,235	100	99,9	75
FA 20:5;2 <sup>o</sup>	RWHZIKMTLJOOEH-UHFFFAOYSA-N	[M-H]-	333,209	0,735	100	99,9	62,4
FA 20:5;O	KONMRYXTSAJFFW-UHFFFAOYSA-N	[M-H]-	317,2138	0,728	100	99,9	70,7
FA 22:0	UKMSUNONTOPOIO-UHFFFAOYSA-N	[M-H]-	339,3277	4,558	100	99,9	75
FA 22:1	DPUOLQHDNGRHS-UHFFFAOYSA-N	[M-H]-	337,3122	3,905	100	99,9	75
FA 23:0	XEZVDURJDFGERA-UHFFFAOYSA-N	[M-H]-	353,3434	4,93	100	99,9	74,3
FA 24:0	QZZGJDVWLFXDLK-UHFFFAOYSA-N	[M-H]-	367,3593	5,304	100	100	75
FA 26:0	XMHIUKTWLZUKEX-UHFFFAOYSA-N	[M-H]-	395,3899	6,146	100	99,9	75
FA 28:0	UTOPWMOLSKOLTQ-UHFFFAOYSA-N	[M-H]-	423,4197	6,958	100	99,9	73,9
FA 30:0	VHOCUJPBKOZGJD-UHFFFAOYSA-N	[M-H]-	451,4516	7,717	100	99,9	74,5
FA 32:0	ICAIHSUWWZJGHD-UHFFFAOYSA-N	[M-H]-	479,483	8,485	100	99,9	74,6



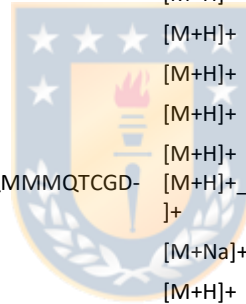
FAHFA 26:0;O FAHFA 12:0/14:0;O	GEAPRHIXZVIFGV-UHFFFAOYSA-N	[M-H]-	425,3625	3,728	100	99,9	74,6
FAHFA 28:0;O FAHFA 12:0/16:0;O	XYJRGHPUHMUHHQ-UHFFFAOYSA-N	[M-H]-	453,3954	4,249	100	99,9	72,8
PA 36:4 PA 18:2_18:2	OBXRDFNCKFWKNY-UHFFFAOYSA-N	[M-H]-	695,4667	4,323	100	99,9	49,5
PA 38:6 PA 18:2_20:4	DLGBYDWDKWEBP-UHFFFAOYSA-N	[M-H]-	719,4656	4,157	95,9	99,9	54,4
PG 32:0 PG 16:0_16:0	BIABMEZBCHDPBV-UHFFFAOYSA-N	[M-H]-	721,5014	4,842	100	99,9	44,6
PG 34:0 PG 17:0_17:0	ZBVHXVKEMAIWQQ-UHFFFAOYSA-N	[M-H]-	749,5347	5,375	100	99,9	55
PG 34:2 PG 16:0_18:2	ATBOMIWRCZXYSZ-UHFFFAOYSA-N	[M-H]-	745,5027	4,458	100	99,9	85,3
PG 34:3 PG 16:0_18:3	MLANVLMRGRHBUJH-UHFFFAOYSA-N	[M-H]-	743,4861	4,098	99,6	99,9	77,1
DG 24:0	ULWFPIOQPKBMLO-UHFFFAOYSA-N	[M+Na]+	479,3688	4,349	100	99,9	69,4
DG 25:4	XJIUNQSPNHVSOG-UHFFFAOYSA-N	[M+Na]+	485,3228	0,597	100	99,8	43,3
DG 26:5	LFQQBMCQSGTBPC-UHFFFAOYSA-N	[M+Na]+	497,3115	1,154	91,9	99,9	14,5
DG 27:1	HNESTVXDVKHGW-UHFFFAOYSA-N	[M+Na]+	519,4007	3,641	100	99,9	58,9
DG 29:1	FTQGBVUFCDQLFK-UHFFFAOYSA-N	[M+Na]+	547,4338	4,079	100	99,9	74
DG 34:1	GXKVCDAVOXTID-UHFFFAOYSA-N	[M+Na]+	617,5143	5,278	100	99,8	16,7
DG 34:2	DPWHHRVJHABNSH-UHFFFAOYSA-N	[M+Na]+	615,4941	4,825	100	99,8	33,3
DG 34:3 A	CJKXNIAUCJAYKE-UHFFFAOYSA-N	[M+Na]+	613,4779	4,422	100	99,8	25,3
DG 34:3 B	CJKXNIAUCJAYKE-UHFFFAOYSA-N	[M+Na]+	613,4814	4,041	97,9	99,8	25,8
DG 34:4	VCQRWKKLJZNMEO-UHFFFAOYSA-N	[M+Na]+	611,4663	4,164	100	99,9	15,7
DG 34:4 DG 16:1_18:3	UUPFPLJLQPYEKS-UHFFFAOYSA-N	[M+NH4]+	606,5065	5,778	100	99,9	52,4
DG 36:3 DG 16:0_20:3	HDLOYNMDVJLGBF-UHFFFAOYSA-N	[M+NH4]+	636,5533	6,803	100	99,9	51,8
DG 36:6 DG 18:3_18:3	RAPBJBKXYMYAY-UHFFFAOYSA-N	[M+NH4]+	630,5099	5,14	100	99,9	37,6
DG 38:6	MAVBOFOXLFASS-UHFFFAOYSA-N	[M+Na]+	663,497	5,849	99,5	99,9	2,3
DG 38:6 DG 18:2_20:4	XQKXAZZSUMABAU-UHFFFAOYSA-N	[M+NH4]+	658,5366	5,835	97,9	99,9	29,2
DG 40:4	VKHVQVHJSQUHDB-UHFFFAOYSA-N	[M+Na]+	695,5608	3,04	100	99,5	48
DG 43:11_w/o MS2:PC 7:0_26:4	NLPVEMQXXOUMGX-UHFFFAOYSA-N_NLVI OGOLRBEOHF-UHFFFAOYSA-N	[M+Na]+_[M+H] ]+	723,5001_740, 5217	4,825_4,82 8	100_99, 7	99,9	8,8
DG 44:10	KERCMTWAJRDWJL-UHFFFAOYSA-N	[M+Na]+	739,5224	4,101	93,9	99,7	15,9
DG 44:4	RKSVJQKAZINLQY-UHFFFAOYSA-N	[M+Na]+	751,6133	4,186	100	99,6	44,5
DG 45:4	VAFHOKSLPWIVOF-UHFFFAOYSA-N	[M+Na]+	765,626	5,097	94,2	99,7	23,8
DG 46:8	VEJMYASEABXMZ-UHFFFAOYSA-N	[M+Na]+	771,6066	9,568	92,9	99,9	70



DG 47:12		XZJRNGBBOYVPBO-UHFFFAOYSA-N	[M+Na]+	777,5463	5,711	100	99,8	68,9
DG 48:10		KUGPCOHBSVFOMJ-UHFFFAOYSA-N	[M+Na]+	795,5718	3,592	87,8	99,6	32
DG 49:13 A		UDRROXCOBRMMC-UHFFFAOYSA-N	[M+Na]+	803,5661	5,762	100	99,8	66,6
DG 49:13 B		UDRROXCOBRMMC-UHFFFAOYSA-N	[M+Na]+	803,5631	5,917	100	99,8	69,3
DGDG	33:3 DGDG							
16:0_17:3		FXIQWNUNSKWHDF-UHFFFAOYSA-N	[M+NH4]+	918,6179	4,489	90,4	99,9	41,4
DGDG	34:1 DGDG							
16:0_18:1		JRCZTCGPEBCBPF-UHFFFAOYSA-N	[M+NH4]+	936,6593	5,716	100	99,9	80,9
DGDG	34:2 DGDG							
16:0_18:2		QZXMUPATKGLZAP-UHFFFAOYSA-N	[M+NH4]+	934,6489	5,203	100	99,9	57,9
DGDG	34:4 DGDG							
16:1_18:3		MHPLFRBUCCWBIP-UHFFFAOYSA-N_null	[M+NH4]+	9.306.226	4.290	92,1	99,9	48,2
DGDG	35:3 DGDG							
17:0_18:3		PUNVOFSUTXXFBB-UHFFFAOYSA-N	[M+NH4]+	946,6468	5,093	100	99,9	51,6
DGDG	35:4 DGDG							
17:1_18:3		AHVPUHVAYBFSNC-UHFFFAOYSA-N	[M+NH4]+	944,6294	4,554	90,8	99,9	39,9
DGDG	35:6 DGDG		[M+NH4]+ [M+NH4]+ <sub>2</sub> [M+H] <sub>2</sub>	940,5951_945,5540	3,812_3,812			
17:3_18:3		GBZGMNJFQHOHOA-UHFFFAOYSA-N_null	[M+NH4]+		2	100	99,9	31,5
DGDG	36:3 DGDG							
18:0_18:3		PPVUDDOGWKXFPF-UHFFFAOYSA-N	[M+NH4]+	960,6625	5,443	100	99,9	53
DGDG	36:4 DGDG							
18:1_18:3		OTTULVKDNCZNKY-UHFFFAOYSA-N	[M+NH4]+	958,6409	4,828	93,1	99,9	46,4
DGDG	36:5 DGDG							
18:2_18:3		GKSHYDZIFVNLSS-UHFFFAOYSA-N	[M+NH4]+	956,6297	4,399	100	99,9	51,1
DGDG	36:6 DGDG							
18:3_18:3		KDYAPQVYJXUQNY-UHFFFAOYSA-N	[M+NH4]+	954,6171	4,04	100	99,9	45,8
DGDG	38:6 DGDG							
18:3_20:3		QCSRHVIANKLEOG-UHFFFAOYSA-N	[M+NH4]+	982,6458	4,525	100	99,9	40,3
LPC 18:0/0:0		IHNKQIMGVNPMTG-UHFFFAOYSA-N	[M+H]+ <sub>2</sub> [M+Na] <sub>2</sub>	524,3688_546,3513	2,327_2,331	91,4_98,6		
LPC 18:1		YAMUFBWLWGFICM-UHFFFAOYSA-N	[M+H]+	522,3478	1,542	91,1	99,9	73,5
LPC 18:1/0:0		YAMUFBWLWGFICM-UHFFFAOYSA-N	[M+H]+	522,3536	1,677	98,1	99,9	47,5
LPC 18:2		SPJFYJXNPEZDW-UHFFFAOYSA-N	[M+H]+	520,3402	1,253	95,6	99,9	76
MGDG	34:3 MGDG							
16:0_18:3		NAUNPPRXNUXMCK-UHFFFAOYSA-N	[M+NH4]+	770,5801	5,246	100	99,9	63
MGDG	34:6 MGDG							
16:3_18:3		ICYUEMSNVJJVHR-UHFFFAOYSA-N	[M+NH4]+	764,531	3,975	100	99,9	44,1
MGDG	36:4 MGDG							
18:2_18:2		BROOMPUVDPTGEG-UHFFFAOYSA-N	[M+NH4]+	796,5929	5,278	100	99,9	45,4



MGDG 36:5		GDYSXKGGNCUYFD-UHFFFAOYSA-N	[M+NH4] <sup>+</sup>	794,5729	4,825	92,3	99,9	16,2
MGDG 18:3_18:3	36:6 MGDG	QUZHZFAQJATMCA-UHFFFAOYSA-N	[M+NH4] <sup>+</sup>	792,5679	4,423	100	99,9	43,7
MGDG 38:6		AAZCMGYBBROTDK-UHFFFAOYSA-N	[M+NH4] <sup>+</sup>	820,5925	5,03	84,1	99,9	20,3
NAE 16:2		KULZUVXNSCAVNT-UHFFFAOYSA-N_null	[M+H] <sup>+</sup>	296,2567_301,2147	2,334_2,337	100	99,9	1,8
NAE 18:4		BSEHZAIYCVZNE-UHFFFAOYSA-N	[M+H] <sup>+</sup>	320,2583	2,513	100	99,9	22,8
NAE 20:1		YDKRGMXLBRWZJR-UHFFFAOYSA-N	[M+H] <sup>+</sup>	354,3348	2,705	100	99,9	1,8
NAE 20:3		IGERBKTWMBMXMC-UHFFFAOYSA-N	[M+H] <sup>+</sup>	350,3021	0,927	100	99,8	4,9
NAE 22:2		OQONQUAYXRQLX-UHFFFAOYSA-N	[M+H] <sup>+</sup>	380,3506	2,833	100	99,9	11
NAE 22:4 A		NCECEOHSWNHORM-UHFFFAOYSA-N	[M+H] <sup>+</sup>	376,3177	1,87	100	99,9	74,5
NAE 22:4 B		NCECEOHSWNHORM-UHFFFAOYSA-N	[M+H] <sup>+</sup>	376,3156	2,541	100	99,9	75
NAE 22:4 C		NCECEOHSWNHORM-UHFFFAOYSA-N	[M+H] <sup>+</sup>	376,3175	2,003	100	99,9	74
NAE 22:5 A		XZURZCGSKALDLA-UHFFFAOYSA-N	[M+H] <sup>+</sup>	374,3032	2,443	100	99,9	70,6
NAE 22:5 B		XZURZCGSKALDLA-UHFFFAOYSA-N	[M+H] <sup>+</sup>	374,3016	2,336	100	99,9	72,7
NAE 22:5 C		XZURZCGSKALDLA-UHFFFAOYSA-N	[M+H] <sup>+</sup>	374,2999	2,126	100	99,9	75
PC 32:3		AGQKQQAJRFTOGL-UHFFFAOYSA-N	[M+H] <sup>+</sup>	728,5211	4,186	83,7	99,9	57,8
PC 34:1		IZGAXEWHRFTGIW-UHFFFAOYSA-N_DPRKXQMMMOTCGD-UHFFFAOYSA-N	[M+H] <sup>+</sup> [M+Na] <sup>+</sup>	760,5817_782,5667	5,696_5,699	85,7_100	99,9	57,3
PC 34:2		DMKGBZJOEARPBA-UHFFFAOYSA-N	[M+Na] <sup>+</sup>	780,5522	5,165	91,1	99,9	52,9
PC 34:4		FJCUMLVANOXIFV-UHFFFAOYSA-N	[M+H] <sup>+</sup>	754,5404	4,498	86,7	99,9	56,8
PC 35:2 PC 17:0_18:2		ZSKWZJYUVZYDQU-UHFFFAOYSA-N	[M+H] <sup>+</sup>	772,5888	5,694	93,6	99,9	80,9
PC 36:1		GQRONIVZDUCCG-UHFFFAOYSA-N	[M+H] <sup>+</sup>	788,6132	6,354	80,5	99,9	56,4
PC 36:2		SNKAWJBQDLSFF-UHFFFAOYSA-N	[M+H] <sup>+</sup>	786,5992	5,826	86,2	99,9	59,2
PC 36:3 A		WSXZDAPARWPHLV-UHFFFAOYSA-N	[M+Na] <sup>+</sup>	806,5651	5,267	81,6	99,9	38,4
PC 36:3 B		FHYXYDNOQOCPNC-UHFFFAOYSA-N_KKVDMSZJVFAMDW-UHFFFAOYSA-N	[M+H] <sup>+</sup> [M+Na] <sup>+</sup>	784,5839_806,5682	5,458_5,451	85,3	99,9	59,1
PC 36:3 PC 18:1_18:2		GDWULUGDXGHJIJ-UHFFFAOYSA-N	[M+H] <sup>+</sup>	784,5887	5,251	100	99,9	86
PC 36:4 PC 18:1_18:3		FVQGNFUBHWGFCY-UHFFFAOYSA-N	[M+H] <sup>+</sup>	782,5661	4,795	100	99,9	85,7
PC 36:5 PC 18:2_18:3_PC 38:8		HZGAVPNEGHQJID-UHFFFAOYSA-N_JAJDBGJIFGOXMW-UHFFFAOYSA-N	[M+H] <sup>+</sup>	780,5523_802,5356	4,388_4,372	100_85,1	99,9	59,3_22,2
PC 36:6		QHAXKXZLHMWFBX-UHFFFAOYSA-N	[M+Na] <sup>+</sup>	800,5192	4,007	82,9	99,9	67
PC 36:6 PC 18:3_18:3		XXKFQTJOZELMD-UHFFFAOYSA-N	[M+H] <sup>+</sup>	778,5359	4,147	100	99,9	86,2



PC 38:2		HJYITXYOCDILBF-UHFFFAOYSA-N	[M+H] <sup>+</sup>	814,6293	6,524	87,4	99,9	40,7
PC 38:5 A		ARDJUHDXABDVFH-UHFFFAOYSA-N	[M+H] <sup>+</sup>	808,5814	5,857	86,6	99,9	28,6
PC 38:5 B		LSNIXSHXTMSKGF-UHFFFAOYSA-N_CANZVNSRAPPYKG-UHFFFAOYSA-N	[M+H] <sup>+</sup> _[M+Na] <sup>+</sup>	808,5775_830,5666	5,008_5,013	84,3_99,9	99,9	55,6
PC 40:6 PC 20:3_20:3		SUSAZHLUBGMSDJ-UHFFFAOYSA-N	[M+H] <sup>+</sup>	834,5966	5,225	100	99,9	81,1
PC 41:2		DJMWTIFDEXNIOA-UHFFFAOYSA-N	[M+H] <sup>+</sup>	856,68	7,511	81,7	99,9	23,2
PE 34:2		GIXVVPGFMACMOZ-UHFFFAOYSA-N	[M+H] <sup>+</sup>	716,5208	5,358	88	99,9	42
PE 34:3		YPQQUIROQBQXEF-UHFFFAOYSA-N	[M+H] <sup>+</sup>	714,5053	4,924	86,7	99,9	39,8
PE 36:3 A		IOCIUBADWAXZRO-UHFFFAOYSA-N	[M+H] <sup>+</sup>	742,5389	5,45	87,4	99,9	53,2
PE 36:3 B		DCPDPBCUPLKQNG-UHFFFAOYSA-N	[M+H] <sup>+</sup>	742,5329	5,588	87,8	99,9	46,8
PE 36:4		SSCDRSKJTAQNNB-UHFFFAOYSA-N	[M+H] <sup>+</sup>	740,5251	5,157	81,4	99,9	34,7
PE 36:5		MBVGZVLTSQSWFJ-UHFFFAOYSA-N	[M+H] <sup>+</sup>	738,5112	4,507	87	99,9	30,5
PE 38:3		KTTDFPCEOHXQBY-UHFFFAOYSA-N	[M+H] <sup>+</sup>	770,5655	6,31	86,7	99,9	28,9
PE 38:4		VASYAYHJSUUNNT-UHFFFAOYSA-N	[M+H] <sup>+</sup>	768,5601	5,674	83,3	99,9	45,3
PI 34:3		SVJIMWKNBYJOKD-UHFFFAOYSA-N	[M+NH <sub>4</sub> ] <sup>+</sup>	850,5474	4,192	100	99,9	64,4
PI-Cer 37:0;3 <sup>o</sup>		FLBVHLLZJOVCV-UHFFFAOYSA-N	[M+H] <sup>+</sup>	840,5933	5,516	97,9	99,9	7,5
PI-Cer 37:1;3 <sup>o</sup>		JOXWGEKNKTYZFB-UHFFFAOYSA-N	[M+H] <sup>+</sup>	838,5727	4,945	95,6	99,9	5,6
TG 16:0_18:2_18:2	52:4 TG	LXAWUIOWWNQCQA-UHFFFAOYSA-N_TVXCNLFXLACFHK-UHFFFAOYSA-N	[M+NH <sub>4</sub> ] <sup>+</sup> _[M+Na] <sup>+</sup>	872,7698_877,7242	10,350_10,350	100_99	99,9	63,5
TG 18:1_18:2_18:2	54:5 TG	VVEBTVMJPTZDHO-UHFFFAOYSA-N_QEUNXFKXMXOSEM-UHFFFAOYSA-N	[M+NH <sub>4</sub> ] <sup>+</sup> _[M+Na] <sup>+</sup>	898,7861_903,7410	10,364_10,357	100	99,9	34,6

\*The spectral similarity and dot product for de identification using the spectrum library were calculated in MS-dial

Table S2-3: Volcano plots results of *P. radiata* needles identified in lipidomics analysis related to early *S. noctilio* infestation

Lipids	FC	log2(FC)	p.adjusted	-log10(p)
FA 18:3;O	18.867	4,2378	1.0478e-21	20.98
LPC 18:1	12.522	3,6464	2.3364e-08	7.6315
FAHFA 26:0;O FAHFA 12:0/14:0;O	8.8873	3,1517	1.9131e-25	24.718
DG 36:6 DG 18:3_18:3	7.9994	2,9999	8.6603e-14	13.062
FA 17:0	6.5926	2,7209	2.7852e-17	16.555
FA 12:0	5.791	2,5338	7.7357e-13	12.111
FA 18:1	4.261	2,0912	9.6785e-15	14.014
PA 38:6 PA 18:2_20:4	4.1519	2,0538	5.6562e-15	14.247
FA 23:0	3.9307	1,9748	3.48e-15	14.458
FA 32:0	3.909	1,9668	0.00036255	3.4406
FAHFA 28:0;O FAHFA 12:0/16:0;O	3.8843	1,9577	9.4188e-17	16.026
FA 20:3	3.218	1,6862	1.857e-11	10.731
PA 36:4 PA 18:2_18:2	3.1551	1,6577	6.9022e-10	9.161
FA 22:0	3.0915	1,6283	8.6603e-14	13.062
PI 34:3	3.0476	1,6077	7.072e-17	16.15
DG 26:5	3.0348	1,6016	0.052302	1.2815
FA 20:0	2.8294	1,5005	1.856e-18	17.731
FA 30:0	2.7635	1,4665	3.2802e-08	7.4841
DG 27:1	2.7157	1,4413	7.0685e-12	11.151
FA 20:4	2.715	1,4409	6.4093e-09	8.1932
FA 28:0	2.6726	1,4182	9.8711e-11	10.006
DG 43:11	2.6673	1,4154	1.9159e-09	8.7176
FA 16:1	2.5856	1,3705	1.8391e-05	4.7354
FA 18:2	2.5508	1,3509	5.6483e-11	10.248
FA 16:0	2.5166	1,3314	1.0432e-08	7.9816
LPC 18:2	2.3992	1,2626	1.9069e-06	5.7197
FA 24:0	2.3106	1,2082	1.857e-11	10.731
FA 26:0	2.1961	1,1349	4.6212e-12	11.335
FA 18:3	2.0001	1	1.0147e-06	5.9937
DG 34:3 A	0.48574	-1,0417	0.00030469	3.5161
MGDG 38:6	0.46034	-1,1192	0.0075982	2.1193
MGDG 36:4 MGDG 18:2_18:2	0.44254	-1,1761	0.0013921	2.8563
DG 49:13 B	0.42057	-1,2496	0.0012594	2.8998
DG 34:2	0.41808	-1,2582	0.0013424	2.8721
PC 36:6 PC 18:3_18:3	0.37854	-1,4015	1.1544e-07	6.9376
PE 36:3 B	0.37128	-1,4294	3.4604e-11	10.461
PC 36:5 PC 18:2_18:3_PC 38:8	0.37015	-1,4338	5.9994e-13	12.222
MGDG 36:5	0.36941	-1,4367	0.00079635	3.0989
PC 36:4 PC 18:1_18:3	0.34935	-1,5173	1.04e-17	16.983
PC 35:2 PC 17:0_18:2	0.34695	-1,5272	2.4968e-05	4.6026

DG 34:4 DG 16:1_18:3	0.3059	-1,7089	0.0068006	2.1675
PC 34:2	0.2688	-1,8954	7.6384e-13	12.117
MGDG 34:3 MGDG 16:0_18:3	0.26656	-1,9075	7.8248e-05	4.1065
PC 36:3 B	0.26535	-1,914	3.8492e-23	22.415
MGDG 34:6 MGDG 16:3_18:3	0.22568	-2,1477	3.7262e-05	4.4287
PC 38:5 B	0.2128	-2,2324	8.2663e-22	21.083
PC 36:6	0.20854	-2,2616	1.7515e-07	6.7566
PC 36:2	0.20824	-2,2637	2.1249e-10	9.6727
PE 36:4	0.17457	-2,5181	7.4737e-07	6.1265
PC 34:1	0.17335	-2,5283	8.6603e-14	13.062
PC 36:3 PC 18:1_18:2	0.17005	-2,556	1.4129e-20	19.85
PC 34:4	0.14431	-2,7928	5.6775e-06	5.2458
DG 47:12	0.12552	-2,9941	1.3051e-07	6.8844
PC 40:6 PC 20:3_20:3	0.12323	-3,0206	8.2663e-22	21.083
PI-Cer 37:0;3 <sup>o</sup>	0.085503	-3,5479	1.5192e-13	12.818
PE 38:4	0.045002	-4,4739	1.2699e-10	9.8962
DG 49:13 A	0.037869	-4,7228	3.1868e-10	9.4966
PC 38:5 A	0.03677	-4,7653	1.1744e-17	16.93
PC 36:3 A	0.032646	-4,9369	3.0547e-20	19.515



Table S3-3: Volcano plots results of *P. radiata* needles identified in lipidomics analysis related to prolonged *S. noctilio* infestation.

Lipids	FC	log2(FC)	p.adjusted	-log10(p)
DG 36:6 DG 18:3_18:3	11.214	3,4872	4.5778e-09	8.3393
LPC 18:1	7.3109	2,8701	3.6572e-16	15.437
FAHFA 26:0;O FAHFA 12:0/14:0;O	6.8824	2,7829	9.9012e-14	13.004
FA 18:3;O	6.722	2,7489	1.2335e-07	6.9089
FA 12:0	3.6909	1,884	9.623e-12	11.017
PI-Cer 37:1;3 <sup>e</sup>	3.6111	1,8524	4.2299e-15	14.374
FA 32:0	3.4484	1,7859	1.005e-05	4.9978
FAHFA 28:0;O FAHFA 12:0/16:0;O	3.3755	1,7551	3.682e-11	10.434
FA 17:0	3.2142	1,6845	1.3163e-11	10.881
FA 20:3	3.1081	1,636	3.6084e-14	13.443
LPC 18:2	2.8977	1,5349	1.9586e-06	5.708
FA 30:0	2.7936	1,4821	4.7799e-11	10.321
DG 26:5	2.7589	1,4641	1.9121e-13	12.718
FA 23:0	2.641	1,4011	1.1117e-10	9.954
FA 18:1	2.6309	1,3956	1.9915e-14	13.701
FA 28:0	2.5568	1,3543	6.1927e-11	10.208
PA 36:4 PA 18:2_18:2	2.5267	1,3373	7.3781e-10	9.1321
FA 22:0	2.4683	1,3035	4.4717e-08	7.3495
DG 29:1	2.4073	1,2674	6.6283e-07	6.1786
FA 18:2	2.3812	1,2517	1.4169e-08	7.8487
DG 49:13 B	2.3532	1,2346	1.3924e-07	6.8562
PA 38:6 PA 18:2_20:4	2.3451	1,2296	1.9857e-08	7.7021
NAE 16:2	2.2319	1,1583	4.8212e-08	7.3168
FA 18:3	2.2189	1,1499	1.2886e-09	8.8899
FA 20:4	2.2143	1,1469	1.3869e-10	9.858
DG 43:11	2.1161	1,0814	9.0409e-11	10.044
FA 26:0	2.1057	1,0743	9.2481e-09	8.0339
FA 24:0	2.0629	1,0447	5.7154e-07	6.243
PE 36:4	0.49146	-1,0248	1.7728e-07	6.7513
TG 54:5 TG 18:1_18:2_18:2	0.49012	-1,0288	0.01744	1.7585
PC 36:6 PC 18:3_18:3	0.48352	-1,0484	1.1675e-07	6.9327
PC 34:4	0.43058	-1,2157	1.2509e-07	6.9028
PC 36:3 PC 18:1_18:2	0.39909	-1,3252	6.6792e-11	10.175
PC 36:3 B	0.35607	-1,4898	1.6319e-19	18.787
PE 38:4	0.35396	-1,4984	3.2895e-09	8.4829
DG 49:13 A	0.33439	-1,5804	6.4024e-07	6.1937
PC 34:1	0.31721	-1,6565	1.7073e-09	8.7677
DG 34:4 DG 16:1_18:3	0.3123	-1,679	0.0059672	2.2242
PC 38:5 B	0.30705	-1,7035	1.2268e-11	10.911
PC 36:2	0.3013	-1,7307	3.4797e-09	8.4585



MGDG 34:6 MGDG 16:3_18:3	0.28525	-1,8097	6.1927e-11	10.208
PC 36:3 A	0.27281	-1,874	1.3592e-11	10.867
PI-Cer 37:0;3º	0.24361	-2,0374	2.4558e-10	9.6098
PC 40:6 PC 20:3_20:3	0.22445	-2,1555	9.623e-12	11.017
PC 38:5 A	0.11014	-3,1827	5.6294e-10	9.2495

**Method S1:** Climatic conditions during sampling time, T1 and T2.

Weather conditions in April 2018 (T1) according to the nearest available stations of the Chilean Meteorological Department, located at Chillán (36°35'8.99"S 72°x2'11.99"W) (code 360011) and Concepción (36°46'49.99"S 73°3'58.99"W) (code 360019), were as follow: mean maximum and minimum temperatures of 19.7 °C and 6.0 °C, respectively; accumulated rainfall of 60.8 mm, with 21.6 mm accumulated only in the day before sampling; a daily average of the UVB (280-315 nm) maximum radiation intensity was 3.2 kWh m<sup>-2</sup>; and relative humidity mean of 82.5%, with 79.9% for the day of sampling. During the second sampling (T2) in July 2018, weather conditions were as follows: mean maximum and minimum temperatures of 12.7 °C and 2.4 °C, respectively; accumulated rainfall of 80.2 mm, with 0.0 mm on the day before sampling; a daily average of the UVB (280-315 nm) maximum radiation intensity was 1.53 kWh m<sup>-2</sup>; and relative humidity mean of 90.4%, with 97.9% for the day of sampling

## 9. REFERENCES

- Beccaccioli, M., Reverberi, M., Scala, V., 2019. Fungal lipids: Biosynthesis and signalling during plant-pathogen interaction. *Frontiers in Bioscience – Landmark* 24, 172–185. <https://doi.org/10.2741/4712>
- Blancaflor, E.B., Kilaru, A., Keereetawee, J., Khan, B.R., Faure, L., Chapman, K.D., 2014. N-Acylethanolamines: lipid metabolites with functions in plant growth and development. *The Plant Journal* 79, 568–583. <https://doi.org/10.1111/TPJ.12427>
- Bordeaux, J.M., Dean, J.F.D., 2012. Susceptibility and response of pine to *Sirex noctilio*, in: Slippers, B., de Groot, P., Wingfield, M.J. (Eds.), *The Sirex Woodwasp and Its Fungal Symbiont: Research and Management of a Worldwide Invasive Pest*. Springer, pp. 31–50.
- Botella, C., Jouhet, J., Block, M.A., 2017. Importance of phosphatidylcholine on the chloroplast surface. *Prog Lipid Res* 65, 12–23. <https://doi.org/10.1016/J.PLIPRES.2016.11.001>
- Brejchova, K., Balas, L., Paluchova, V., Brezinova, M., Durand, T., Kuda, O., 2020. Understanding FAHFAs: From structure to metabolic regulation. *Prog Lipid Res* 79, 101053. <https://doi.org/10.1016/J.PLIPRES.2020.101053>
- Cajka, T., Fiehn, O., 2016. Increasing lipidomic coverage by selecting optimal mobile-phase modifiers in LC–MS of blood plasma. *Metabolomics* 12, 1–11. <https://doi.org/10.1007/s11306-015-0929-x>
- Cajka, T., Fiehn, O., 2014. Comprehensive analysis of lipids in biological systems by liquid chromatography-mass spectrometry. *TrAC – Trends in Analytical Chemistry* 61, 192–206. <https://doi.org/10.1016/j.trac.2014.04.017>
- Cajka, T., Smilowitz, J.T., Fiehn, O., 2017. Validating Quantitative Untargeted Lipidomics Across Nine Liquid Chromatography-High-Resolution Mass Spectrometry Platforms. *Anal Chem* 89, 12360–12368. <https://doi.org/10.1021/acs.analchem.7b03404>

- Canonne, J., Froidure-Nicolas, S., Rivas, S., 2011. Phospholipases in action during plant defense signaling. *Plant Signal Behav* 6, 13–18. <https://doi.org/10.4161/psb.6.1.14037>
- Correa, S.M., Fernie, A.R., Nikoloski, Z., Brotman, Y., 2020. Towards model-driven characterization and manipulation of plant lipid metabolism. *Prog Lipid Res* 80, 101051. <https://doi.org/10.1016/j.plipres.2020.101051>
- Coutts, M., 1969a. The Mechanism of Pathogenicity of *Sirex Noctilio* on *Pinus Radiata* II. Effects of *S. Noctilio* Mucus. *Aust J Biol Sci* 22, 1153. <https://doi.org/10.1071/bi9691153>
- Coutts, M., 1969b. The Mechanism of Pathogenicity of *Sirex Noctilio* on *Pinus Radiata* II. Effects of *S. Noctilio* Mucus. *Aust J Biol Sci* 22, 1153. <https://doi.org/10.1071/bi9691153>
- Coutts, M., 1969c. The Mechanism of Pathogenicity of *Sirex Noctilio* on *Pinus Radiata* I. Effects of the Symbiotic Fungus *Amylostereum* Sp. (Thelophoraceae). *Aust J Biol Sci* 22, 915. <https://doi.org/10.1071/BI9690915>
- Coutts, M.P., Dolezal, J.E., 1966. Some effects of bark cincturing on the physiology of *Pinus radiata*, and on *Sirex* attack. *Australian Forestry Research* 2, 17–28.
- DeFelice, B.C., Mehta, S.S., Samra, S., Čajka, T., Wancewicz, B., Fahrman, J.F., Fiehn, O., 2017. Mass Spectral Feature List Optimizer (MS-FLO): A Tool To Minimize False Positive Peak Reports in Untargeted Liquid Chromatography-Mass Spectroscopy (LC-MS) Data Processing. *Anal Chem* 89, 3250–3255. <https://doi.org/10.1021/acs.analchem.6b04372>
- Ding, Z., Jia, S., Wang, Y., Xiao, J., Zhang, Y., 2017. Phosphate stresses affect ionome and metabolome in tea plants. *Plant Physiology and Biochemistry* 120, 30–39. <https://doi.org/10.1016/j.plaphy.2017.09.007>
- Dixon, R.A., Paiva, N.L., 1995. Stress-induced phenylpropanoid metabolism. *Plant Cell* 7, 1085–1097.
- Dong, W., Lv, H., Xia, G., Wang, M., 2012. Does diacylglycerol serve as a signaling molecule in plants? *Plant Signal Behav* 7, 472–475. <https://doi.org/10.4161/psb.19644>

- Ferrer, J.L., Austin, M.B., Stewart, C., Noel, J.P., 2008. Structure and function of enzymes involved in the biosynthesis of phenylpropanoids. *Plant Physiology and Biochemistry* 46, 356–370. <https://doi.org/10.1016/j.plaphy.2007.12.009>
- Fett-Neto, A.G., Rodrigues-Corrêa, K.C.S., 2012. Pine resin : biology, chemistry and applications. Research Signpost, T. C.
- Gullner, G., Komives, T., Király, L., Schröder, P., 2018. Glutathione S-Transferase Enzymes in Plant-Pathogen Interactions. *Front Plant Sci* 9. <https://doi.org/10.3389/FPLS.2018.01836>
- Ha, K.S., Thompson, G.A., 1991. Diacylglycerol Metabolism in the Green Alga *Dunaliella salina* under Osmotic Stress : Possible Role of Diacylglycerols in Phospholipase C-Mediated Signal Transduction. *Plant Physiol* 97, 921. <https://doi.org/10.1104/PP.97.3.921>
- He, M., Ding, N.Z., 2020. Plant Unsaturated Fatty Acids: Multiple Roles in Stress Response. *Front Plant Sci*. <https://doi.org/10.3389/fpls.2020.562785>
- Hong, Y., Wang, T.-W., Hudak, K.A., Schade, F., Froese, C.D., Thompson, J.E., 2000. An ethylene-induced cDNA encoding a lipase expressed at the onset of senescence *PLANT BIOLOGY* 97, 8717–8722.
- Ide, S., Beeche, M., Sandoval, A., Opazo, A., Velazquez, P., Schafer, M., Aravena, J.C., Barrientos, C., Sievert, H., Gonzalez, M., Valenzuela, J., Peragallo, M., Muños, C., Gallardo, R., 2018. Programa control biológico de *Sirex noctilio* F. (Hymenoptera: Siricidae): 2006-2017.
- Kenwood, B.M., Merrill, A.H., 2016. Lipidomics, in: *Encyclopedia of Cell Biology*. Elsevier, pp. 147–159. <https://doi.org/10.1016/B978-0-12-394447-4.10024-0>
- Klapwijk, M.J., Bylund, H., Schroeder, M., Björkman, C., 2016. Forest management and natural biocontrol of insect pests. *Forestry* 89, 253–262. <https://doi.org/10.1093/forestry/cpw019>

- Lantschner, M.V., Villacide, J.M., Garnas, J.R., Croft, P., Carnegie, A.J., Liebhold, A.M., Corley, J.C., 2014. Temperature explains variable spread rates of the invasive woodwasp *Sirex noctilio* in the Southern Hemisphere. *Biol Invasions* 16, 329–339. <https://doi.org/10.1007/s10530-013-0521-0>
- Laxalt, A.M., Munnik, T., 2002a. Phospholipid signalling in plant defence. *Curr Opin Plant Biol.* [https://doi.org/10.1016/S1369-5266\(02\)00268-6](https://doi.org/10.1016/S1369-5266(02)00268-6)
- Laxalt, A.M., Munnik, T., 2002b. Phospholipid signalling in plant defence. *Curr Opin Plant Biol.* [https://doi.org/10.1016/S1369-5266\(02\)00268-6](https://doi.org/10.1016/S1369-5266(02)00268-6)
- Li-beisson, Y.N.Y., 2016. Lipids in Plant and Algae Development 86. <https://doi.org/10.1007/978-3-319-25979-6>
- Lightner, J., Wu, J., Browse, J., 1994. A mutant of *Arabidopsis* with increased levels of stearic acid. *Plant Physiol* 106, 1443–1451. <https://doi.org/10.1104/pp.106.4.1443>
- Lim, G.-H., Singhal, R., Kachroo, A., Kachroo, P., 2017. Fatty Acid-and Lipid-Mediated Signaling in Plant Defense. *Annu Rev Phytopathol.* <https://doi.org/10.1146/annurev-phyto-080516>
- Lloyd, J.A., 1975. FATTY ACIDS, RESIN ACIDS AND PHENOLS IN *PINUS MURICATA* 14, 483–485.
- Lopez-Molina, L., Mongrand, S., Chua, N.H., 2001. A postgermination developmental arrest checkpoint is mediated by abscisic acid and requires the ABI5 transcription factor in *Arabidopsis*. *Proc Natl Acad Sci U S A* 98, 4782–4787. <https://doi.org/10.1073/PNAS.081594298>
- Matthew, X., Kolar, J., Konduri, S., Chang, T., Wang, H., Mcnerlin, C., Ohlsson, L., Härröd, M., Siegel, D., Saghatelian, A., 2019. Linoleic acid esters of hydroxy linoleic acids are anti-inflammatory lipids found in plants and mammals. <https://doi.org/10.1074/jbc.RA118.006956>
- Mehta, S., Chakraborty, A., Roy, A., Singh, I.K., Singh, A., 2021. Fight hard or die trying: Current status of lipid signaling during plant–pathogen interaction. *Plants.* <https://doi.org/10.3390/plants10061098>

- Millner, A., Ekin Atilla-Gokcumen, G., 2020. Lipid Players of Cellular Senescence. *Metabolites* 10, 1–17. <https://doi.org/10.3390/METABO10090339>
- Ohlrogge, J., Browse, J., 1995. Lipid biosynthesis. *Plant Cell* 7, 957–970. <https://doi.org/10.1105/tpc.7.7.957>
- Olajide, T.M., Cao, W., 2022. Exploring foods as natural sources of FAHFAs—A review of occurrence, extraction, analytical techniques and emerging bioactive potential. *Trends Food Sci Technol* 129, 591–607. <https://doi.org/10.1016/J.TIFS.2022.11.005>
- Pierrugues, O., Brutesco, C., Oshiro, J., Gouy, M., Deveaux, Y., Carman, G.M., Thuriaux, P., Kazmaier, M., 2001. Lipid phosphate phosphatases in Arabidopsis. Regulation of the AtLPP1 gene in response to stress. *J Biol Chem* 276, 20300–20308. <https://doi.org/10.1074/JBC.M009726200>
- Raffaele, S., Leger, A., Roby, D., 2009. Plant Signaling & Behavior Very long chain fatty acid and lipid signaling in the response of plants to pathogens VLCFA Biosynthesis, Regulation and Use for Wax and Sphingolipid Production. *Plant Signal Behav* 4. <https://doi.org/10.4161/psb.4.2.7580>
- Reszczyńska, E., Hanaka, A., 2013. Lipids Composition in Plant Membranes Classification of Fatty Acids in Plants. *Cell Biochem Biophys* 78, 401–414. <https://doi.org/10.1007/s12013-020-00947-w>
- Rojas, C.M., Senthil-Kumar, M., Tzin, V., Mysore, K.S., 2014. Regulation of primary plant metabolism during plant-pathogen interactions and its contribution to plant defense. *Front Plant Sci* 5, 1–12. <https://doi.org/10.3389/fpls.2014.00017>
- Ryan, K., Hurley, B.P., 2012. Life History and Biology of *Sirex noctilio*, in: Slippers, B., de Groot, P., Wingfield, M.J. (Eds.), *The Sirex Woodwasp and Its Fungal Symbiont*: Springer Netherlands, Dordrecht, pp. 15–30. [https://doi.org/10.1007/978-94-007-1960-6\\_2](https://doi.org/10.1007/978-94-007-1960-6_2)

- Schmid, K.M., 2016a. Lipid Metabolism in Plants, in: Biochemistry of Lipids, Lipoproteins and Membranes. Elsevier, pp. 113–147. <https://doi.org/10.1016/B978-0-444-63438-2.00004-3>
- Schmid, K.M., 2016b. Lipid Metabolism in Plants, in: Biochemistry of Lipids, Lipoproteins and Membranes. Elsevier, pp. 113–147. <https://doi.org/10.1016/B978-0-444-63438-2.00004-3>
- Shiva, S., Enniful, R., Roth, M.R., Tamura, P., Jagadish, K., Welti, R., 2018. An efficient modified method for plant leaf lipid extraction results in improved recovery of phosphatidic acid. *Plant Methods* 14, 1–8. <https://doi.org/10.1186/S13007-018-0282-Y/FIGURES/4>
- Tan, W.J., Yang, Y.C., Zhou, Y., Huang, L.P., Xu, L., Chen, Q.F., Yu, L.J., Xiao, S., 2018. DIACYLGLYCEROL ACYLTRANSFERASE and DIACYLGLYCEROL KINASE Modulate Triacylglycerol and Phosphatidic Acid Production in the Plant Response to Freezing Stress. *Plant Physiol* 177, 1303. <https://doi.org/10.1104/PP.18.00402>
- Teaster, N.D., Motes, C.M., Tang, Y., Wiant, W.C., Cotter, M.Q., Wang, Y.S., Kilaru, A., Venables, B.J., Hasenstein, K.H., Gonzalez, G., Blancaflor, E.B., Chapman, K.D., 2007. N-acylethanolamine metabolism interacts with abscisic acid signaling in *Arabidopsis thaliana* seedlings. *Plant Cell* 19, 2454–2469. <https://doi.org/10.1105/tpc.106.048702>
- Tobias, K., Kwang-Hyeon, L., Do Yup, L., Brian, D., John K., M., Fiehn, O., 2013. LipidBlast in silico tandem mass spectrometry database for lipid identification. *Nat Methods* 10, 755–758. <https://doi.org/10.1038/nmeth.2551.LipidBlast>
- Tripathy, S., Venables, B.J., Chapman, K.D., 1999. N-Acylethanolamines in Signal Transduction of Elicitor Perception. Attenuation of Alkalinization Response and Activation of Defense Gene Expression. *Plant Physiol* 121, 1299–1308. <https://doi.org/10.1104/pp.121.4.1299>
- Troncoso-Ponce, M.A., Cao, X., Yang, Z., Ohlrogge, J.B., 2013. Lipid turnover during senescence. *Plant Science* 205–206, 13–19. <https://doi.org/10.1016/J.PLANTSCI.2013.01.004>

- Tsugawa, H., Cajka, T., Kind, T., Ma, Y., Higgins, B., Ikeda, K., Kanazawa, M., Vandergheynst, J., Fiehn, O., Arita, M., 2015. MS-DIAL: Data-independent MS/MS deconvolution for comprehensive metabolome analysis. *Nat Methods* 12, 523–526. <https://doi.org/10.1038/nmeth.3393>
- Valledor, L., Escandón, M., Meijón, M., Nukarinen, E., Cañal, M.J., Weckwerth, W., 2014. A universal protocol for the combined isolation of metabolites, DNA, long RNAs, small RNAs, and proteins from plants and microorganisms. *Plant Journal* 79, 173–180. <https://doi.org/10.1111/tpj.12546>
- van der Hoeven, R.S., Steffens, J.C., 1995. Biosynthesis and Elongation of Short-and Medium-Chain-Length Fatty Acids, Charlton and Roeloffs. Hartman and Reimann.
- Wang, C., Wang, X., 2001. A novel phospholipase D of 208rabidopsis that is activated by oleic acid and associated with the plasma membrane. *Plant Physiol* 127, 1102–1112. <https://doi.org/10.1104/PP.010444>
- Worley, B., Powers, R., 2016. PCA as a predictor of OPLS-DA model reliability. *Curr Metabolomics* 4, 97–103. <https://doi.org/10.2174/2213235X04666160613122429.PCA>
- Worley, Bradley, Powers, R., 2016. PCA as a Practical Indicator of OPLS-DA Model Reliability. *Curr Metabolomics* 4, 97–103. <https://doi.org/10.2174/2213235x04666160613122429>
- Worley, B., Powers, R., 2013. Multivariate Analysis in Metabolomics. *Curr Metabolomics* 1, 92–107. <https://doi.org/10.2174/2213235x130108>
- Xu, Q., Sun, X., Lu, P., Luo, Y., Shi, J., 2019. Volatile profiles of three tree species in the northeastern China and associated effects on *Sirex noctilio* activity 9145. <https://doi.org/10.1080/17429145.2019.1629035>
- Zhao, J., 2015. Phospholipase D and phosphatidic acid in plant defence response: from protein-protein and lipid-protein interactions to hormone signalling. <https://doi.org/10.1093/jxb/eru540>





## 4. CHAPTER 4

### 1. CONCLUSION

#### 1.1 General conclusions

- Due to the overall complexity of the metabolome of individuals, new methods of analysis have been developed. Lipidomics focuses on non-polar metabolites, such as lipids and phospholipids, that are as extensive as specialized metabolites. The application of libraries in lipidomics has enabled the identification of hundreds of thousands of compounds, altering the paradigms regarding their functions in organisms, which were previously limited to energy storage and membrane structural components.
- Using specialized software and platforms such as Metaboanalyst, Metaboscape, MSDIAL and CSI:Finder allowed us to perform the workflow involving chromatogram processing, feature extraction, statistical analysis and subsequent biomarker identification.
- With the combined metabolomic and lipidomic approach, it was possible to identify metabolites that are directly associated with the resistance and defensive response of *Pinus radiata* to *S. noctilio* attack. However, new research avenues are now available to investigate their functions and roles in plant-insect interaction.

- Pine bark did not show significant changes comparing the metabolome IT and HT through metabolomics by LC-MSMS. However, it was possible to differentiate both groups by identifying specific biomarkers in wood and needles.
- Changes in the metabolome and lipidome were identified in both early and prolonged infestation.
- The identification of lipid biomarkers was established by calculating their exact mass, fragmentation pattern and coincidence of the mass spectral pattern with available libraries and analysis of pure spectrum.



## 1.2 Specific conclusions:

The metabolomics strategy used in this study revealed the fundamental roles of plants' chemical defence on *P. radiata* during the infestation of *S. noctilio*

- The infestation of *S. noctilio* caused in needles of *P. radiata* the upregulation of flavonols, catechins, oxycneolignans, auxins, proline, and tryptophan during the early stage. The accumulation of catechins suggests a photoprotective response for weakened photosynthetic tissues. Instead, proline accumulation during the early stage of infestation and its subsequent decline may be associated with an alternative respiration mechanism that uses proline as an alternative substrate when the photosystem collapses during chlorosis. Glutathione, glutamate, and ascorbate levels dropped in needles, indicating high oxidative stress triggered during the infestation. The redox balance was not fully replenished in the prolonged infestation stage, compromising tree survival. Auxin accumulation may be associated with an attempt to produce new needles during the early stage of infestation to produce new photosynthetic tissues.
- The alteration in the translocation of the tree produced by the mucus of *S. noctilio* prevents the oxycneolignans accumulated in the needles from reaching the wood.

The lipidomics analysis applied in needles of *P. radiata* showed the alteration of the lipidome of *P. radiata* during the *S. noctilio* infestation.

- Fats were the most abundant upregulated lipids. Among the FA, the accumulation of lipids C16 and C18 can regulate the tree's defensive response. Also, VLCFA and LCFA with activity in the synthesis of resins increased significantly during both early and late infection. In addition, the high level of LPC and PA and the downregulation of PC suggest a high activity of phospholipases.
- Finally, a statistical model using ROC curve was evaluated to identify *P. radiata* trees presumably infested by *S. noctilio*. The model will be applied in cases of suspected attack by *S. noctilio*, confirming or not its presence in forest land. The ROC curve of the constructed biomarker model demonstrated excellent performance. These results validated the efficacy of a biomarker model based on the combination of 21 up-regulated metabolites to detect an early infestation of *P. radiata* trees by *S. noctilio*. The developed ROC models can serve as a platform for confirming the presence of *S. noctilio* in trees.
- We anticipate that our work will contribute to the development of new research line and breeding programs for resistant plant production.

## 2. Anexos

Other antecedent of the candidate:

### 2.1 Research project participation

Research project contribution list developed during the doctorate period:

CORFO 21CVC2-183630- Unidad de Desarrollo Tecnológico UDT, Enginier

2022: “Espuma agrícola biobasada, de buen desempeño técnico, costo competitivo y baja huella ambiental”

FONDEF ID19I10206 IDeA: Universidad de Concepción, Engenier, 2019-2021. “Development of a product for the control of eucalyptus weevil, based on scientific evidence obtained from new metabolomics approaches”

CONTEC83617- Universidad de Concepción, Engenier, 2018 - 2019. Project: "Vinculación asociativa para el desarrollo de un proceso de obtención de colágeno de alta pureza a partir de los subproductos de la pesquería de la jibia”

UCO1795- Universidad de Concepción, Chemist, 2017 - 2018. Project: “Fortalecimiento de las capacidades y gestión analítica de la Universidad de Concepción para contribuir a la producción y comercialización de productos hortofrutícolas inocuos en las VI, VII y VIII regiones”

CORFO 14IDL2-30156- Universidad de Concepción/Unidad de Desarrollo Tecnológico UDT, Área Productos Químicos. Chemist, 2015 - 2017. Project: “Estílbenos y procianidinas extraídas de residuos de poda de *Vitis vinífera*:

Producto purificado y micro encapsulado para la industria cosmética y/o nutracéutica”

## **2.2Scholarship**

Doctoral scholarship ANID N° 21161407, from 2016 to 2020

## **2.3Collaboration in other publications**

García, D. E., Carrasco, J. C., Salazar, J. P., Pérez, M. A., Cancino, R. A., & Riquelme, S. (2016). Bark polyflavonoids from *Pinus radiata* as functional building-blocks for polylactic acid (PLA)-based green composites. *Express Polymer Letters*, 10(10), 835–848.

García, D.E., Salazar, J. P., Riquelme, S., Delgado, N., & Paczkowski, S. (2017). Condensed Tannin-Based Polyurethane as Functional Modifier of PLA-Composites. *Polymer - Plastics Technology and Engineering*.

García, Danny Eugenio, Salazar, J. P., Riquelme, S., Delgado, N., & Paczkowski, S. (2018). Condensed Tannin-Based Polyurethane as Functional Modifier of PLA-Composites. *Polymer - Plastics Technology and Engineering*, 57(8), 709–726.

Sáez, V., Pastene, E., Vergara, C., Mardones, C., Hermosín-Gutiérrez, I., Gómez-Alonso, S., ... von Baer, D. (2018). Oligostilbenoids in *Vitis vinifera* L. Pinot Noir grape cane extract: Isolation, characterization, in

vitro antioxidant capacity and anti-proliferative effect on cancer cells. Food Chemistry, 265.

Riquelme, S., Sáez, V., Escobar, D., Vergara, C., Fuentealba, C., Bustamante, L., ... Mardones, C. (2019). Bench-scale extraction of stilbenoids and other phenolics from stored grape canes (*Vitis vinifera*): optimization process, chemical characterization, and potential protection against oxidative damage. Journal of the Chilean Chemical Society, 2

Guedes, L. M., Aguilera, N., Ferreira, B. G., Riquelme, S., Sáez-Carrillo, K., Becerra, J., ... Isaias, R. M. S.(2019). Spatiotemporal variation in phenolic levels in galls of calophyids on *Schinus polygama* (Anacardiaceae). Journal of Plant Research, 132(4), 509–520.

Escobar-Avello D, Mardones C, Saéz V, Riquelme S, von Baer D, Lamuela-Raventós RM, Vallverdú-Queralt A. 2021. Pilot-plant scale extraction of phenolic compounds from grape canes: Comprehensive characterization by LC-ESI-LTQ-Orbitrap-MS. Food Research International 143.



## 2.4 Patents

Formulación de micropartículas de extracto de sarmiento de *Vitis vinifera* útil en la industria nutraceútica y cosmética que comprende extracto de sarmiento con estilbenos y flavon-3-oles, ciclodextrina y maltodextrina; proceso para su elaboración y usos. N° 201702902

Un procesamiento para aumentar el contenido de estilbenos, esencialmente resveratrol, en sarmientos provenientes de las podas de *Vitis vinífera*. N°2014-03417

